The isolation and characterisation of a novel siderophore from the marine bacterium *Thalassomonas viridans*

UNIVERSITY *of the*
WESTERN CAPE

By

AMY COOPER

Submitted in the fulfilment of the requirements for the degree
Magister Scientiae

In the

Department of Biotechnology
University of the Western Cape
Bellville

Supervisor: Prof. Marla Trindade

Co-supervisor: Dr. Leonardo van Zyl

Declaration

I, Amy Cooper, declare that "The isolation and characterisation of a novel siderophore from the marine bacterium *Thalassomonas viridans*" is my own work, that it has not been submitted for any degree or examination in any other tertiary institution, and that all the sources I have used or quoted have been indicated and acknowledged by complete references.

Date ……19/12/2022……

Signature…….

Abstract

Natural products (NPs) produced by bacteria, fungi, plants, and marine animals include a large group of diverse chemical entities that display a broad range of biological activities. NPs are widely used for various applications, particularly in the fields of agriculture and medicine. Siderophores are a type of NP produced by various microorganisms to scavenge iron from the environment. They are characterised as low-molecular-mass (500-1500 Da) free ligands with a high affinity for iron. In recent years, organisms inhabiting the world's oceans have moved into the spotlight of NP discovery studies.

Thalassomonas viridans is a strictly aerobic, halophilic, chemo-organotrophic marine bacterium that was first isolated from cultivated oysters off the Mediterranean coast of Spain. When tested, this organism was seen to produce siderophores when grown under iron-limited conditions. Chemical characterisation tests were able to deem the siderophore as a carboxylate type. No antimicrobial activity was seen by the purified siderophore. It was determined that the siderophore is able to bind both iron and aluminium, but not vanadium or arsenic.

antiSMASH analysis of the genome of *T. viridans* revealed no detected similarity to known siderophore producing pathways. This indicates that the siderophore in question is novel, at least in its genetic method of production. A putative siderophore T1PKS/NRPS pathway was identified and analysed.

The approach of proteomic MS was selected in attempt to confirm whether or not the suspected genomic pathway was responsible for siderophore synthesis in *T. viridans*. Unfortunately, MS results showed a number of missing data points, possibly as a result of low protein concentrations. Despite low levels of protein, a peptide synthase belonging to a different genomic pathway was found in higher amounts in the test sample, suggesting that this alternative pathway may be responsible for siderophore synthesis.

MS analysis of purified siderophore extract revealed the fragmentation of a novel compound that could possibly be the siderophore, with a molecular weight of 1050.39 Da, that contains carboxylate groups. In order to elucidate the structure of this novel molecule, it is recommended that further studies, involving NMR techniques are performed.

Acknowledgements

I would like to thank my supervisor, Professor Marla Trindade and my co-supervisor, Dr Lonnie van Zyl for granting me the opportunity to conduct this research as well as for all their guidance. Both of whom I consider not only to be great scientists, but also great mentors. I will carry their lessons of critical thinking, curiosity, and resilience with me for the rest of my life.

I would also like to thank all of the students and staff at the IMBM for all of their help, support, and suggestions. I have thoroughly enjoyed my time at the IMBM, which is a true example of a positive and collaborative workspace.

Thank you to both the National Research Foundation (NRF) and the Institute for Microbial Biotechnology and Metagenomics (IMBM) for funding this project.

Thank you to my father, for trying so hard to understand exactly what it is that this thesis is about, even if I did have to explain over 100 times. Dad, thank you for trying. I really appreciate you putting in the effort to learn new and challenging things just so that you can discuss my interests with me.

Lastly, I would like to thank my partner Juandre. Although less inclined to attempt to understand what exactly it is that I do, I am very grateful of his support and motivation towards my “sciencing”.

Abbreviations

%SU	Percentage siderophore units
Δ	Delta
°C	Degrees Celsius
µl	Microlitre
µm	Micrometre
µM	Micromolar
rRNA	Ribosomal RNA
2,3-DAP	2,3-Diaminopropionic acid
2x	Two times
A domain	Adenylation domain
Aad	Aminoadipic acid
ABC	ATP-binding cassette
Abu	Aminobutyric acid
CAN	Acetonitrile
ACP	Acyl carrier protein
AGC	Automatic grain control
Ala	Alanine
AMT	Aminotransferase
antiSMASH	Antibiotics and Secondary Metabolite Analysis Shell
APS	Ammonium Persulfate
Ar	Absorbance of reference at 630 nm
ARTS	Antibiotic Resistance Target Seeker
As	Absorbance of the sample at 630 nm
Asn	Asparagine
Asp	Aspartic acid
AT	Acyltransferase
ATP	Adenosine 5′-triphosphate
BGC	Biosynthetic gene cluster
Bht	Butylated hydroxytoluene
BLAST	Basic local alignment search tool
Bp	Base pair
C domain	Condensation domain
CAS	Chromazurol Sulphonate

CDPS	tRNA-dependent cyclodipeptide synthases
CLSI	Clinical and laboratory standards institute
Cm	Centimetre
CTAB	Cetyltrimethylammonium bromide
Da	Dalton
DFOB	Deferoxamine B
dH_2O	Distilled water
Dhpg	Dihydroxyphenylglycine
DNA	Deoxyribonucleic acid
DtxR	Diphtheria toxin regulator
ESIMS	Electrospray ionization mass spectrometry
EST	Expressed Sequence Tags
Fur	Ferric iron uptake regulator
G	Grams
GC	Guanine-cytosine
Gln	Glutamine
Glu	Glutamic acid
Gly	Glycine
HCD	Higher energy collisional dissociation
HCl	Hydrochloric acid
HILIC	Hydrophilic interaction liquid chromatography
HMM	Hidden Markov model
Hpg	Homopropargylglycine
HPLC	High-pressure liquid chromatography
ICPMS	Inductively coupled plasma mass spectrometry
Ile	Isoleucine
Iva	Isovaline
Kd	Dissociation constant
kDa	Kilodalton
KS	Ketosynthase
kV	Kilovolts
L	Litre
LA	Luria Agar
LB	Luria Broth
LC-ESIMS	Liquid chromatography electrospray ionization mass spectrometry
LC-ICPMS	Liquid chromatography-inductively coupled plasma mass spectrometry

Leu	Leucine
M	Molar
m/z	Mass to charge ratio
MA	Marine Agar
MALDI-TOF	Matrix-assisted laser desorption/ionization-time of flight
Mb	Mega base pairs
MbtH	Methylbenzothiazolinone hydrazonehydrochloride
MeOH	Methanol
Met	Methionine
MFS	Major facilitator superfamily
Mg	Milligram
mg/l	Milligrams per litre
Min	Minutes
Ml	Millilitre
mM	Millimolar
MMM Fe-	Iron Deficient Minimal Marine Media
MMM Fe+	Iron sufficient Minimal Marine Media
mol%	Molar percentage
MS	Mass Spectrometry
Ms	Millisecond
N	Normal
NaOH	Sodium Hydroxide
NaPDos	Natural Product Domain Seeker
NCBI	National Center for Biotechnology Information
NIS	NRPS-independent synthetases
nL	Nanolitre
nM	Nanomolar
Nm	Nanometer
NMR	Nuclear magnetic resonance
NPs	Natural products
NRPS	Non-ribosomal peptide synthetase
NRPs	Non-ribosomal peptides
OD	Optical density
OMRPs	Outer membrane receptor proteins
ORF	Open reading frame
PBS	Phosphate buffered saline

pH	Potential hydrogen
Phe	Phenylalanine
Phg	Phenylglycine
PKS	Polyketide synthase
Ppm	Parts per million
PRISM	PRediction Informatics for Secondary Metabolomes
RNA	Ribonucleic acid
RND	Resistance, nodulation, and cell division
SAGE	Serial Analysis of Gene Expression
SDS	Sodium dodecyl-sulfate
SDS-PAGE	Sodium dodecyl-sulfate polyacrylamide gel electrophoresis
Ser	Serine
sgRNA	Single guide ribosomal nucleic acid
spp.	Species
T domain	Thioester domain
T1PKS	Type 1 polyketide synthase
T3PKS	Type 3 polyketide synthase
TD	Terminal reductase
TEAB	Triethylammonium bicarbonate
TEMED	Tetramethylethylenediamine
Thr	Threonine
TILLING	Targeting Induced Local Lesions In Genomes
tRNA	Transfer ribonucleic acid
Trp	Tryptophan
Tyr	Tyrosine
V	Volts
v/v	Volume to volume
Val	Valine
w/v	Weight to volume
X*g*	G force

Table of Contents

Declaration i
Abstract ii
Acknowledgements iii
Abbreviations iv
Table of Contents viii
List of Figures xi
List of Tables xiii
Chapter 1: Literature Review 1
1.1 Introduction 2
1.2 Importance of Iron 3
1.3 Iron Acquisition 4
1.4 Siderophores 4
1.5 Other Roles of Siderophores in Bacteria 5
1.5.1 Virulence 5
1.5.2 Other Metals 6
1.5.3 Biofilms 8
1.5.4 Signalling Molecules 9
1.6 Classification of Siderophores 10
1.6.1 Hydroxamate Siderophores 10
1.6.2 Catecholate Siderophores 12
1.6.3 Carboxylate Siderophores 14
1.6.4 Mixed Functional Group Siderophores 16
1.7 Siderophore Mediated Iron Uptake Mechanism 16
1.8 Siderophore Biosynthesis 20
1.8.1 NRPS-Mediated Siderophore Biosynthesis 20
1.8.2 NRPS-Independent Siderophore Biosynthetic Pathway 21
1.9 Iron Regulation in Bacteria 22
1.10 Application of Siderophores 23
1.11 Marine Siderophores 25
1.11.1 Identifying Marine Siderophores 26
1.12 Functional Genomics 28
1.12.1 Genome Mining Tools 29
1.13 *Thalassomonas viridans* 31
1.14 Research Objectives 32

Chapter 2: Methods and Materials 34
2.1 General Laboratory Chemicals and Reagents 35
2.2 Bacterial Strains and Growth Conditions 35
2.3 Preparation of Glassware 37
2.4 Preparation of Inoculums 37
2.5 Detection of Siderophore Production 37
2.5.1 Cas Assay (Schwyn and Neilands, 1987) 37
2.5.2 $FeCl_3$ Test (Snow, 1954) 38
2.5.3 Hydroxyquinoline-mediated Siderophore Test (De Brito et al., 1995) 38
2.5.4 CAS-Shuttle Assay (Schwyn and Neilands, 1987) 38
2.6 Growth and Siderophore Production 39
2.7 Chemical Siderophore Characterisation 39
2.7.1 Arnow's Assay (Arnow, 1937) 39
2.7.2 Tetrazolium Salt Test (Snow, 1954) 40
2.7.3 Vogel's Test (Vogel,1987) 40
2.7.4 Spectrophotometric Tests 40
2.8 Antimicrobial Activity Assay 41
2.9 Chelation of Other Metals 41
2.10 Compound Purification 42
2.10.1 Hydrophobic-Resin Chromatography 42
2.10.2 Size Exclusion Filtration 42
2.11 Mass Spectrometry of Siderophore Extract 43
2.11.1 Mass Spectrometry Data Analysis 44
2.12 Total Protein Extraction 44
2.13 Sodium Dodecyl Sulphate-Polyacrylamide Gel Electrophoresis (SDS-PAGE) 44
2.14 Proteomics 46
2.14.1 On-bead Protein Digestion 46
2.14.2 Liquid Chromatography 46
2.14.3 Mass Spectrometry of Protein Extracts 47
2.14.4 Data Analysis 47
2.15 Genome Mining for Secondary Metabolite Pathways 47
Chapter 3: Results and Discussion 49
3.1 Initial Detection of Siderophore Production 50
3.2 Growth and Siderophore Production 51
3.3 Siderophore Purification 54
3.4 Antimicrobial Assays 56
3.5 Chemical Characterisation 57

3.6 Chelation of Other Metals 61
3.7 Genome Mining of *Thalassomonas viridans* 62
3.7.1 Cluster 8 Open Reading Frames with Possible Siderophore-Related Activity 67
3.7.2 Modular Organisation of Cluster 8 68
3.7.3 Prediction of A-domain Amino Acid Specificity of Cluster 8 NRPS Domain 70
3.7.4 Specificity Prediction of A-domain Amino Acid Specificity of Cluster 8 T1PKS Domain 72
3.7.5 Cluster 8 C-domain Classification 72
3.7.6 Gene Cluster Comparison 74
3.7.7 Structure Prediction 75
3.8 Mass Spectrometry 77
3.8.1 SIRIUS Analysis of Compounds Less Than 1000 Da 79
3.8.2 SIRIUS Analysis of Compounds Larger Than 1000 Da 82
3.9 Proteomic Analysis 98
Chapter 4: General Discussion and Conclusion 104
References 109
Appendices 145
Appendix A 146
Appendix B 146

List of Figures

Figure 1: Diagram showing the process of biofilm formation. 8

Figure 2: Chemical structures of the hydroxamate functional group and the hydroxamate siderophores: aerobactin produced by *E. coli*, pyoverdin Pa A produced by *Pseudomonas aeruginosa*, and ferrichrome A produced by *Ustilago sphaerogena*. 11

Figure 3: Chemical structures of the catecholate functional group and the catecholate siderophores enterobactin produced by *E. coli*, pyochelin I produced by *Pseudomonas aeruginosa*, bacillibactin C produced by *Bacillus subtilis*, and protochelin produced by *Azotobacter vinelandii*. 13

Figure 4: Chemical structures of the carboxylate functional group and the carboxylate siderophores rhizobactin produced by *Ensifer meliloti* and vibrioferrin produced by *Vibrio parahaemolyticus*. 15

Figure 5: Enterobactin import (A) and export (B) mechanisms in *E. coli*. 17

Figure 6: Aerobactin synthesis by *E. coli*. 23

Figure 7: antiSMASH version 6.1.1 analysis parameters used in this study. 48

Figure 8: CAS assay results.. 50

Figure 9: Results of $FeCl_3$ test.. 51

Figure 10: Growth curve of *T. viridans* and *T. viridans* Δ*1*, both grown with and without iron for a period of 14 days. 52

Figure 11: Siderophore production of *T. viridans* and *T. viridans* Δ*1*, both grown with (Fe+) and without (Fe-) iron for a period of 14 days. 54

Figure 12: Siderophore activity detection of various SEPABEADS® SP207 extraction fractions as determined via the CAS-shuttle assay.. 55

Figure 13: Siderophore activity tests at various steps of size exclusion filtration performed using the CAS-shuttle assay. 56

Figure 14: Results of tetrazolium salt test for hydroxamates. 58

Figure 15: Results of Arnow's method of catecholate detection. 59

Figure 16: Results of Vogel's test for carboxylates. 60

Figure 17: Secondary metabolite pathways identified in the genome of *T. viridans* Δ*1* using antiSMASH version 6.1.1.. 63

Figure 18: Prediction of ORFs within cluster 8 using antiSMASH 6.1.1. 64

Figure 19: Modular organisation of cluster 8 in *T. viridans* as detected by antiSMASH version 6.1.1. 69

Figure 20: Comparison of cluster 8 of *T. viridans* and similar cluster found in *Pseudoalteromonas piscicida.* 74

Figure 21: Structures of Pseudoalteropeptide A and Pseudochelin A. 75

Figure 22: antiSMASH predicted structures of *T. viridans* cluster 8 and similar *P. piscicida* cluster. 76

Figure 23: MS1 chromatograms of siderophore positive and siderophore negative samples run in positive mode. 78

Figure 24:MS1 chromatograms of siderophore positive and siderophore negative samples run in negative mode. 78

Figure 25: MS2 chromatograms for three compounds with masses larger than 1000 Da as detected by SIRIUS. 84

Figure 26:SIRIUS structure prediction results (A) and substructure peak matching results(B) for the predicted formula $C_{45}H_{57}N_{13}O_{17}$ for the detected compounds of 1050.39 Da and 1032.38 Da. 88

Figure 27: antiSMASH and PRISM predicted structures of *T. viridans* cluster 3 and SIRIUS predicted structure of compounds with masses of 1050.39 Da and 1032.38 Da. 92

Figure 28: SDS-PAGE of total protein extracts from *T. viridans* cultures grown with and without iron to asses extraction quality prior to proteomic analysis 100

Figure 29: Graph displaying relative amounts of the peptides identified in the iron-starved (Fe-) and iron-sufficient (Fe+) protein extracts of *T. viridans* 1007

List of Tables

Table 1: Examples of siderophores found to bind other metals in addition to iron. 7

Table 2: Bacterial strains used in this study. 35

Table 3: Growth media used in this study. 36

Table 4: Preparation of 4% stacking gel. 45

Table 5: Preparation of 12% separating gel. 45

Table 6: Summary of metal binding ability of siderophore extract. 61

Table 7: Predicted ORFs within cluster 8, their top BLAST hits, and their putative functions. 64

Table 8: Prediction of A-domain amino acid specificity in *T. viridans* cluster 8 using NRPSpredictor2. 71

Table 9: Prediction of A-domain amino acid specificity in *T. viridans* cluster 8 using PRISM. 72

Table 10: Summary of NRPS C-domain subcategories. 73

Table 11: C-domain subtypes as determined by the NaPDos server 74

Table 12: Summary of SIRIUS results for compounds less than 1000 Da under the time frame of Peak 1. 79

Table 13: Summary of SIRIUS results for compounds less than 1000 Da under the time frame of Peak 2. 80

Table 14: Summary of SIRIUS results for compounds less than 1000 Da under the time frame of Peak 3. 81

Table 15: Summary of SIRIUS results for compounds less than 1000 Da under the time frame of Peak 4. 82

Table 16: Masses of MS2 peaks with intensities of 0.1 and above for the compounds of 1050.39 Da, 1032.38 Da and 1034.40 Da. 85

Table 17: Summary of top five SIRIUS predictions for the compound with a mass of 1050.39 Da. 86

Table 18: Summary of top five SIRIUS predictions for the compound with a mass of 1032.38 Da. 87

Table 19:A-domain amino acid specificity in *T. viridans* cluster 3 using NRPSpredictor2 and PRISM. Amino acids predicted to be incorporated in the compounds of 1050.39 Da and 1032.38 Da also shown. 91

Table 20: Summary of top five SIRIUS predictions, as well as the eighth prediction (highlighted in green) for the compound with a mass of 1034.40 Da 90

Table 21: Currently known sulphur-containing siderophores 94

Table 22: Table Summarising peptides that were found in higher amounts in the case of the iron-starved protein sample when compared to the iron-sufficient protein sample and the corresponding proteins from which the peptides originate.....100

Table 23: Summary of the presence or absence of three housekeeping proteins seen in both the Iron-starved and iron-sufficient protein extracts.....102

Chapter 1: Literature Review

1.1 Introduction

Historically, the human pharmaceutical armamentarium has been greatly indebted to nature, particularly to the secondary metabolites or natural products (NPs) of bacteria, fungi, plants, and marine animals (Luo et al., 2014). NPs embody a large group of diverse chemical entities that display a broad range of biological activities and thus have been seen to have many uses, particularly in the fields of agriculture and medicine (Bhanot et al., 2011; Demain, 2014). Since penicillin was discovered over 90 years ago, more than 400 000 NPs have been identified, most of which are produced by bacteria (Sorokina and Steinbeck, 2020).

Unfortunately, a decline in NP discovery rates following the 1990s was seen. This was partially because of the inaccurate belief that microorganisms had been fully exploited as a source of NPs, as well as high rates of molecule rediscovery caused by a lack of complete compound databases and the limited availability of high-resolution and sensitive detection methods (Li and Vederas, 2009). Following the advent of fast and inexpensive next-generation genome sequencing technologies, however, the field of NP discovery was revived (Luo et al., 2014). The sequencing of several microbial genomes, such as *Streptomyces coelicolor* M145 and *Salinispora tropica*, revealed that approximately 70% of the NPs encoded by these genomes had yet to be characterised (Li and Vederas, 2009; Gerea et al., 2012). Since then and following the genome sequencing of organisms across all domains of life, it has been seen that the presence of multiple NP gene clusters that encode uncharacterised products is a common occurrence. This has resulted in NP discovery efforts again flourishing, particularly at the academic level (Luo et al., 2014).

In recent years the focus of NP discovery has shifted away from those produced solely by terrestrial organisms, and scientists have begun to also search the oceans for novel compounds (Montaser and Leusch, 2011). The oceans cover over 70% of our planet's surface and represent a largely unexplored resource (Bérdy, 2012). It has been estimated that a biological diversity exceeding that of tropical rainforests can be found in certain areas, such as coral reefs and the deep-sea floor (Haefner, 2003). It is thought that because organisms that inhabit marine environments are exposed to conditions that are so very different from terrestrial ones, many marine organisms may produce a variety of NPs with unique structural features when compared to those produced by terrestrial organisms (Lam, 2006). The search for novel marine NPs has already resulted in the isolation of tens of thousands of metabolites

(Fusetani, 2000) with diverse biological activities, including; antibiotic, antifungal, toxic, cytotoxic, neurotoxic, antimitotic, antiviral, antineoplastic, and immunosuppression activities (Kelecom, 1999; Blunt et al., 2018).

One such type of NPs is siderophores. These molecules are produced by organisms with the goal of iron acquisition and will be the focus of this study. This review will cover the importance of microbial siderophore production, the production mechanisms, the different known classes of siderophores, and the potential applications of these molecules. The use of bioassay-guided isolation and genome mining approaches in the context of natural product discovery will also be discussed.

1.2 Importance of Iron

Iron is an essential element that is required by virtually all bacteria, with only a few exceptions, for growth and survival. It is required for many vital biological processes, such as electron transport, oxygen transport, amino acid synthesis, respiration, methanogenesis, nitrogen fixation, the citric acid cycle, photosynthesis, DNA biosynthesis, detoxification of oxygen radicals, tRNA modifications, and gene regulation (Granger and Price, 1999; Andrews et al., 2003; Miethke and Marahiel, 2007). Additionally, iron acts as a cofactor for many enzymes, such as ribonucleotide reductase, nitrogenase, peroxidase, catalase, and succinic dehydrogenase (Litwin and Calderwood, 1993).

Iron is the fourth most abundant element found in the Earth's crust, following oxygen, silicon, and aluminium. However, due to the insolubility of Fe(III) at physiological pH in aerobic environments, the availability of this element to most microorganisms is severely limited (Sandy and Butler, 2009). Marine bacteria are faced with the challenge of even lower iron availability since ocean waters have a higher pH when compared to terrestrial environments. This results in an even lower solubility and thus iron availability (Butler, 2005). This problem is also compounded by the low total concentration of iron found in surface ocean waters. Bacteria usually require between 0.4 μM and 1 μM concentrations of iron for growth (Raymond et al., 2003), yet ocean surface waters typically only contain between 0.01 and 2 nM of iron (Sandy and Butler, 2009).

1.3 Iron Acquisition

To overcome the extremely low solubility of ferric iron within ocean waters, micro-organisms have developed various exquisitely selective and precisely regulated mechanisms of acquiring iron (Matzanke et al., 1990). It appears that the competition among species for ferric iron has acted as a selection pressure during evolution and thus has resulted in the generation of a broad spectrum of diverse ferric iron uptake methods in prokaryotes and eukaryotes. In bacteria, iron acquisition can be achieved by either reducing ferric iron to the relatively soluble ferrous form, lowering the external pH to render ferric iron more soluble, or employing ferric ion chelators as solubilizing agents (Matzanke et al., 1990). These systems are regulated by iron concentration (Lankford, 1973) and are only expressed under iron-deficient conditions and suppressed under high iron concentrations. Most bacteria use the chelation and reduction approach, and many do so through the production of iron-chelating molecules known as siderophores (Winkelmann, 2002).

1.4 Siderophores

Siderophores are secondary metabolites produced by various microorganisms to scavenge iron from the environment. They are characterised as low-molecular-mass (500-1000 Da) free ligands with a high affinity for iron (Neilands, 1984). The availability of iron regulates the production of these molecules, and more significant quantities are produced as the availability of iron decreases. Siderophores are not only able to provide iron to the cell, but they also regulate and control iron uptake (Guerinot, 1994). Although a large amount of variation can be seen between the siderophore structures of different species, most have a peptide backbone with several non-protein amino acids (Drechsel and Jung, 1998).

Compared to the amount of knowledge available regarding siderophores produced by terrestrial microorganisms, less is known about the siderophores produced by marine microorganisms. This is because open ocean bacteria that produce siderophores have not been studied for as long as terrestrial microbes, and thus much fewer structures of marine siderophores have been characterized (Butler, 2005). More recent studies by Chen et al. (2019) have shown that marine siderophores are both abundant and diverse.

1.5 Other Roles of Siderophores in Bacteria

1.5.1 Virulence

Several studies (Demir and Kaleli, 2004; Abergel et al., 2006; Jin et al., 2006; Lawlor et al., 2007: Crouch et al., 2008; Fetherston et al., 2010; Jimenez et al., 2010; Beasley et al., 2011; Caza et al., 2011; Chim et al., 2011) have shown that siderophores play a role in mediating pathogen multiplication and the development of virulence in some bacteria. Pathogens infecting mammalian hosts are faced with the challenge that extracellular iron is bound to proteins of the transferrin family to ensure a supply of iron to all the cells throughout the host's body. This strategy reduces the amount of iron available to the pathogenic bacteria, thus forming a critical element of the innate immune system. The siderophores of the pathogenic bacteria must compete with the host's iron-binding proteins for iron, which is crucial for its survival (Lawlor et al., 2007; Skaar, 2010). An example of this is seen by the siderophore pyoverdine, which is produced by *Pseudomonas aeruginosa* and can sequester iron from the human host's lactoferrin and transferrin to enable biofilm formation and thus facilitate infection (Xiao and Kisaalita, 1997; Singh et al., 2002). In bacteria such as *Escherichia coli*, *Bacillus cereus*, *P. aeruginosa*, and *Staphylococcus aureus*, the transmembrane signalling system that is involved in the uptake of iron-siderophore complexes is, in addition to siderophores, essential for the development of virulence factors (Wilderman et al., 2001; Lamont et al., 2002; Zawadzka et al., 2009). The siderophore pyoverdine in *P. aeruginosa* is known to regulate the production of other virulence factors such as exotoxin A and PrpI in addition to sequestering iron (Wilderman et al., 2001). The siderophore nigribactin, produced by the marine bacterium *Vibrio nigripulchritudo*, has been seen to enhance the expression of *spa*, a gene encoding a major surface-bound virulence factor in this species (Nielsen et al., 2012). Other siderophores produced by marine bacteria that are essential virulence factors include anguibactin produced by *Vibrio anguillarum* or *Vibrio* sp. DS40M4 (Soengas et al., 2006; Balado et al., 2008), and piscibactin, produced by *Photobacterium damselae* subsp. *piscicida* and *V. anguillarum* (Souto et al., 2012; Balado et al., 2017; Balado et al., 2018).

1.5.2 Other Metals

Bacterial siderophores, in addition to iron, are also known to chelate other metals. Table 1 summarises some examples of siderophores that have been found to bind other metals in addition to iron. Studies have shown that metals other than iron can also regulate the production of siderophores, depending upon the concentration of metals in the growth medium (Braud et al., 2009). For instance, pyoverdine production was upregulated in the presence of silver, aluminium, copper, chromium, gallium, manganese, and nickel in *P. aeruginosa* (Braud et al., 2009). In *Azotobacter vinelandii* azotochelin biosynthesis was stimulated by molybdenum (Duhme et al., 1998), and high aluminium concentrations activated the production of schizokinen and *N*-deoxyschizokinen in *Bacillus megaterium* (Hu and Boyer 1996). The amphiphilic siderophore imaqobactin, produced by the marine bacterium *Variovorax* sp. RKJM285 can form stable adducts with iron, gallium, and aluminium (Robertson et al., 2018). The siderophores of the marine bacterium *Streptomyces olivaceus* FXJ8.012, tetroazolemycin A and B, are able to bind iron, copper, and zinc (Liu et al., 2013).

Since the molecular mass of a siderophore–metal complex is too large for diffusion via porins, sequestering heavy metals outside of the cell by siderophores can prevent the entry of these metals into the cell. The ability of other metals to induce siderophore production thus plays an important role in the heavy/toxic metal tolerance of bacteria (Michel et al., 2005; Schalk et al., 2011).

Table 1: Examples of siderophores found to bind other metals in addition to iron.

Source Organism	**Siderophore**	**Structure**	**Metals Complexed in addition to iron**
Streptomyces pilosus	Desferrioxamine	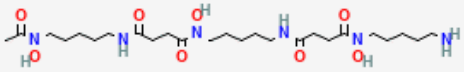	nickel, cadmium, gallium, aluminium, vanadium, and plutonium (Dimkpa et al., 2008a).
Streptomyces coelicolor	Coelichelin	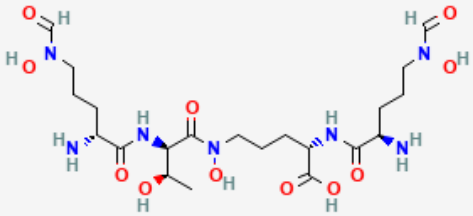	nickel and cadmium (Dimkpa et al., 2008a).
Pseudomonas aeruginosa	Pyoverdine	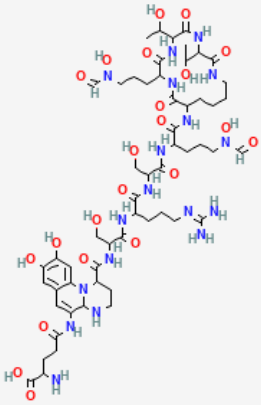	silver, aluminium, cadmium, cobalt, chromium, copper, europium, gallium, mercury, manganese, nickel, lead, tin, terbium, thallium, and zinc (Dimkpa et al., 2008b; Braud et al., 2009
Pseudomonas aeruginosa	Pyochelin	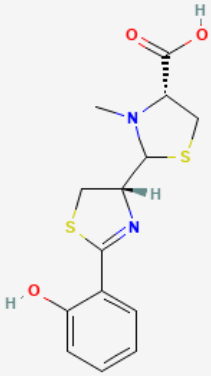	silver, aluminium, cadmium, cobalt, chromium, copper, europium, gallium, mercury, manganese, nickel, lead, tin, terbium, thallium, and zinc (Dimkpa et al., 2008b; Braud et al., 2009)

1.5.3 Biofilms

Microbial biofilms are complex communities of microorganisms that grow on biotic or abiotic surfaces in aqueous environments (Donlan, 2001; Lynch and Robertson, 2008). They can include multiple organisms, including Gram-positive or Gram-negative bacteria, protozoa, and yeast (Bell, 2001). Biofilm development depends on the availability of a surface for attachment and nutrients required for growth (Costerton et al., 1999; Stoodley et al., 2002). As illustrated in Figure 1, the development of biofilms occurs in five steps: first, planktonic cells attach to a surface, next a monolayer is formed, and a matrix is produced, microcolonies form, the microcolonies mature, and the biofilm structure is detached. The microorganisms that establish biofilm communities are very different from their planktonic counterparts regarding which genes they express and have highly complex and heterogeneous physiology. They are difficult to control since they are less susceptible to antimicrobial agents (Xu et al., 2000; Stewart and William Costerton, 2001). Studies have shown that intracellular iron concentrations play an important role in biofilm formation and development.

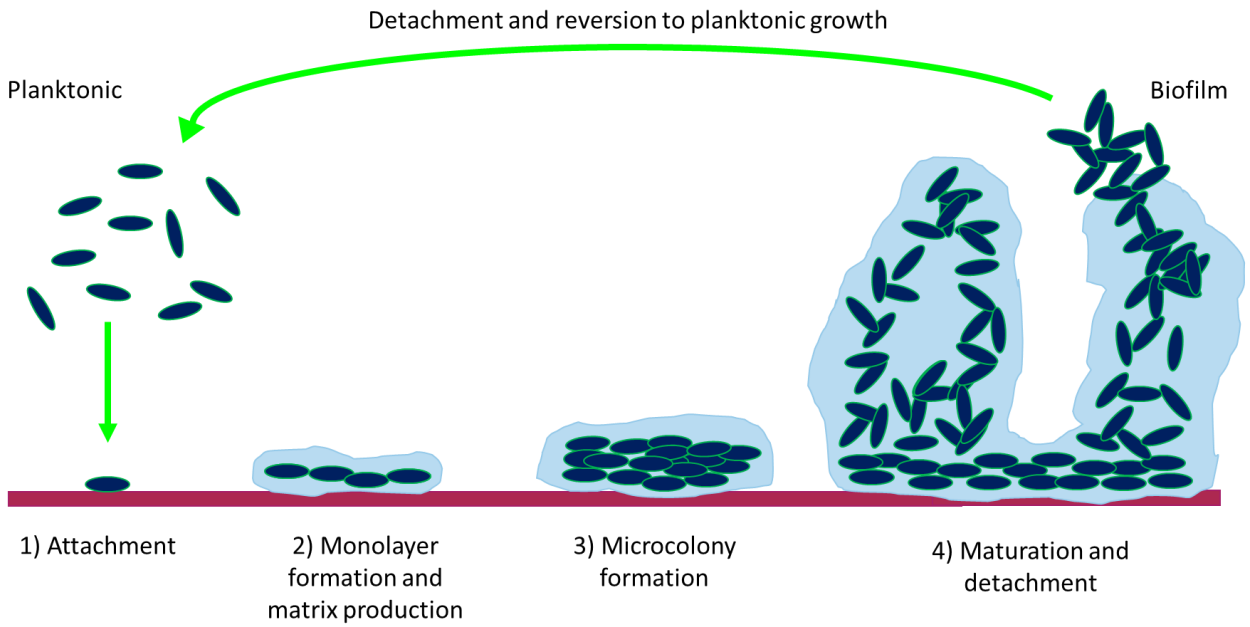

Figure 1: Diagram showing the process of biofilm formation.

In a study by Singh et al. (2002), it was seen that the iron chelator in mammalian blood called lactoferrin could restrict the maturation of *P. aeruginosa* biofilms. This was caused by the twitching motility displayed by *P. aeruginosa* cells at a low iron concentration, preventing

the formation of microcolonies. *P. aeruginosa* can form the typical mushroom-shaped biofilms by utilizing pyoverdine, pyochelin, ferric citrate, or ferrioxamine siderophores (Banin et al., 2005). It was shown by Banin et al. (2005) that thin biofilms are formed in the absence of iron by *P. aeruginosa* mutants that are incapable of pyoverdine and pyochelin biosynthesis. Hence, depending on different environments, different iron uptake systems may be vital for the development and maturation of biofilms in *P. aeruginosa*. Similarly, the exochelin siderophore biosynthesis and uptake systems have been seen to be essential in *Mycobacterium smegmatis* for the development of biofilms, though not for planktonic growth (Ojha and Hatfull, 2007). This is thought to be due to iron playing a regulatory role in the transition to biofilm growth and exochelin being required to obtain the needed iron (Ojha and Hatfull, 2007).

1.5.4 Signalling Molecules

It has also been seen that siderophores play essential roles as signalling molecules. Quorum sensing bacteria release low molecular weight chemical "messenger" molecules into the environment. When a critical concentration of these molecules is reached outside the cell, a signal transduction cascade is triggered, leading to an alteration of gene expression. It has been reported that siderophore production and other iron transport genes are under the control of quorum sensing (Guan and Kamino, 2001). Additionally, several reports have suggested that in addition to their roles in iron uptake and transport, siderophores can have cell signalling functions.

An example of this can be seen by pyoverdine, which is reported to regulate its own production and the production of at least two other virulence factor proteins (an exotoxin and an endoprotease) in *Pseudomonas aeruginosa* (Lamont et al., 2002). It is proposed that this pyoverdine-mediated signalling provides pathogenic bacteria with a mechanism to delay the production of virulence factors and detection by the host immune system until bacterial cell numbers have reached a sufficient level to enable a productive infection (Passador et al., 1993; Whitehead et al., 2001). An early example of siderophores being used as signalling molecules came from the observation that some marine bacteria use exogenous siderophores to stimulate the production of endogenous siderophores (Johnstone and Nolan, 2015). For example, the growth of the α-proteobacterium strain V0210 was stimulated by the addition of *N*,*N′*-bis(2,3-dihydroxybenzoyl)-*O*-serylserine, a siderophore produced by *Vibrio* spp. (Guan, Kanoh and Kamino, 2001).

1.6 Classification of Siderophores

Siderophores can be classified into different groups based on their functional groups and hydrophobicity. These include α-hydroxycarboxylates, hydroxamates, catecholates, and mixed-type siderophores (Neilands, 1990).

1.6.1 Hydroxamate Siderophores

Hydroxamate siderophores are produced by both fungi and bacteria and include ferrioxamines, ferrichromes, and coprogens (Winkelmann, 1991). Hydroxamates originate from either of the amino acids, L- ornithine or lysine. Bacterial hydroxamates usually consist of Nδ hydroxylated and Nδ acylated alkyl amines. These siderophores are predominantly hexadentate with three secondary hydroxamate groups. Each hydroxamate group can be described as C(=O)N-(OH)R, where R is an amino acid or a derivative (Hider, 1984). The structure of the hydroxamate group and a few examples of hydroxamate siderophores can be seen in Figure 2.

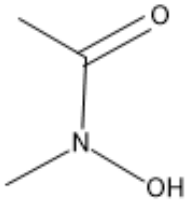

Hydroxamate Functional Group

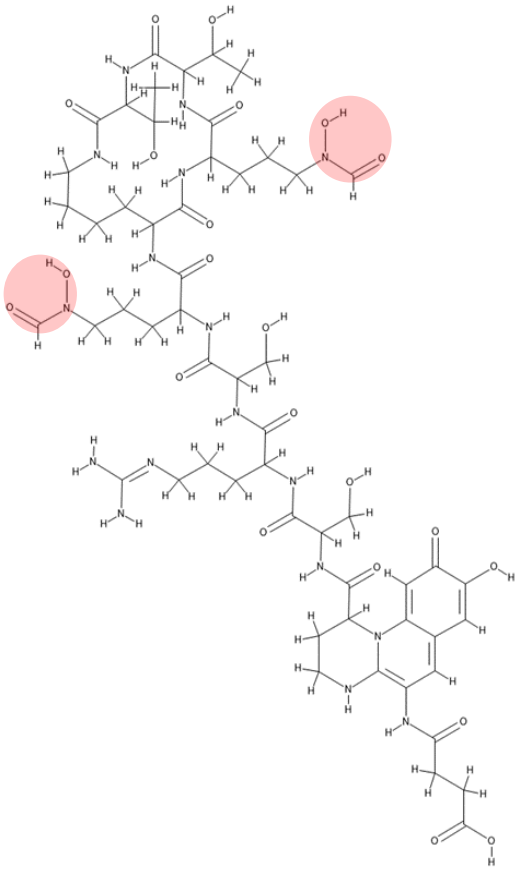

Pyoverdin Pa A

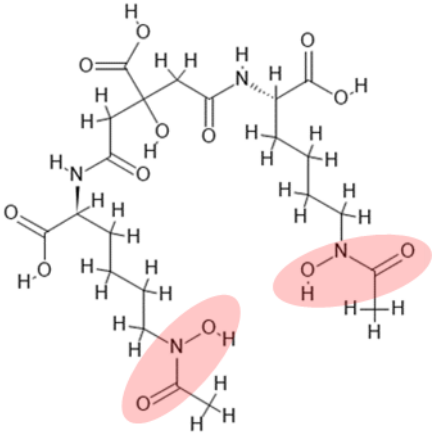

Aerobactin

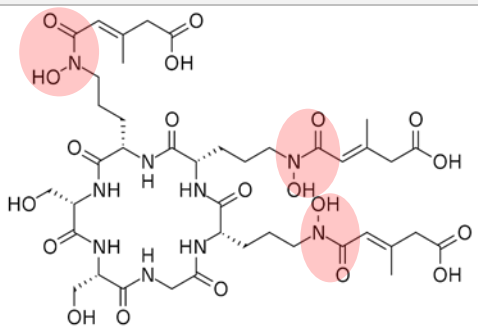

Ferrichrome A

Figure 2: Chemical structures of the hydroxamate functional group and the hydroxamate siderophores: aerobactin produced by E. coli, pyoverdin Pa A (Demange et al., 1990) produced by Pseudomonas aeruginosa, and ferrichrome A produced by Ustilago sphaerogena. Hydroxamate functional groups within these siderophores are highlighted in red.

In the synthesis of aerobactin (*E. coli*) and mycobactin (*Mycobacterium* spp.), lysine derivatives are used (Miethke and Marahiel, 2007). Ornithine derivatives are utilised in the synthesis of fusarinine (*Fusarium roseum*), ferrichrome (variety of fungi), coprogens (variety of fungi), pyoverdine (*P. aeruginosa*), ornibactin (strains of pseudomonads), and exochelin

(*Mycobacterium* spp.) (Neilands 1981; Miethke and Marahiel, 2007). The hydroxamate group is assembled in a two-step process, beginning with hydroxylation of the primary side-chain amine of ornithine or lysine by a flavin adenosine dinucleotide-dependent monooxygenase (Challis, 2005). The second step involves formylation by a methyltransferase for pyoverdin and ornibactin or acetylation by an acetylase for all other hydroxamate siderophores (Miethke and Marahiel, 2007). Each hydroxamate group provides two oxygen molecules that react with iron to form a bidentate ligand through the acylation of hydroxylamine. Two major resonance forms, one with a distributed negative charge over the two oxygen atoms and one with a negative charge on a single oxygen atom, can be found (Hider, 1984). An essential role in the charge distribution is played by the carbonyl and nitrogen substituents. These substituents promote the donation of electron density from the nitrogen lone pair to the carbonyl oxygen. This results in both the oxygen atoms being negatively charged and thus enhances the stability of the metal complex (Hider, 1984). In hydroxamate siderophores, the nitrogen atoms of oxazoline and thiazoline chelate iron. Ferrioxamines are both linear and cyclic compounds containing l-amino-5-hydroxylaminopentane, in some cases 1-amino-5-hydroxylaminobutane, and succinic acid as building blocks (Winkelmann, 1991). Ferrichromes, except for tetraglycyl-ferrichrome, a heptapeptide, all possess cyclic hexapeptide backbones containing a tripeptide sequence of Nδ-acyl-Nδ-hydroxy-l-ornithine. The variety of ferrichromes is caused by variations in the remaining tripeptide sequence and the N-acyl substituents (Winkelmann, 1991). Coprogens are linear trihydramates composed of Nδ-acyl-Nδ-hydroxy-l-ornithine, anhydromevalonic acid, acetic acid, and additional variable building blocks (Winkelmann, 1991).

1.6.2 Catecholate Siderophores

Catecholate siderophores, also known as phenolates, are the second most widely produced siderophores. This class of siderophore has so far only been seen to be produced by bacteria and contains a catecholate group that is derived from either dihydroxybenzoic acid or salicylate. When compared to hydroxamate siderophores, catecholates display very few structural variations (Winkelmann, 1991). A range in iron-binding affinities of different catecholate siderophores is seen, from very tight binding for enterobactin from *E. coli* (Kd = 10-52 M) to fairly weak binding seen in pyochelin from *P. aeruginosa* (Kd = 5 x 10^{-5} M) (Cox and Graham, 1979). These siderophores all contain a cyclic trimester scaffold of L-serine or L-threonine, and examples include enterobactin, vibriobactin, salmochelin,

bacillibactins, and yersiniabactin (Raymond and Dertz, 2004). The catecholate functional group, as well as the structures of a few catecholate-type siderophores, can be seen in Figure 3.

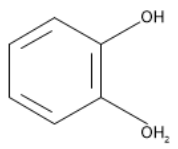

Catecholate Functional Group

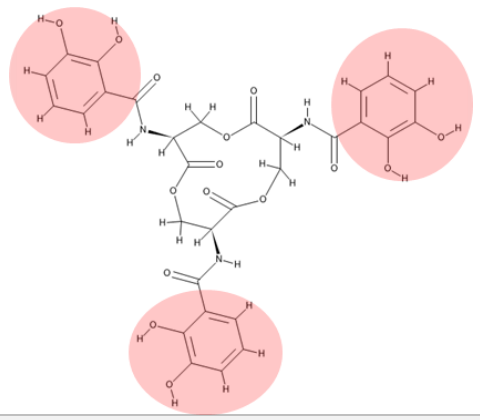

Enterobactin

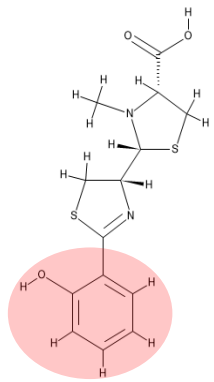

Pyochelin I

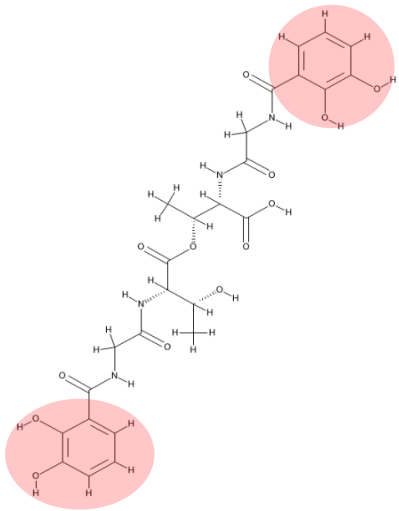

Bacillibactin C

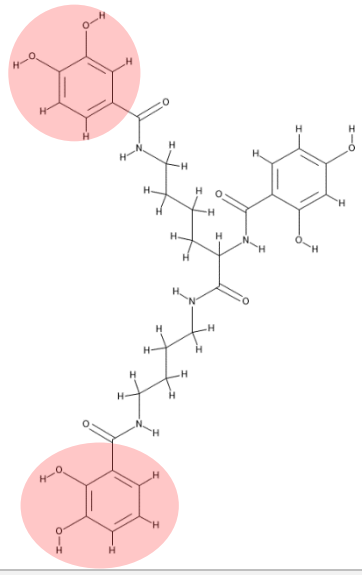

Protochelin

Figure 3: Chemical structures of the catecholate functional group and the catecholate siderophores enterobactin produced by E. coli, pyochelin I produced by Pseudomonas aeruginosa, bacillibactin C produced by Bacillus subtilis, and protochelin produced by Azotobacter vinelandii. Catecholate functional groups within these siderophores are highlighted in red.

Enterobactin is a cyclic trimer of 2,3-dihydroxybenzoyl-L-serine, with each group providing two oxygen atoms that form a hexadentate octahedral complex with iron, similar to hydroxamate siderophores (Hofte, 1993). This catecholate siderophore has a remarkably large stability constant, a high affinity for Fe(III), and can be isolated from a range of pathogenic and enteric bacteria (Hofte, 1993). Salmochelin is a glucosylated derivative of enterobactin that was isolated from *Salmonella enterica* (Raymond et al., 2003). Bacillibactin was isolated from some *Bacillus* species and has been seen to incorporate a cyclic trimester scaffold of L-threonine. The glycine that is ligated by 2,3-dihydroxybenzoic acid appends each threonine amine. Thus, the glycine spacers extend the three chelating arms (Dertz et al., 2006). In addition, various linear catecholates, including cepaciachelin, protochelin, aminochelin, and azotobactin, have also been identified (Page et al., 1991; Khodr et al., 2002).

In addition to the hydroxamate type siderophore pyoverdin, *P. aeruginosa* produces a catecholate type siderophore called pyochelin. This is a 324 Da peptide that forms a thiazoline and a thiazolidine heterocyclic ring that is composed of salicylate and two cysteines (Cox and Graham, 1979). Contrasting the high levels of divergence of pyoverdin among strains of *P. aeruginosa*, the same pyochelin molecule is produced by a wide variety of *Pseudomonas* species and in some *Burkholderia cenocepacia* strains (Poole and McKay, 2003). It has been seen that the production of pyochelin by *P. aeruginosa* leads to an increase in the lethality of virulent strains but not in nonvirulent strains. This indicates that pyochelin is not a crucial virulence factor (Cox, 1982).

1.6.3 Carboxylate Siderophores

Carboxylate siderophores are produced by various organisms including *Rhizobium*, *Staphylococcus*, *Zygomycota*, and various marine bacteria species (Butler and Theisen, 2010). This type of siderophore use carboxyl and hydroxyl groups to chelate iron. These siderophores have a structure comparable to the siderophore mycobactin (produced by *Mycobacterium* species), wherein the case of carboxylates, the long alkyl chain of mycobactin is replaced by a short acyl chain that terminates in a carboxylic acid group (Lane et al., 1995; Crosa and Walsh, 2002). Carboxylates, mainly produced by marine bacteria, are bidentate ligands. The carboxylate siderophore achromobactin has two α-hydroxycarboxylate groups that are derived from α-ketoglutarate as well as a third α-hydroxycarboxylate that comes from citric acid (Schmelz et al., 2009). Bis α-hydroxycarboxylic acid siderophores, such as aerobactin, consist of one α-hydroxycarboxylate from citrate and one from α-

ketoglutarate, whereas the α-hydroxycarboxylates in staphyloferrin and rhizoferrin come from two citrate groups (Schmelz et al., 2009). Vibrioferrin is a carboxylate-type siderophore which was originally isolated from an enteropathogenic estuarine bacterium, *Vibrio parahaemolyticus* and which has since been seen to also be produced by *Marinobacter* species collected from Pacific and Atlantic Oceans (Soengas et al., 2006). Shown in Figure 4 is the carboxylate functional group as well as the chemical structures of a few carboxylate siderophores.

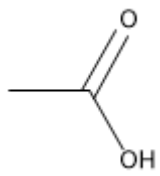

Carboxylate Functional Group

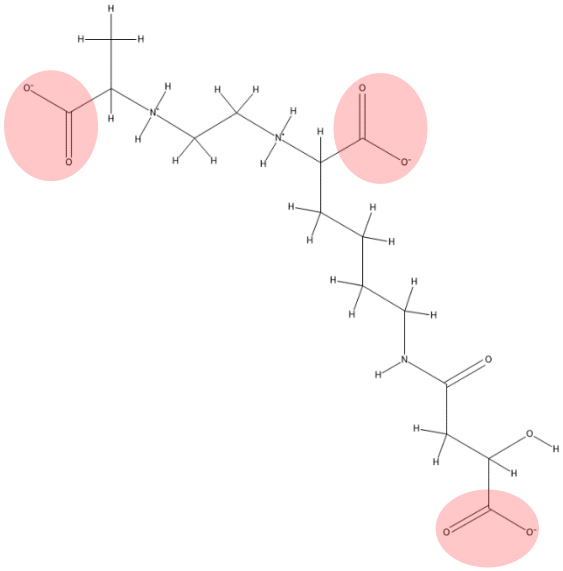

Rhizobactin

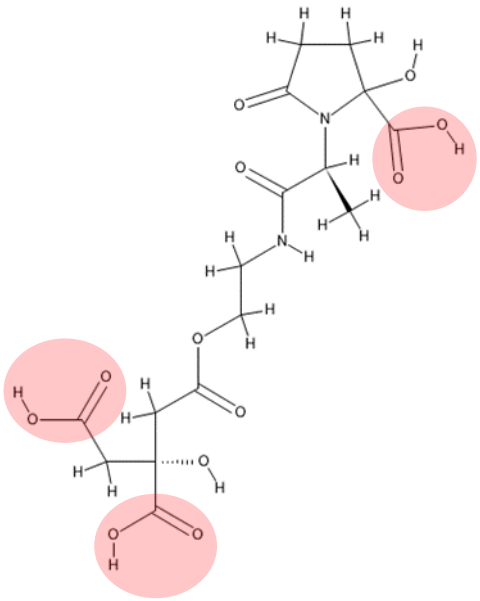

Vibrioferrin

Figure 4: Chemical structures of the carboxylate functional group and the carboxylate siderophores rhizobactin (Smith et al., 1985) produced by Ensifer meliloti and vibrioferrin produced by Vibrio parahaemolyticus. Carboxylate functional groups within these siderophores are highlighted in red.

1.6.4 Mixed Functional Group Siderophores

Mixed-type siderophores, which contain more than one category of functional group moiety, have been isolated from various species. These siderophores include several carboxylate-hydroxamate mixed siderophores, such as aerobactin, arthrobactin, shizokinen, acinetoferrin, and nannochelin (Fadeev et al., 2004; Kupper et al., 2006). *Mycobacterium* spp. produce unusual siderophores called mycobactins, which are a hybrid of hydroxamate and catecholate classes and are highly lipid-soluble. This class of siderophore is speculated to reside in the outer membrane of *Mycobacterium* spp. and work in conjunction with water-soluble chelating agents for iron acquisition (Meneely, 2007).

1.7 Siderophore Mediated Iron Uptake Mechanism

Siderophore-mediated iron acquisition by Gram-negative bacteria is a multicomponent and versatile strategy that allows the transport of iron into the cell under iron-deficient conditions from varied sources. Other components within the system include specific outer membrane protein receptors, protein complexes in the inner membrane, periplasmic binding proteins, and ABC transporters and Ton protein complex systems (Chakraborty et al., 2003). The process involves several distinct steps such as the secretion of the siderophore from the cell, the binding and solubilization of Fe(III) by the siderophore; the recognition of the Fe(III)-siderophore complex at the surface of the cell by the outer membrane receptors; the transport of the complex into the periplasmic space via TonB-dependent receptors; the iron-loaded siderophore is then transported through the cytoplasmic membrane into the cytoplasm by ABC transporters, or iron exchange with a membrane-bound carrier occurs; and finally the release and deposition of iron at an appropriate site within the cell, typically via reduction of Fe(III) to Fe(II) by microbe-mediated redox processes (Miethke and Marahiel, 2007; Wencewicz et al., 2013; Schalk, 2018). The basic mechanisms of enterobactin excretion and uptake by *E. coli* are shown in Figure 5.

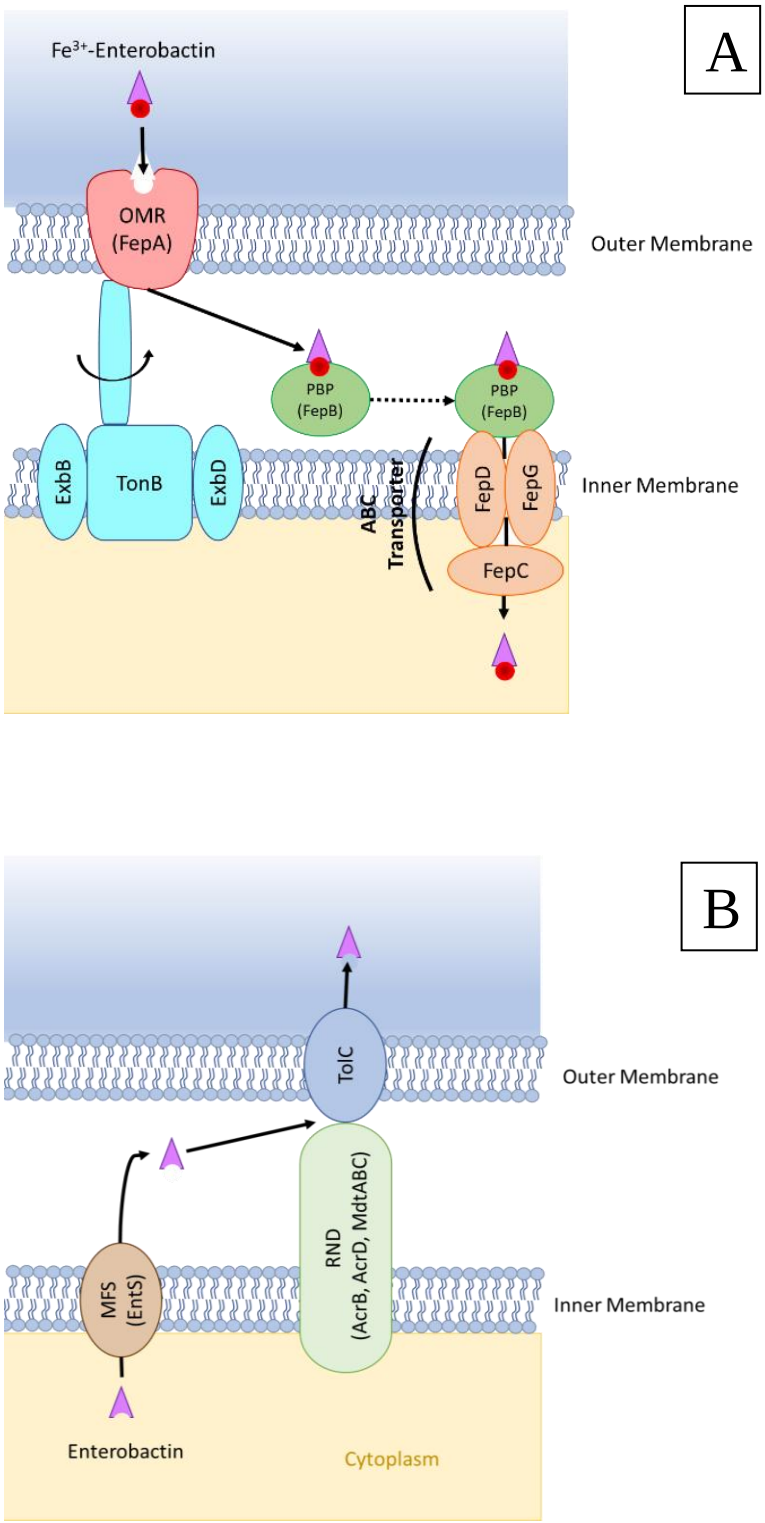

Figure 5: Enterobactin import (A) and export (B) mechanisms in E. coli. (A)- Enterobactin forms a complex with iron outside of the cell. The complex is recognised by FepA and actively imported across the outer cell membrane into the periplasmic space, with energy being provided by the TonB complex. FepB then shuttles the complex towards the cytoplasmic membrane, where it is actively transported through the cytoplasmic membrane by the ABC-type transporter composed of FepD, FepG, and FepC. (B)- the secretion of enterobactin involves the transport of this molecule through the EntS MFS protein from the cytoplasm into the periplasmic space. It is then transported across the outer membrane by a TolC complex and an associated Resistance-Nodulated-Cell Division (RND) efflux pump. (Adapted from Wilson et al., 2016)

The secretion of siderophores from cells is carried out by three major types of transport proteins or pumps. These are the major facilitator superfamily (MFS), the resistance, nodulation, and cell division (RND) superfamily, and the ABC superfamily. An MFS protein called EntS which is encoded by the gene *ybdA,* is responsible for enterobactin export in *E. coli* (Furrer et al., 2002; Bleuel et al., 2005). The secretion of bacillibactin by *B. subtilis* is carried out by a similar MFS-type transporter named YmfE (Miethke et al., 2008). The typical RND superfamily transport protein MexA-MexB-OprM is accountable for pyoverdine secretion in *P. aeruginosa* (Poole et al., 1993; Vettoretti et al., 2009). ABC-type transporters are responsible for siderophore secretion in several bacteria, such as; *S. aureus* (Grigg et al., 2010; Beasley et al., 2011), *Mycobacterium tuberculosis* (Rodriguez and Smith, 2006), and *M. smegmatis* (Farhana et al., 2008)

After forming a complex with the iron outside of the cell, the siderophore brings the iron into the cell in one of two ways. In filamentous algae and fungi, this is done by the iron being released from the complex and entering the cell as a single ion, whereas in most bacterial systems, the entire iron-siderophore complex enters the cell (Saha et al., 2012). An essential component of Gram-negative bacteria is the outer membrane, as it provides an increase in resistance to detergents, digestive enzymes, and antibiotics (Krewulak and Vogel, 2008). It also contains several receptor proteins that function in the recognition, binding, and transport of Fe(III)-siderophore complexes into the periplasm of the cell. These receptor proteins, termed high-affinity outer membrane receptor proteins (OMRPs), are necessary since Fe(III)-siderophore complexes are too large to enter the cell through porins as various other nutrients do (Aravinth, 2012). The production of these siderophore-specific OMRPs is induced under iron-starved conditions and thus is not usually present in iron-sufficient environments. Examples of these receptor proteins include FepA (for enterobactin), FhuA (for ferrichrome), and FecA (for ferric citrate) in *E. coli* (Braun and Braun, 2002) and FpvA and FptA in *P. aeruginosa* (Greenwald et al., 2008). OMPRs consist of two domains, a β-barrel region and a plug region. The β-barrel of each protein is composed of 22 antiparallel β-strands that are connected in the periplasm by short turns and external loops that extend above the cell surface. It inserts across the lipid bilayer of the outer membrane and is closed completely by the plug region (Braun and Braun, 2002). Conformational changes in the OMRP are induced by the binding of the Fe(III)-siderophore complex. This binding results in the α-helix at the N-terminal of the plug unwinding and extending. This facilitates the interaction between the

outer membrane receptor protein and the TonB complex, which provides the energy required for the active transport of the complex into the periplasm (Aravinth, 2012).

Once inside the periplasm, the Fe(III)-siderophore complex is recognised and bound by periplasmic binding proteins that are required to 'shuttle' the complex towards the cytoplasmic membrane. The complex is then actively transported through the cytoplasmic membrane either by ABC-type transporters (ferrichrome and ferrienterobactin in *E. coli*) or permeases (ferripyoverdine in *P. aeruginosa*) located in the cytoplasmic membrane (Hannauer et al., 2010; Aravinth, 2012). ABC-type transporters are considered ATP dependent and are members of the ABC superfamily, a highly conserved family of active transporters. They consist of an ATPase, one or two transmembrane permease proteins, and a lipoprotein substrate receptor found on the external surface of the membrane. They pump substrates into the cytoplasm against the concentration gradient by using the energy released by the hydrolysis of ATP (Aravinth, 2012).

The process of iron uptake is not just driven by ABC-type transporters but also by the TonB-ExbB-ExbD complex system (Larsen et al., 1994; Higgs et al., 1998). This complex consists of three cytoplasmic membrane proteins, TonB, ExbB, and ExbD, and functions to provide energy to the outer membrane receptor proteins by taking advantage of the proton motive force of the cytoplasmic membrane. This allows for the active transport of Fe(III)-siderophore complexes through the outer membrane. TonB and ExbB are anchored by their N-termini and located in the cytoplasmic membrane, whereas ExbB spans the cytoplasmic membrane three times; its N-terminus is in the periplasm, and most of the protein lies in the cytoplasm (Braun and Killmann, 1999). An allosteric signal that is generated by the binding of the Fe(III) siderophore complex to the outer membrane receptor is transmitted through the outer membrane by the plug region of the transporter (Aravinth, 2012). The transduction of energy is then permitted through conformational changes in the TonB box region of the transporter that is caused by the loading of the outer membrane receptor protein (Ferguson and Deisenhofer, 2004). Once energized, TonB stretches across the periplasm and binds to the TonB box region of the outer membrane receptor protein. It is then completely released from the cytoplasmic membrane and transduces stored potential energy to the outer membrane receptor protein, which allows for the active transport of the Fe(III) siderophore complex (Aravinth, 2012).

The final step of iron release or dechelation then occurs. This happens in different ways depending on the organism and siderophore. Methods include reduction via ferric reductases, protonation of iron siderophore complexes, or chemical modification or breakdown of ferric siderophore complexes by acetylation and esterases, respectively (Neilands et al., 1987; Boukhalfa and Crumbliss, 2002).

1.8 Siderophore Biosynthesis

Based on the enzymatic machinery involved, there are two routes of siderophore biosynthesis, with the method used determining the chemical nature of the resulting siderophores. These routes are either a Non-Ribosomal Peptide Synthetase (NRPS) dependent or NRPS independent route (Barry and Challis, 2009). Both routes make use of a wide range of enzymatic activities such as decarboxylases, monooxygenases, aminotransferases, amino acid ligases, acetyltransferases, and aldolases.

1.8.1 NRPS-Mediated Siderophore Biosynthesis

The NRPS-dependent pathway of siderophore synthesis is responsible for the synthesis of peptide siderophores. This approach makes use of NRPS, which are large multienzyme complexes that form an assembly line that builds and activates a broad array of structurally complex peptides from small building blocks such as amino or carboxyl acids without an RNA template (Mootz and Marahiel, 1997; Crosa and Walsh 2002; Strieker et al., 2010). The wide range of possible subunits and subunit combinations give rise to greatly diverse non-ribosomal peptides (NRPs) and thus chemical scaffolds (Challis, 2005). These mega-enzymes are made up of multifunctional modules, with each module being made up of several catalytic domains and responsible for a particular function (Challis et al., 2000).

For an NRPS enzyme to be able to synthesise a non-ribosomal peptide, it must contain at least three core domains, including a condensation domain (C), an adenylation domain (A), and either a thiolation (T) or a peptidyl carrier protein (PCP) domain (Martínez-Núñez and López López, 2016). The A domain recognizes and selects the amino acid substrate that makes up the final product and, through the catalysis of the hydrolysis of ATP, activates it as an aminoacyl-adenylate. The PCP domain, which through covalent bonds is linked to its 4-phosphopantetheine cofactor as a thioester, then accepts the activated aminoacyl-adenylate (Nikolouli and Mossialos, 2012). The substrate can then undergo modifications such as N-

methylation and epimerization (Martínez-Núñez and López López, 2016). The condensation domain is then in charge of the formation of the peptide bond. It does this through the catalysis of the transesterification of the chosen amino acid onto the amino end of the growing peptide chain (Kohli et al., 2001).

A module may also, in addition to these three domains, contain a methylation domain. Methylation domains add a methyl group to either the epimerisation, oxidation, and reduction domains or the amine backbone (Mootz and Marahiel, 1997; Kyung Kim and Fuerst, 2006; Wang et al., 2014). This results in further diversity through the modification of the peptide backbone.

Usually, the number and order of molecules in NRPS systems determine the number and order of amino acids in the peptide product. Exceptions to this have, however, been seen in the synthesis of some molecules such as coelichelin and fusachelin A. In coelichelin biosynthesis, a tetrapeptide structure is assembled from a single trimodular NRPS (Lautru et al., 2005). This appears to be possible through the iterative use of the A and T domains of module 1 and the C domain of either module 2 or module 3 (Lautru et al., 2005; Haynes and Challis, 2007), with the skipping of module 2's A and T domains and either module 2 or 3's C domain in the second iteration. Fusachelin A synthesis follows a similar unusual enzymatic logic. These examples indicate that this non-linear enzymatic logic (Haynes and Challis, 2007) may be fairly common in NRPS-mediated siderophore synthesis and that, in some cases, products are formed that cannot be predicted from the sequences of the enzymes that are responsible for their assembly.

1.8.2 NRPS-Independent Siderophore Biosynthetic Pathway

Certain hydroxamate and carboxylate siderophores are assembled by the NRPS independent mechanism (Saha et al., 2012). NRPS-independent siderophore (NIS) synthetases are dissimilar to NRPS in both structure and sequence yet are also responsible for the synthesis of siderophores. NRPS-independent siderophore synthesis occurs through condensation of alternating amino alcohols, alcohols, dicarboxylic acids, and diamines through synthetase enzymes that catalyze amide and ester bond formation between these siderophore subunits (Challis, 2005). NIS synthetases can be classified into types A, B, or C based on sequence similarity (Aravinth, 2012). The catalysis of the condensation of amines or alcohols with a prochiral carboxyl group of citric acid is performed by type A NIS synthetases, Type B NIS

synthetases catalyze the condensation of amines with a γ-carboxyl group of α-ketoglutarate, and the catalysis of either the oligomerization and macrocyclisation of ω-amino-carboxylic acids or an amine or alcohol with a monoamide derivative of citric acid is performed by Type C NIS synthetases (Aravinth, 2012). Generally, hydroxamates are generated through two reactions. The first reaction is the N-hydroxylation which is catalyzed by reduced flavin adenine dinucleotide (FAD)-dependent monooxygenases that use oxygen, a set of amino acids, and polyamines as substrates. The second step is catalyzed by acyl-coenzyme A transferases and involves the acylation of the hydroxylated amine, yielding the functional hydroxamate (Grunewald and Marahiel, 2006).

1.9 Iron Regulation in Bacteria

In Gram-negative bacteria, the ferric iron uptake regulator (Fur) protein is responsible for iron regulation (Mchugh et al., 2003; Ollinger et al., 2006). In many low G-C content, Gram-positive bacteria such as *B. subtilis* Fur-like proteins are also found (Bsat et al., 1998). In *E. coli* the Fur protein acts as an iron-dependent transcriptional repressor and has a molecular weight of 17 kDa (Figure 6). It negatively regulates the transcription of iron transport through its binding to the Fur box, which is a 19 bp inverted repeat sequence found upstream of the iron transport gene (Saha et al., 2012). Divalent iron acts as a co-repressor that activates the Fur protein, which then goes on to repress the downstream iron transport genes. Only under conditions of excess iron does Fur bind to DNA. Under iron-deficient conditions, the metal dissociates from the protein, RNA polymerase is no longer blocked, and the genes are expressed (Mchugh et al., 2003). In *E. coli*, around 90 genes are controlled by the Fur protein at the transcriptional level (Escolar et al., 1999). In pathogens, Fur proteins have also been seen to assist in the regulation of several virulence determining factors involved in attachment to host cells, biofilm formation, and manipulation of host wound healing (Hantke, 1981).

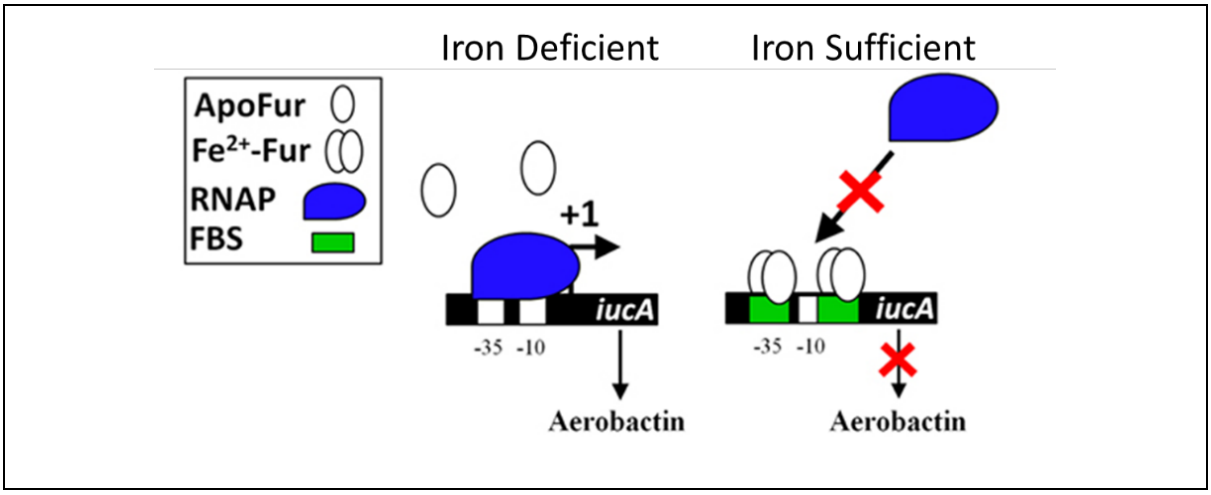

Figure 6: Aerobactin synthesis by E. coli. In this example, there are two Fur-binding sites (FBS) for the Fe-dependent regulation of iucA. iucA is the first of several genes involved in aerobactin synthesis that are found in the iucABCD, iutA operon. Both FBS are located within the P1 promoter, which overlaps the −35 and −10 sites. Under iron-deficient conditions (left), the transcription of the iucABCD genes is increased. Under sufficient conditions (right), Fur binds to DNA at the FBS (green box) and blocks access to the −35 and −10 sites by RNA polymerase (RNAP, blue shape). (Adapted from Troxell and Hassan, 2013)

In the case of high GC-content Gram-positive bacteria such as *Mycobacteria* and *Streptomyces*, the function of iron regulation is performed by the diphtheria toxin regulator (DtxR) (Hantke, 2001). In addition, there are several transcriptional regulators that control the synthesis and utilisation of siderophores. These mostly act as activators by sensing the iron-siderophore complex, either extracellularly or intracellularly (Saha et al., 2012).

1.10 Application of Siderophores

Siderophores have been seen to be involved in various processes besides iron acquisition. These processes include heavy metal biosorption, iron overload disease treatment, antibiosis, quorum sensing, and plant growth promotion (Aravinth, 2012).

Recently, the negative effects of traditional strategies of disease control through the use of artificial chemical agents have been highlighted. These drawbacks include resistance development, epidemiological consequences, and altering the nature of the ex-situ environment (Aravinth, 2012). This has resulted in the exploration of several alternate approaches, such as the use of siderophores as prophylactics or disease treatments. Examples of the use of siderophores in disease treatment include; the siderophore produced by *Pseudomonas aeruginosa* PAO1 being labelled with Gallium-68 for specific imaging of *Pseudomonas* infections through positron emission tomography (PET) (Dell' Anno et al.,

2022), desferrioxamine (a structural mimic of hydroxamate siderophores) that is used in the treatment of iron overload/haemochromatosis (Richardson et al., 2009), sideromycins produced by *Streptomyces pilosus* that are used in the treatment of iron overload (thalassemia) disease (Braun et al., 2009) as well as having been seen to have antimicrobial activity, and the use of hydroxamic siderophores in the treatment of infections such as malaria, tuberculosis, leprosy, and cholera due to their ability to access infected cells and remove iron from intracellular parasites (Mabeza et al., 1999; Stirrett et al., 2008). It is also thought that siderophores can be developed as novel antimicrobial compounds through the covalent attachment of clinical antibiotics to siderophores which would then be taken up by the target cells via their iron-uptake machinery. (Page 2013; Souto et al., 2013; Wencewicz and Miller, 2013; Dell' Anno et al., 2022). This concept has been adopted from naturally occurring siderophore-antibiotic conjugate molecules called sideromycins (Ratledge and Dover, 2000). Studies have shown that the penetration of antibiotics such as β-lactam and sulfonamides through bacterial outer membranes was increased when these antibiotics were conjugated to synthetic analogues of siderophores (Heinisch et al., 2003; Mollmann et al., 2009).

The application of siderophores as commercial biocontrol agents has also grown in significance. Siderophores are safe, do not result in biomagnification, and the fact that they are produced by self-replicating microbes means that there is no need for repeated applications and thus prevents the target organisms from building up resistance (Aravinth, 2012). When looking at plant growth development, the prevention of disease and promotion of growth by siderophore-producing soil bacteria is a promising technology. The enzymes involved in nitrogen-fixation require large amounts of iron, and so it is likely that the efficient acquisition of iron is crucial to nitrogen-fixing organisms (Geider, 1999). It has been reported by Sayyed et al. (2005) that the growth and yield of various plants are increased by pseudobactin that is produced by *Pseudomonas putida*. Pyoverdins produced by *P. aeruginosa* have been seen to increase the phytoavailability of nickel instead of cadmium in hydroponics and can enhance plant growth and induce plant pathogen suppression (Dell' Anno et al., 2022)

It has been seen that bacterial strains that produce siderophores have a higher tolerance to high metal concentrations than those that cannot. Several mechanisms for survival under metal stress have been evolved by these metal-tolerant bacteria (Aravinth, 2012). As

described in Section 1.5.2, studies have shown that although specific to iron, some siderophores bind to other metals including aluminium, cadmium, copper, gallium, manganese, lead, and zinc amongst others, which are of environmental concern. Siderophores have also been seen to bind to radionuclides, including uranium and neptunium (Kiss and Farkas, 1998; Neubauer et al., 2000). Due to the ability of siderophores to chelate metals other than iron, they have the potential to be used in metal recovery and remediation strategies. Several studies have looked into the possibility of using siderophore-producing bacteria to enhance the phytoextraction capacity of plants in contaminated soils (Glick et al., 2003; Crowley and Kraemer, 2007; Dimkpa et al., 2008a; Dimkpa et al., 2008b: Dimkpa et al., 2009a: Dimkpa et al., 2009b; Braud et al., 2009; Rajkumar et al., 2010). Pyoverdins have been used to remove iron from asbestos waste, altering the structure of the asbestos fibres (Anno et al., 2022).

Siderophores have possible applications in bacterial typing. An example of this application is the siderophore pyoverdine could potentially be used as a taxonomic marker to differentiate between closely related strains of fluorescent pseudomonads (Fuchs et al., 2001; Meyer et al., 2007; Mulet et al., 2007). When typing siderophores, techniques such as mass spectrometry and isoelectrophoresis can be used as effective methods (Meyer et al., 2008, Meyer et al., 2010). In order for this technique to be efficiently used, however, further research and development are needed to develop a dedicated database and platform.

D'Onofrio et al. (2010) reported in an interesting study that a significant role in the growth of uncultured bacteria on synthetic media is played by the siderophores produced by cultured bacteria. This means that the large number of bacteria that are unculturable on traditional media may be cultured on modified synthetic media containing helper siderophores, which could lead to the discovery of novel microorganisms.

1.11 Marine Siderophores

Several structurally diverse siderophores produced by marine bacteria have been identified in culture (Chen et al., 2019). They are often amphiphilic compounds containing a peptidic head group from which a fatty acid tail is linked, such as the amphibactins, aquachelins, loihichelins, marinobactins, and moanachelins, all of which use three hydroxamate groups to bind iron (Kanoh et al., 2003; Holt et al., 2005; Martinez and Butler, 2007; Homann et al., 2009a; Zhang et al., 2009; Vraspir et al., 2011; Gauglitz and Butler, 2013). Another type of

marine amphiphilic siderophore includes mixed mode compounds such as the synechobactins and ochrobactins, which contain both citrate and two hydroxamate groups (Ito and Butler, 2005; Martin et al., 2006; Chen et al., 2019). Many catechol-based siderophores, such as alterobactins, amonabactin, anguibactin, petrobactin (which also contains citrate), pseudoalterobactins, and vancrobactin have also been seen to be produced by marine bacteria (Telford and Raymond, 1997; Homann et al., 2009b; Sandy et al., 2010; Chen et al., 2019). Also seen in marine bacteria is the well-known group of tris-hydroxamate siderophores ferrioxamines B and E and the citrate-based siderophores aerobactin (a di-hydroxamate siderophore) and vibrioferrin (Martinez et al., 2001; Mawji et al., 2011; Cordero et al., 2012; Chen et al., 2019).

Through the use of metagenomic surveys in low iron regions of the ocean, it has been seen that genes involved in siderophore uptake are common in these environments. In many cases, however, the corresponding siderophore synthesis genes, as well as the siderophores themselves, are yet to be identified (Hopkinson and Barbeau, 2012; Toulza et al., 2012). This indicates that our oceans are home to many undiscovered siderophores.

1.11.1 Identifying Marine Siderophores

When structurally characterising ligands in a bacterial culture, a preconcentration step is usually required to remove salts and media components as well as to concentrate the biomolecules. This preconcentration step usually includes the extraction of the molecules onto a solid phase resin. The highest dissolved organic matter extraction efficiencies are often seen following the acidification of culture supernatants to a pH of 2, which protonates low pKa functional groups (such as carboxylates) to form natural species, which will bind to hydrophobic resins with a higher affinity (Dittmar et al., 2008). Doing this, however, can result in the hydrolysis of labile bonds that are found in many siderophores, and so many studies have instead focused on the portion of organic compounds that can be isolated through extraction at a pH equal to that of ocean waters. This method has been seen to be effective when isolating numerous marine bacterial siderophores, such as amphiphilic compounds and ferrioxamines. When attempting to isolate highly polar or deprotonated negatively charged siderophores, including vibrioferrin and citrate, this method has been seen to fail to capture some of these siderophores (Loomis and Raymond, 1991; Gledhill and Buck, 2012).

The chemical composition of iron-binding compounds can be investigated following their extraction. This can be done through a combination of the chromatographic separation of organic compounds and mass spectrometry. In previous studies, there has been the use of two complementary mass spectrometry methods; inductively coupled plasma mass spectrometry (ICPMS) and electrospray ionization mass spectrometry (ESIMS). ICPMS can be used to screen for organic-metal complexes within samples and has major advantages in that the chemical species of the organic ligand does not affect the sensitivity and that a quantitative measurement is provided for each analyte (Lobiński et al., 2006). This method is not, however, without drawbacks since it is unable to provide information on the identity of the species. ESIMS is thus a useful technique to use alongside ICPMS. This technique can be used to determine the mass and fragmentation pattern of metal-containing compounds and to determine their chemical structure (Szpunar, 2005; Mounicou et al., 2009).

When looking at mass spectrometry-based methods, studies were done by Gledhill et al. (1994) that take advantage of the similar binding affinities of gallium and iron, which have laid down the foundation (McCormack et al., 2003; Gledhill et al., 2004; Mawji et al., 2008, 2011). In these studies, organic extracts were spiked with excess gallium and then acidified to a pH of less than three, which allowed the gallium to swap into the siderophores. Samples were then analyzed via liquid chromatography-mass spectrometry, with LC-ICPMS being used first to detect gallium-associated compounds. After they had been calibrated using a standard curve, the resulting chromatograms provided information on the number of organic metal ligands in a sample as well as their retention times and abundances. Masses exhibiting distinctive gallium isotope patterns (69Ga:71Ga of 3:2) were then identified through the coupling of this chromatography with LC-ESIMS. In order to further validate these masses, they then searched for the apo or iron forms of the compounds in samples that had not been spiked with gallium. This method has been used to identify several ligands, such as the trishydroxamates ferrioxamine E and G (Mawji et al., 2008) and amphibactins.

High-resolution mass spectrometry presents another auspicious method for identifying microbial marine siderophores through the detection of the distinct isotopic ratio of 54Fe:56Fe (0.056). Following the incorporation of iron into an organic compound, the relative intensity and mass difference of the major iron isotopes are reflected by the detection of two isotopologues. This has previously been successfully used to identify novel

siderophores from cultures of the nitrogen-fixing bacteria *Azotobacter vinelandii* and the filamentous fungus *Trichoderma* (Lehner et al., 2013; Baars et al., 2014, 2015).

1.12 Functional Genomics

Since the advent of high throughput DNA sequencing, the ability to identify genes has extensively surpassed the ability to determine the functions of these genes. Numerous complete genome sequences are now available, and so the focus of many researchers across the world has been directed towards functional genomics and assigning functions to newly identified DNA sequences (Srinivasan et al., 2005).

Once a new sequence has been identified, the easiest way to obtain functional information is the comparison of the sequence with those in databases. Nowadays, there are several efficient bioinformatics tools for the annotation of available genome sequences. Unfortunately, this method of *in silico* analysis is only indicative on its own and is usually not enough to definitively determine the function of a gene (Srinivasan et al., 2005). An additional limitation of this method is that many newly sequenced genomes contain novel regions of sequence (Bennett, 1997), which cannot be functionally classified through comparative genomics (Scheidegger and Payne, 2003).

In addition to comparative genomics, various additional approaches can be used to gather information about the function of genes. Genomic strategies such as microarray analysis, Serial Analysis of Gene Expression (SAGE), differential display, and Expressed Sequence Tags (EST's) can be used in large-scale gene expression analysis studies as these methods are multiplex and look at multiple genes simultaneously (Cooke et al., 1996; Singh-Gasson et al., 1999). Other methods of functional genomics include proteomic-based methods such as SDS-PAGE, MS, MALDI-TOF, and Yeast two-hybrid systems (Bouchez and Hofte, 1998), as well as methods such as Targeting Induced Local Lesions In Genomes (TILLING) (Henikoff et al., 2004) and map-based cloning (Sun et al., 2004).

Methods involving the suppression or over-expression of genes allow for a gene sequence to be linked to a particular phenotype and thus allow for the function of the gene to be deduced (Matzke and Matzke, 1995). The disruption of genes is a powerful tool for the acquisition of knock-out mutants which assist in determining the biological function of uncharacterized genes that have been revealed by sequencing (Srinivasan et al., 2005). Gene knock-out

systems provide a direct route to determining function as opposed to most other approaches of determining gene function that are correlative (Srinivasan et al., 2005). Another strategy for identifying gene function is through antisense or overexpression mutations. These, however, are laborious approaches that often result in inconclusive or impossible to interpret data (Azpiroz-Leehan and Feldmann, 1997).

An example of functional genomic techniques being used in the field of siderophore studies is seen in a study by Louvel et al. (2006). This study, with a focus on iron-related genes found in *Leptospira biflexa*, made use of quantitative reverse transcription-PCR (qRT-PCR) to analyse the expression of seven genes of interest, including four *fur*-related genes, the ferrous iron transporter gene (*feoB*), and two TonB-dependent receptors involved in iron transport (*fecA* and *tbr3*). Results showed that the relative expression of *fur1* was unchanged in response to iron availability, levels of *tbr3* (encoding the receptor for desferrioxamine) increased threefold in response to iron depletion, and that other genes (*fecA*, *feoB*, *fur2*, *fur3*, and *fur4*) showed more than a 10-fold decrease in expression in response to iron depletion. From their results, they were able to determine that under iron limitation, the expression of *tbr3* is induced to utilize siderophores, whereas the expression of *fecA*, which encodes a receptor for a relatively large number of iron sources (i.e., iron citrate, iron sulfate, iron chloride, and aerobactin), is more important in the presence of higher iron concentrations.

1.12.1 Genome Mining Tools

Since the start of the genome sequencing of microorganisms, treasures of previously unseen natural product biosynthetic genes have been revealed (Leal et al., 2012; Chaudhary et al., 2013). Genome sequencing gives clues to understanding the biosynthesis of novel drug molecules and unlocking novel chemistry (Rutledge and Challis, 2015). It also provides direct access to the genome, allowing researchers to “mine” for a wide range of novel compounds at a nucleotide level. This allows for compound discovery to be directed away from previously described or known compounds (Pickens et al., 2011; Lane and Moore, 2012; Yamanaka et al., 2014).

Several computational tools, such as antibiotics and Secondary Metabolite Analysis Shell (antiSMASH), NRPS predictor 2, Natural Product Domain Seeker (NaPDoS), the PRediction Informatics for Secondary Metabolomes (PRISM), and CLUSEAN have been developed to assist researchers with ‘genome mining’ (Blin et al., 2019). Additionally, several independent

tools that interpret and provide additional information regarding the results generated by antiSMASH, such as a reverse-tailoring tool to match finished NRPS/PKS structures to antiSMASH-predicted core structures (Shirley et al., 2018), the sgRNA design tool CRISPy-web (Blin et al., 2016), the 'Antibiotic Resistance Target Seeker' ARTS (Alanjary et al., 2017), the mass-spectrometry guided peptide mining tool Pep2Path (Medema et al., 2014), and the BGC clustering and classification platform (Navarro-Muñoz et al., 2018) have been developed.

antiSMASH is a comprehensive and open-source pipeline that bioinformatically allows the rapid genome-wide identification, annotation, and analysis of loci within bacterial and fungal genomes that are responsible for the coding of enzymes that are involved in a wide range of specialized metabolite biosynthesis pathways. It includes specialised metabolite classes such as melanins, siderophores, butyrolactones, beta-lactams, nucleosides, bacteriocins, lantibiotics, indolocarbazoles, aminocoumarins, aminoglycosides, terpenes, polyketides, and non-ribosomal peptides (Weber et al., 2015). This pipeline has integrated several well-known bioinformatics tools such as CLUSEAN for gene cluster prediction (Weber et al., 2009), BLAST for gene annotation, HMMER and Pfam for protein domain identification (Finn et al., 2008), and NRPSpredictor (Röttig et al., 2011) for the assessment of conserved motifs in NRPS/PKS enzymes as well as substrate specificity prediction for NRPS 'A' domains.

PRISM is an open-source, user-friendly web application that can identify biosynthetic gene clusters, predict genetically encoded nonribosomal peptides and type I and II polyketides, and predict the bio- and cheminformatic dereplication of known natural products (Skinnider et al., 2015).

Genome mining techniques have aided in the discovery of the following siderophores: variochelin, a lipopeptide siderophore from the bacterium *Variovorax boronicumulans* (Kurt hey al., 2016); and, pseudonochelin from the marine-derived *Pseudonocardia* spp. (Zhang et al., 2022). Furthermore, a study in which 48 gapless genomes of *Burkholderia* species were genome-mined for significant secondary metabolites, led to the prediction of potentially new forms of known siderophores in strains not previously known to produce these compounds. For example, a new malleobactin-like siderophore was predicted to be produced by *B. phymatum* STM815 through the identification of a cluster with some characteristics for malleobactin synthesis but also predicted to have different specificities in the NRPS A domains (Esmaeel et al., 2016). Siderophore activity was confirmed for this strain and masses

corresponding to known siderophores belonging to the ornibactin or malleobactin families could not be identified. Although the structure was not fully characterised, the authors attribute the siderophore activity to a new malleobactin-like siderophore called phymabactin. Moreover, this comparative genomics approach facilitated the identification of the cluster responsible for biosynthesis of the siderophore cepaciachelin. Although the structure of cepaciachelin has been known for a long time (Barelmann et al., 1996), the mechanism of its synthesis was not known. Through analysis of the genome of *Burkholderia ambifaria* AMMD, the relationship between genes and the product could finally be established (Esmaeel et al., 2016). A study by Kreutzer and Nett (2012) demonstrated how genome mining techniques can be useful in the discovery of completely novel siderophores. This genome mining study led to the identification of a previously unrecognised siderophore biosynthesis gene cluster in the nitrogen-fixing bacterium *Cupriavidus taiwanensis* LMG19424. Based upon predicted structural residues, a convenient strategy for an NMR-assisted isolation of the associated metabolite was designed. The structure of the purified siderophore, taiwachelin, was fully characterized by spectroscopic methods and chemical derivatisation and was seen to be a novel lipopeptide siderophore. These examples serve to demonstrate the power of genome mining techniques in the discovery of novel secondary metabolites, and siderophores in particular

1.13 *Thalassomonas viridans*

Thalassomonas viridans is a strictly aerobic, halophilic, chemo-organotrophic marine bacterium that was first isolated from cultivated oysters off the Mediterranean coast of Spain near Valencia (Macián et al., 2001). *T. viridans* has not been identified as a pathogen of its host and is thought to possibly play a role in the host's health as part of their natural microflora. As reported by Macián et al. (2001), this bacterium takes the form of Gram-negative rods that are approximately 1.5-2 µm long and 0.8-1 µm wide, each cell with a single polar flagellum. It has been seen to produce a green/blue-green diffusible and unstable pigment and has a DNA GC content of 48.4 mol%. It is unable to ferment sugars under anaerobic conditions, is catalase and oxidase-positive, and is unable to reduce nitrate to nitrite. It is a mesophilic strain that grows within the temperature range of 13 °C to 37 °C. It is able to hydrolyse starch, lecithin, casein, and gelatin, but not alginate or agar. It does not oxidise sulphite. No indole production, arginine dihydrolase, ornithine decarboxylase, or lysine decarboxylase activities by the strain have been detected. The predominant cellular

fatty acids found within the strain are saturated and monounsaturated straight-chain fatty acids.

Analysis of the *T. viridans* 16S rRNA gene sequence has shown that this isolate represents a branch within the class γ-Proteobacteria, and is similar to the genus *Colwellia*. It has a 93.2–94.8% range in 16S rRNA gene sequence similarity values when compared to *Colwellia* species, with the highest similarity being shown by the *Colwellia demingiae* sequence (Macián et al., 2001).

The sequencing and analysis of the genome of *T. viridans* by Olonade et al. (2015) revealed that this organism has 6,667 (2,476 hypothetical) coding sequences and 76 tRNAs. Their analysis using the antiSMASH secondary metabolite prediction server uncovered that this strain contains several potentially novel, nonribosomal peptide and polyketide biosynthetic clusters (or hybrids thereof), as well as bacteriocins and lantipeptides. It was also thought that because its genome of approximately 7.4 Mb is roughly 2 Mb larger than its closest relative, it could be harbouring interesting metabolic pathways as well as information on the relationship of this bacterium with its host (Olonade et al., 2015).

1.14 Research Objectives

Preliminary studies have shown that *Thalassomonas viridans* is positive for siderophore production. Yet, genome mining tools such as antiSMASH and PRISM cannot detect gene clusters with significant similarity to known siderophore genes. This study aimed to isolate and characterise the siderophore produced by *T. viridans,* which is expected to be novel, at least in the sequence of the corresponding biosynthetic gene cluster and possibly in the actual siderophore structure. Additionally, the genes responsible for the synthesis of the siderophore were attempted to be identified. These aims dictated the following objectives:

1. To functionally screen *T. viridans* for siderophore activity

2. To isolate and purify the compound responsible for siderophore activity using liquid chromatography

3. To identify the compound using mass spectrometry

4. To identify the biosynthetic gene(s) within the *T. viridans* genome that are responsible for the observed siderophore activity.

Chapter 2: Methods and Materials

2.1 General Laboratory Chemicals and Reagents

All chemicals, reagents, and culture media used in this study were supplied by Merck Chemicals and Laboratory Supplies (Darmstadt, Germany), Sigma Aldrich Chemical Company (Deissenhofen, Germany), and Kimix Chemical Laboratory Supplies (South Africa).

2.2 Bacterial Strains and Growth Conditions

The bacterial strains used in this study can be seen in Table 2.

Table 2: Bacterial strains used in this study.

Bacterial strain	Description	Reference	Source
Thalassomonas viridans	Halophilic, strictly aerobic, chemo-organotrophic, marine bacterial strain	(Macián et al., 2001).	IMBM culture collection
Thalassomonas viridans* Δ*1	A strain of *T. viridans* containing a 1.1 Mb deletion mutation		IMBM culture collection
***Escherichia coli* ATCC 35218**	This strain is used in the assay of beta-lactam antibiotics, evaluation of Mueller-Hinton agar, and the quality control strain for susceptibility testing,	(Castellani and Chalmers, 1919)	Anatech Microbiologics
***Escherichia coli* ATCC 25922**	This strain does not produce verotoxin. This organism is a CLSI control strain for antimicrobial susceptibility testing.	(Castellani and Chalmers, 1919)	IMBM culture collection
***Staphylococcus aureus* ATCC 29213**	A Gram-positive bacterium that causes a wide variety of clinical diseases	(Ogston, 1984)	IMBM culture collection

***Pseudomonas aeruginosa* PAO1**	A common encapsulated, Gram-negative, strictly aerobic, rod-shaped bacterium that can cause disease in plants and animals, including humans	(Gessard, 1982)	IMBM culture collection
***Klebsiella pneumoniae* ATCC 700603**	Gram-negative bacterium within the family Enterobacteriaceae, found in the environment and the alimentary tract of animals. Cause of various diseases in animals.	(Friedlaender, 1882)	IMBM culture collection
***Enterobacter cloacae* ATCC BAA-1143**	Multiple antibiotic-resistant nosocomial pathogen	(Hormaeche and Edwards, 1960)	Anatech Microbiologics

The growth media used in this study are listed in Table 3. Following preparation, all media were autoclaved at 121 °C for 20 minutes unless otherwise specified. Any pH adjustments were made using either 6 M HCl or 3 M NaOH before autoclaving.

Table 3: Growth media used in this study.

	Constituent	**Grams per Litre**
Luria Broth (LB)	Tryptone	10
	Yeast Extract	5
	NaCl	10
Luria Agar (LA)	Tryptone	10
	Yeast Extract	5
	NaCl	10
	Bacteriological Agar	15
Iron Deficient Minimal Marine Media (MMM Fe-)	NaCl	20
	$MgSO_4 \cdot 7H_2O$	7
	$MgCl_2 \cdot 5H_2O$	5.3
	KCl	0.7
	$CaCl_2$	1.25
	$CuSO_4$	0.005
	K_2HPO_4	0.075
	Sodium glutamate	2
	Tris base	6.1
Iron sufficient Minimal Marine	MMM Fe- medium	

Media (MMM Fe+)	$FeSO_4 \cdot 7H_2O$	5.3
Marine Agar (MA)	Peptone	5
	Yeast extract	1
	$C_6H_5FeO_7$	0.1
	NaCl	19.45
	$MgCl_2$	5.9
	$MgSO_4$	3.24
	$CaCl_2$	1.8
	KCl	0.55
	$NaHCO_3$	0.16
	KBr	0.08
	$SrCl_2$	0.034
	H_3BO_3	0.022
	Na_2SiO_3	0.004
	NaF	0.0024
	NH_4NO_3	0.0016
	Na_2HPO_4	0.008
	Agar	15

2.3 Preparation of Glassware

To remove any contaminating iron from the glassware used in the preparation, growth, and processing of iron-deficient cultures, glassware was first soaked in 6 M HCl overnight before being thoroughly rinsed at least four times with MilliQ water.

2.4 Preparation of Inoculums

Seed cultures were prepared from fresh, isolated colonies grown on either MA plates (*T. viridans* strains) or LA plates (other strains). *T. viridans* was grown in 250 ml Erlenmeyer flasks containing 50 ml of MMM Fe- at room temperature on a rotary shaker until an optical density (OD) of between 0.18 and 0.2 was reached before being used as inoculum. All other strains were grown in LB under the same conditions until reaching an OD of 0.3-0.35 before being used as inoculum.

2.5 Detection of Siderophore Production

2.5.1 Cas Assay (Schwyn and Neilands, 1987)

One of the methods of determining siderophore production was via the Chromazurol Sulphonate (CAS) agar method. CAS agar plates were prepared as described by Schwyn and Neilands (1987). Wells were bored into the CAS plates using the back of a sterile pipette tip,

and 100 µl of either culture supernatant or purified sample was added to the wells. The formation of yellow/orange halos around wells containing the sample indicated the presence of a siderophore. This colour change could occur within 30 minutes or up to 8 hours depending on the concentration of siderophore and the temperature, and so plates were left at room temperature overnight before being analysed. Sterile media was used as a negative control.

2.5.2 $FeCl_3$ Test (Snow, 1954)

An equal volume of freshly prepared 2% $FeCl_3$ solution was added to 0.5 ml of culture supernatant, which was then immediately examined for the appearance of an orange/reddish-brown colour. If this colour change is seen, it indicates a positive result for siderophore production.

2.5.3 Hydroxyquinoline-mediated Siderophore Test (De Brito et al., 1995)

In this test, marine agar (MA) plates were supplemented with 50 mg/l of the strong iron chelator, 8-hydroxyquinoline. Plates were then streaked with *T. viridans* strains and incubated at room temperature for 48 hours before being checked for growth. Only organisms that produce iron chelators stronger than 8-hydroxyquinoline will be able to grow, and thus unhindered growth indicates siderophore production.

2.5.4 CAS-Shuttle Assay (Schwyn and Neilands, 1987)

Quantitative estimation of siderophore production was done using the CAS-Shuttle assay. Freshly prepared CAS-Shuttle solution (0.5 ml) (Schwyn and Neilands, 1987) was mixed with 0.5 ml of culture supernatant, allowing 30 minutes at room temperature for the reaction to occur, and then measuring the absorbance at 630 nm against a reference consisting of 0.5 ml of uninoculated broth and 0.5 ml of CAS-Shuttle solution. Absorbance measurements were taken using a BioMate3 spectrophotometer (Thermo Electron Corporation). The amount of siderophore, in percentage Siderophore Units (%SU), within the supernatant was then calculated using the formula below as described by Ghosh et al., 2015.

$$\%SU = \frac{Ar - As}{Ar}\ x\ 100$$

Ar = Absorbance of reference at 630 nm

As = Absorbance of the sample at 630 nm

2.6 Growth and Siderophore Production

Growth and siderophore production as a function of time was determined for both the original and deletion strains of *T. viridans.* Each strain was grown in MMM Fe- from a single colony isolated from MA plates until an OD of 0.18-0.2 was reached. From these starter cultures, 20 µl were then added to 10 ml of either MMM Fe- or MMM Fe+ within 30 ml McCartney bottles. This was done in such a way that there would be three available cultures of each strain, with each media each day (3 x *T. viridans* /Fe+, 3 x *T. viridans* /Fe-, 3 x *T. viridans* Δ*1*/Fe+, 3 x *T. viridans* Δ*1*/Fe-), over a period of 2 weeks. Cultures were grown at room temperature with shaking.

The growth of each strain under each condition was measured each day by first thoroughly vortexing the cultures until they appeared homogenous. This was necessary since *T. viridans* forms a biofilm and so cells are not evenly dispersed before vertexing. The cultures' optical density (OD) was then measured at 660 nm using a BioMate 3 spectrophotometer (Thermo Electron Corporation), with the appropriate uninoculated media being used as blanks.

The same cultures that were used to take OD readings were then centrifuged at 21000 x*g* for 10 minutes before the supernatants were used to determine the amount of siderophore production using the CAS Shuttle assay (Section 2.5.4). These results, in percentage siderophore units (%SU), were then converted to Deferoxamine B (DFOB) equivalent units. To calculate DFOB equivalent units, a standard curve was constructed by measuring the %SU units of a range of known DFOB concentrations (2 µM, 4 µM, 6 µM, 8 µM, 10 µM, 12 µM, 14 µM, 16 µM, 18 µM, 20 µM, 25 µM).

The average of three results was calculated for each culture type test (technical repeats). Additionally, the entire process was repeated a further three times (biological repeats).

2.7 Chemical Siderophore Characterisation

2.7.1 Arnow's Assay (Arnow, 1937)

This assay was used to test for the presence of catecholate functional groups that would be found in the case of a catechol siderophore. Although not specific to siderophores, this test gives an indication as to the presence or absence of catecholate containing molecules within a

sample. First, 1 ml of crude siderophore extract (obtained by extraction with SEPABEADS® SP207 resin, Section 2.10.1) was mixed with 1 ml 0.5 M HCl. Then, 1 ml of nitrite-molybdate reagent (10% M/V sodium nitrite, 10% M/V sodium molybdate in ddH_2O) was added, at this point a yellow colour should be observed in the case of catecholates. Finally, 1 ml of 1 M NaOH was added. The mixture was allowed to incubate for 5 minutes at room temperature before being observed for a colour change. The formation of a red colour indicates a positive result. Uninoculated media was used as a negative control, and 0.1 mM and 1 mM pyrocatechol were used as positive controls.

2.7.2 Tetrazolium Salt Test (Snow, 1954)

This test is used to detect hydroxamate siderophores and is based on the ability of hydroxamic acids to reduce tetrazolium salts in the presence of strong alkali. As in the case of Arnow's assay, this test is specific for a particular functional group and not for siderophores. First, 50 µl of 2 M NaOH was added to 8-10 mg of tetrazolium salt. Next, 1 ml of crude siderophore extract was added to the solution. An instant appearance of a deep red colour indicates a positive result for hydroxamate functional groups. Uninoculated media was used as a negative control, and 10 mM and 1 mM hydroxylamine hydrochloride were used as positive controls.

2.7.3 Vogel's Test (Vogel,1987)

This assay tests for the presence of carboxylate functional groups. In this test, 50 µl phenolphthalein was added to 150 µl of 2 N NaOH. Sterile deionized water was then added to the mixture until the appearance of a light pink colour. The disappearance of colour by the addition of culture supernatant indicates the presence of molecules with a carboxylate nature. Uninoculated media was used as a negative control.

2.7.4 Spectrophotometric Tests

In addition to the methods described above, spectrophotometric assays were performed to determine the nature of the siderophore produced. The $FeCl_3$ test (Neilands, 1981) was used to check for hydroxamate and catecholate types. Due to the fact that this assay is based on binding of iron by the test sample, it is more specific to siderophore molecules than previous tests. In this assay, 1 ml of crude extract was added to 1 ml of freshly prepared 2% $FeCl_3$ solution. The absorbance spectra of the sample were then measured using a Varian Cary 50

Bio UV-Visible Spectrophotometer. A peak between 420 and 450 nm indicates a hydroxamate siderophore, whereas a peak at 495 nm indicates a catecholate. The method of (Shenker et al., 1992) was used to investigate the possibility of a carboxylate siderophore. Briefly, 1 ml of 250 µM $CuSO_4$ and 2 ml of acetate buffer (pH 4) were added to 1 ml crude extract. An absorbance maximum between 190 and 280 nm indicates a carboxylate.

2.8 Antimicrobial Activity Assay

The agar well diffusion assay was utilized to determine whether or not the extract displays antimicrobial activity. Wells were bored in LA plates using the back of a sterile pipette tip. Next, 50 µl of the extract was added to each well, in addition to 50 µl of sterile media being added to a negative control well. The plates were left for 4-5 hours to allow the extracts to diffuse into the agar. Bacterial test strains were cultured by adding 100 µl of overnight culture to 10 ml of LB broth and growing at 37 °C with shaking until their ODs (600 nm) reached 0.30-0.35. Next, 100 µl of these cultures were spread plated onto the previously prepared plates. Plates were then incubated at 37 °C for 24 hours before being checked. Clear zones with no microbial growth around wells indicated the antimicrobial activity of the respective extracts.

2.9 Chelation of Other Metals

To investigate the extracted siderophores' ability to chelate metals other than iron, the method of (Mehnert et al., 2017) was used. In this method 1.5 ml each of 1 mM $FeCl_3 \cdot 6H_2O$, 1 mM $AlCl_3 \cdot 6H_2O$, 5 mM VCl_3, and 10 mM $NaAsO_2$ (dissolved in 10 mM HCl) was mixed with 7.5 ml of 2 mM CAS solution. The mixtures were then each slowly added to 6 ml of 10 mM cetyltrimethylammonium bromide (CTAB). Next, 9.76 g MES was dissolved in 80 ml water, and pH was adjusted using 50% KOH to 5.6 in the case of Fe-CAS and Al-CAS, pH 4 for V-CAS, and pH 12 for As-CAS. The volumes of the buffers were then brought up to 85 ml using dH2O before being added to the dye solutions.

Next, 250 µl of crude extract was mixed with 250 µl of each metal-CAS solution. Following incubation at room temperature, in the dark, for 4 hours (or 6 hours in the case of Al-CAS), the absorbance at 630 nm of each mixture was recorded. Zero absorbance (A0) was calibrated with a mixture of metal-CAS solution and 2 mM DFOB. Sterile culture medium was used as

a reference solution containing no siderophores. To calculate the %SU units for each metal, the same formula as described in Section 2.5.4 was used.

2.10 Compound Purification

2.10.1 Hydrophobic-Resin Chromatography

For purification of the siderophore, a large volume of culture was needed. Batch cultures of 3-4 litres of *T. viridans* Δ*1* were grown in MMM Fe- at room temperature with shaking until the culture reached a %SU of at least 70% (approx. 2 weeks). Each one litre of culture was grown within 3 L Erlenmeyer flasks. Cultures were centrifuged at 3100 x*g* for 45 minutes, and the supernatant was collected.

To activate SEPABEADS® SP207 resin, the amount of resin needed was weighed out before being shaken in dH_2O for 1 hour. The dH_2O was discarded, and the resin was shaken in 100% MeOH for another hour. The MeOH was discarded, and the resin was rinsed 3 times with dH_2O.

The cell-free supernatant was then added to activated SEPABEADS® SP207 with the ratio of 20 g of dry resin per 1 L of supernatant. An overnight incubation at room temperature with shaking was done to allow for compounds to bind to the resin. The resin/supernatant mixture was then transferred to a separation funnel, and the first flow-through fraction was collected. A 2x bed volume of 25% acetone was added to the funnel and left for 1 hour with occasional stirring before this fraction was collected. This process was repeated using 50% acetone, 75% acetone, 100% acetone, and finally dH_2O, with each fraction being collected. Each fraction was then tested for siderophore activity using the CAS-Shuttle assay (Section 2.5.4) to identify in which fraction(s) the siderophore had been eluted. Fractions showing high siderophore activity were then dried by evaporation and resuspended in 2 ml of dH_2O.

2.10.2 Size Exclusion Filtration

To further purify the siderophore extracts and prepare them for HPLC analysis, following hydrophobic-resin chromatography, extracts were centrifuged at 21000 x*g* for 20 minutes, and the resulting precipitate-free supernatants were then filtered using Amicon® Ultra Centrifugal Filters. This was done by first adding the supernatant to a 50 kDa filter tube and

centrifuging at 3100 x*g* for 30 minutes. The same was repeated using the filtrate from the 50 kDa filter in a 3 kDa filter tube. At each stage of the process, fractions were tested for siderophore activity using the CAS-Shuttle assay (Section 2.5.4) to monitor the location of the siderophore activity.

2.11 Mass Spectrometry of Siderophore Extract

In this study two forms of MS were conducted. The first, as described here, pertains to the MS of siderophore extracts with the aim of structural elucidation. The second, as described in Section 2.14.3 refers to the MS of protein extracts with the goal of identifying the biosynthetic gene cluster responsible for siderophore synthesis.

Two samples were subjected to mass spectrometry analysis. These were the purified siderophore sample (post size exclusion filtration) and a sample that had been prepared in the same way except for the original culture media containing sufficient iron to suppress siderophore synthesis. Samples were analysed at CCMAR (Centro de Ciências do Mar) at the University of the Algarve, Portugal, by liquid chromatography coupled with high-resolution mass spectrometry as described below.

Chromatographic separation was performed on a Thermo Scientific ultimate 3000 UHPLC. The column was a Thermo Scientific Accucore RP-18 (2.1 × 100 mm, 2.6 µm). The mobile phase composition was prepared with water (A) and acetonitrile (B), both containing 0.1 % of formic acid. The gradient (in v/v %) started with 100% of A for 2 minutes, followed by a linear increase in B to 30 % over 13 minutes, then to 100% over 16 minutes, and maintained at 100% for additional 4 minutes. The mobile phase then returned to 100% of A over 1 minute and then was maintained at 100% of A for 4 minutes. The flow rate was 0.3 ml/min. The injection volume was 5 ml.

Mass analysis was performed on an Orbitrap Elite (Thermo Scientific) mass spectrometer with a Heated EletroSpray Ionization source (HESI-II). HR-MSn data were acquired using the following ionization parameters: spray voltages, 3.7 kV (positive polarity) and 4.0 kV (negative polarity); sheath gas, 40 arbitrary units; auxiliary gas, 10 arbitrary units; heater temperature, 300 °C; capillary temperature, 350 °C; S-Lenses RF level, 64.9%. The scan range was 100-1500 m/z.

Samples were analyzed in data-dependent mode, which was achieved by selecting the three most intense ions under dynamic exclusion and collision-induced dissociation (CID) activation.

2.11.1 Mass Spectrometry Data Analysis

Raw data files were converted to SIRUS compatible mgf format using MZmine version 2.53 (Pluskal at al., 2010; Dührkop et al., 2019). Analysis was performed using SIRIUS version 5.5.1 (Böcker et al., 2008; Dührkop et al., 2015; Böcker and Dührkop, 2016; Djoumbou Feunang et al., 2016; Dührkop et al., 2019; Ludwig et al., 2019; Dührkop et al., 2020; Hoffmann et al., 2021; Kim et al., 2021).

2.12 Total Protein Extraction

Total protein extraction was performed on 100 ml *T. viridans* Δ*1* cultures grown both with and without iron for 5 days at room temperature with shaking. Cultures were centrifuged at 3100 x*g* for 30 minutes before the supernatants were discarded and pellets resuspended in 5 ml of 1xPBS (0.137 M NaCl, 2.7 mM KCl, 10 mM Na_2HPO_4, 1.8 mM KH_2PO_4). Samples were sonicated using a BANDELIN *SONOPLUS* ultrasonic Homogenizer (230 V) for 10 minutes with 15 seconds breaks every 30 seconds. Cellular debris was separated from the extracts via centrifugation at 21000 x*g* for 15 minutes. The supernatants were collected in clean tubes before being quantified using a Nanodrop® ND-1000 (Nanodrop Technologies, Inc., USA) as well as being analysed by SDS-PAGE to access the quality and quantity of the protein in the extracts before they were stored at -80 ^{o}C until further analysis.

2.13 Sodium Dodecyl Sulphate-Polyacrylamide Gel Electrophoresis (SDS-PAGE)

The integrity and purity of total protein extracts (Section 2.12) were assessed using SDS-PAGE. When performing SDS-PAGE, two gels are prepared. These are an upper stacking gel (Table 4) for protein loading and a lower resolving gel for protein separation (Table 5). A volume of 10 µl of 4× sample buffer (100 mM Tris-HCl, pH 8; 4% [w/v] SDS; 0.2% [w/v] bromophenol blue; 200 mM β-mercaptoethanol) was added to 30 µl of protein sample. The protein mixture was then heated at 95 ˚C in a heating block for 10 minutes before being subjected to pulse centrifugation. Both the total protein samples and 4 µl of protein molecular

weight marker were loaded into wells on the stacking gel wells. Electrophoresis was then performed on the gels using 1× running buffer (25 mM Tris-HCl, pH 8; 200 mM glycine; 0.1% [w/v] SDS) in a Mini-PROTEAN system (Bio-Rad Laboratories, Hercules, CA, USA) at 80 V for 20 minutes, followed by 120 V for 40 minutes. Following electrophoresis, the Polyacrylamide gels were stained with Coomassie Brilliant Blue G250 solution (40% [v/v] methanol; 10% [v/v] acetic acid; 0.05% [w/v] Coomassie Brilliant Blue G250) overnight before being destained by placing in a destaining solution (40% [v/v] methanol; 10% [v/v] acetic acid) overnight.

Table 4: Preparation of 4% stacking gel.

dH_20	3.075 ml
0.5 M Tris-HCl, pH 6.8	1.250 ml
20% (w/v) SDS	0.025 ml
Acrylamide/ Bisacrylamide (30%/ 0.8% w/v)	0.670 ml
10% Ammonium Persulfate (APS)	0.025 ml
Tetramethylethylenediamine TEMED	0.01 ml

Table 5: Preparation of 12% separating gel.

dH_20	3.4 ml
1.5 M Tris-HCl, pH 8.8	2.5 ml
20% (w/v) SDS	0.05 ml
Acrylamide/ Bisacrylamide (30%/ 0.8% w/v)	4.3 ml
10% Ammonium Persulfate (APS)	0.05 ml
Tetramethylethylenediamine TEMED	0.01 ml

2.14 Proteomics

Protein extracts were analysed at the Stellenbosch University's Central Analytical Facility for qualitative proteomic analysis, where the below methodology was performed.

2.14.1 On-bead Protein Digestion

All reagents were analytical grade or equivalent. Samples were diluted in 100 mM Tris-HCl containing 100 mM NaCl and 1% SDS before being reduced with 5 mM triscarboxyethylphosphine in 100 mM Tris buffer for 1 hour at 60 °C. Cysteine residues were thiomethylated for 30 minutes at room temperature with 20 mM S-Methyl methanethiosulfonate in 100 mM TEAB. Next, samples were diluted two-fold with binding buffer (100 mM ammonium acetate, 30% acetonitrile, pH 4.5). The protein solutions were then added to MagResyn (Resyn Biosciences) HILIC magnetic particles prepared according to the manufacturer's instructions and incubated overnight at 4 °C. After binding, the supernatant was removed, and the magnetic particles were washed twice with washing buffer (95% acetonitrile (ACN; Romil). The magnetic particles were then suspended in 25 mM ammonium bicarbonate containing trypsin to a final ratio of 1:50 and incubated for 18 hours at 37 °C. The peptides were then extracted once with 50 ml of 15 trifluoro acetic acid. The samples were then dried and re-suspended in 50 ml of 2% acetonitrile: water; 0.1% Formic acid for analysis.

2.14.2 Liquid Chromatography

Liquid chromatography was performed on a Thermo Scientific Ultimate 3000 RSLC equipped with a 5 mm x 300 µm C_{18} trap column and a CSH 25 cm x 75 µm 1.7 µm particle size C_{18} analytical column. The solvent system employed was loading: 2% acetonitrile: water; 0.1% formic acid; Solvent A: 2% acetonitrile: water; 0.1% formic acid and Solvent B: 100% acetonitrile: water. The samples were loaded onto the trap column using loading solvent at a flow rate of 2 µl per minute from a temperature-controlled autosampler set at 7 °C. Loading was performed for 5 minutes before the sample was eluted onto the analytical column. The flow rate was set to 300 nL/minute, and the gradient was generated as follows: 5.0% -30% B over 60 minutes and 30-50% B from 60-80 minutes. Chromatography was performed at 45 °C, and the outflow was delivered to the mass spectrometer.

2.14.3 Mass Spectrometry of Protein Extracts

Mass spectrometry was performed using a Thermo Scientific Fusion mass spectrometer equipped with a Nanospray Flex ionization source. The sample was introduced through a stainless-steel nano-bore emitter. Data were collected in positive mode with spray voltage set to 1.8 kV and ion transfer capillary set to 275 °C. Spectra were internally calibrated using polysiloxane ions at m/z = 445.12003.

MS1 scans were performed using the orbitrap detector set at 120 000 resolution over the scan range 375-1500 with AGC target at 4 E5 and a maximum injection time of 50 ms. Data were acquired in profile mode.

MS2 acquisitions were performed using monoisotopic precursor selection for ions with charges +2 - +7 with error tolerance set to +/- 10ppm. Precursor ions were excluded from fragmentation for 60 seconds. Precursor ions were selected for fragmentation in HCD mode using the quadrupole mass analyser with HCD energy set to 30%. Fragment ions were detected in the Orbitrap mass analyzer set to 30 000 resolution. The AGC target was set to 5E4, and the maximum injection time to 100 ms. The data were acquired in centroid mode.

2.14.4 Data Analysis

The raw files generated by the mass spectrometer were imported into Proteome Discoverer version 1.4 (Thermo Scientific) and processed using the Sequest algorithm. Database interrogation was performed against a user-supplied database. Semi-tryptic cleavage with two missed cleavages was allowed. Precursor mass tolerance was set to 10 ppm, and fragment mass tolerance was set to 0.02 Da. Deamidation (NQ) and oxidation (M) were allowed as dynamic modifications. Peptide validation was performed using the Target-Decoy PSM validator node. The search results were analysed using MaxQuant version 2.1.3.0 and Persius version 2.0.6.0 according to the developers' instructions (Tyanova et al., 2016).

2.15 Genome Mining for Secondary Metabolite Pathways

To identify siderophore-related secondary metabolite biosynthetic gene clusters within the genome sequence of *T. viridans Δ1* (genome sequenced using Oxford Nanopore's MinION Sequencing Device, unpublished), antiSMASH version 6.1.1 was used (https://antismash.secondarymetabolites.org/) in combination with PRISM version 4.4.5

(https://prism.adapsyn.com/). The analysis parameters were set as shown in Figure 7. Additionally, the NCBI BLAST web server (www.ncbi.nlm.nih/BLAST) was used to compare regions within the genome to similar regions found in other genomes.

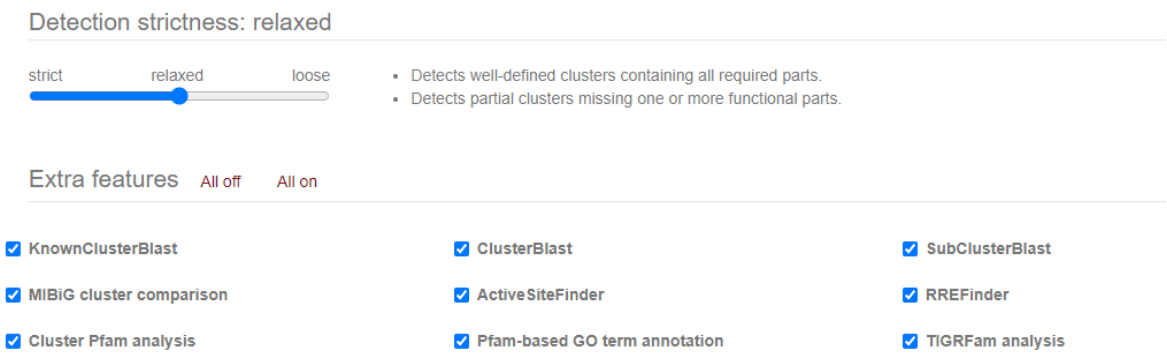

Figure 7: antiSMASH version 6.1.1 analysis parameters used in this study.

Chapter 3: Results and Discussion

3.1 Initial Detection of Siderophore Production

Three different assays were used for the initial determination of siderophore production in *Thalassomonas viridans*. The first assay, the CAS assay, is a sensitive and universal method for detecting and determining siderophores. It involves the use of agar containing CAS dye and Fe (III), which, when bound to each other, give the agar a rich blue colour. On the addition of a solution containing iron-chelating compounds, the Fe (III) is removed from the CAS dye complex, and a colour change to orange is seen (Schwyn and Neilands, 1987). It should be noted that the blue colour resulting from the CAS-Fe complex is highly sensitive to variations in pH. In order account for this, the CAS agar includes the buffering agent PIPES. Orange halos formed around wells that were loaded with iron-starved culture supernatants of *T. viridans* and not around those loaded with iron-sufficient culture supernatants (Figure 8). This indicates that when grown under low iron conditions, this bacterium does indeed produce siderophores.

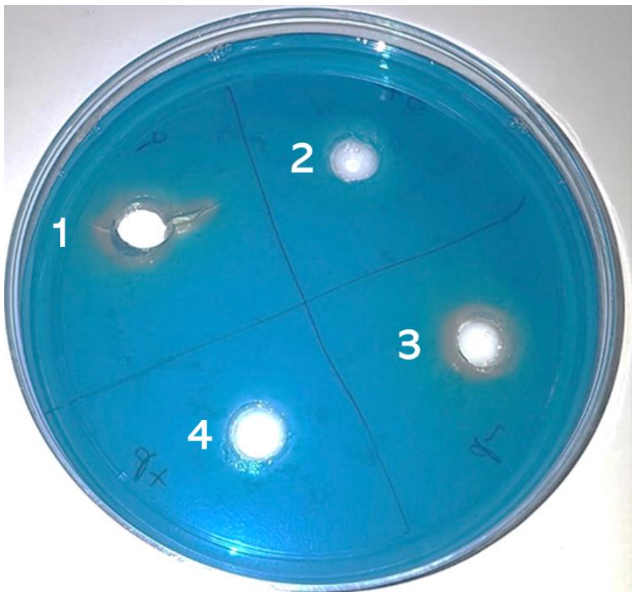

Figure 8: CAS assay results. Positive results for siderophore activity were seen in wells 1 (T. viridans grown without iron) and 3 (T. viridans Δ1 grown without iron) but not in wells 2 (T. viridans grown with iron) and 4 (T. viridans Δ1 grown with iron).

The second test performed was the $FeCl_3$ test (Neilands, 1981). In this test, culture supernatant is mixed with ferric chloride solution. The presence of siderophores is indicated by the formation of red or purple colour. As with the CAS test, this assay again gave positive results for both iron starved samples and not for the sufficient iron samples (Figure 9).

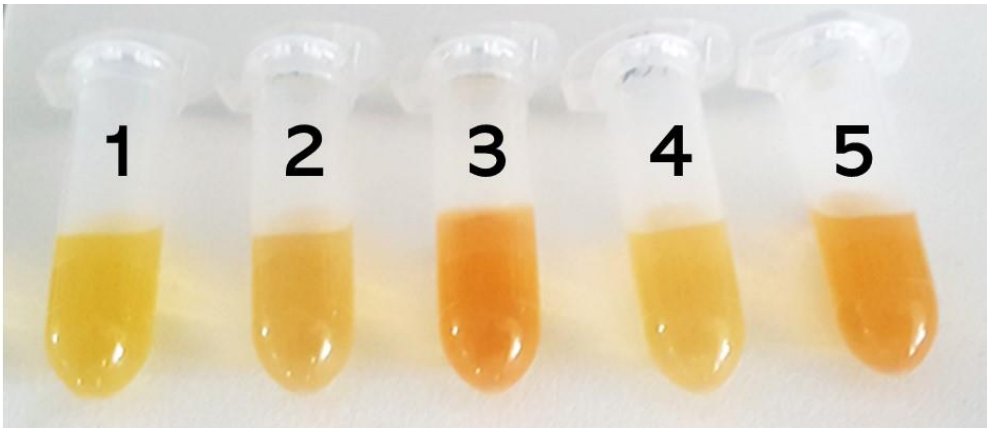

Figure 9: Results of $FeCl_3$ test. Tube 1 represents a negative control containing $FeCl_3$ and MMM Fe- and no colour change is seen. Tubes 2 (T. viridans) and 4 (T. viridans Δ1) contain $FeCl_3$ and cultures grown with iron. Again, no significant colour changes were seen. Tubes 3 (T. viridans) and 5 (T. viridans Δ1) contain $FeCl_3$ and cultures grown without iron. In these two tubes, a clear colour change is seen.

The final test for siderophore production by *T. viridans* involved inoculating *T. viridans* on marine agar supplemented with the strong iron chelator, 8-hydroxyquinoline (50 mg/l) (De Brito et al., 1995). In this assay, the added amount of 8-hydroxyquinoline is more than sufficient to bind all the available iron within the medium, making it unavailable to the inoculated bacteria. Only bacteria that produce a more powerful iron chelator, which can liberate the iron from the 8-hydroxyquinoline complex will be able to grow. The growth of *T. viridans* was unhindered by the addition of 8-hydroxyquinoline to the agar, and thus it can be said that it does indeed produce a potent siderophore.

All three of the above tests indicated that siderophore activity is produced by both *T. viridans* and *T. viridans Δ1* when these strains are grown under iron-limited conditions. When iron is added, however, no activity is seen. This lack of siderophore production seen in media containing iron is expected since, as explained by Johnson (2008) and Chi et al. (2012), although the majority of microbes require iron to grow, excess iron can have toxic cellular effects, and so the biosynthesis of siderophores must be strictly regulated according to the presence or absence of iron in the medium.

3.2 Growth and Siderophore Production

To assess the growth and siderophore production of the two strains as a function of time, growth and siderophore curves were constructed over 2 weeks.

The absence of iron hindered the biomass yield in both strains (Figure 10). This is expected since iron is essential for bacterial growth. Although no additional iron was added, and glassware was treated with 6 M HCl to remove absorbed iron, it can still be expected that trace amounts of iron can be found in other media components. This study showed that this trace amount of iron is sufficient to allow for the survival and limited growth of both *T. viridans* strains. This growth in the presence of very low iron levels further supports the theory that *T. viridans* does indeed have a highly effective method of iron acquisition.

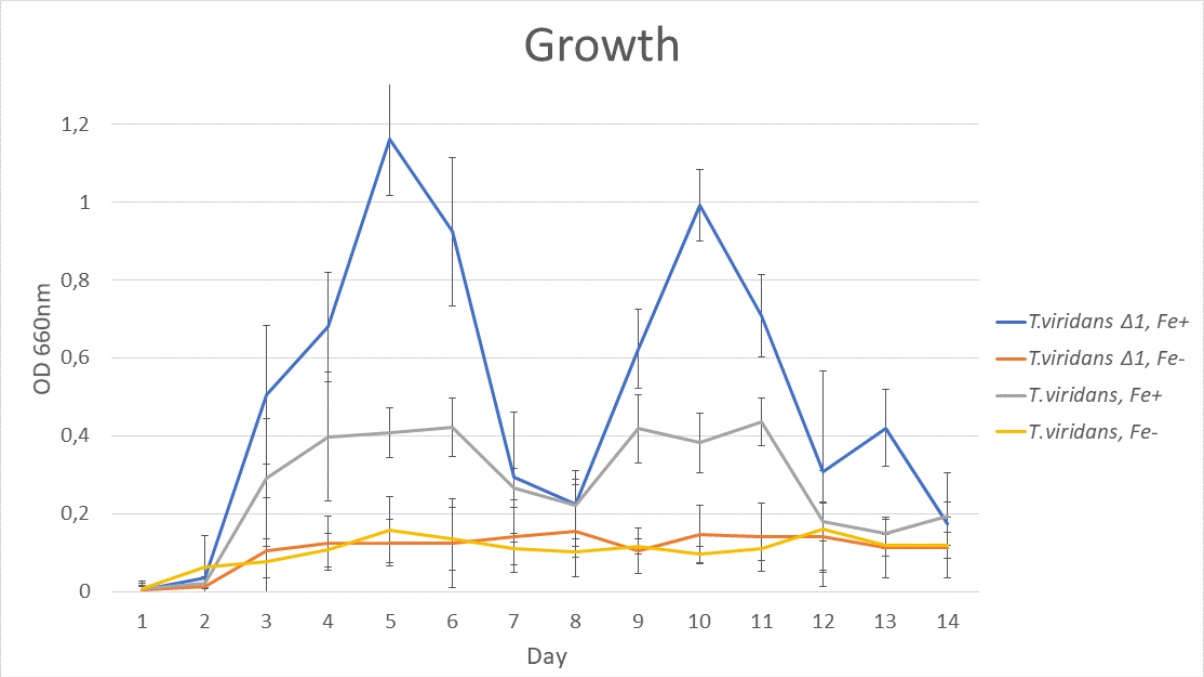

Figure 10: Growth curve of T. viridans and T. viridans Δ1, both grown with and without iron for a period of 14 days.

When comparing the growth of the two strains in the presence of iron, it can be seen that *T. viridans Δ1* has a faster growth rate. This is likely due to the 1 Mb of the genome that is deleted in the case of *T. viridans Δ1* placing a metabolic burden on the cell. In theory the loss of such a significant portion of the genomes is expected to result in cells with reduced complexity, enhanced genetic stability, and improved cellular economy, and has been the subject of many studies. However, most of these studies have ironically found the opposite to be true. Various studies aiming to develop deletion mutation strains with increased growth have found reduced growth rates in mutant strains (Hashimoto et al., 2004, Kurokawa et al., 2016, Nishimura et al., 2017, Yuan et al., 2017). A study by Vernyik et al. (2020) has, however, shown that a multiple-deletion strain of *E. coli* had outcompeted the wild-type and showed increased biomass yield. It is believed that this was obtained by Vernyik et al. (2020)

and not in other studies because, in contrast to targeted methods, Vernyik et al. (2020) made use of an iterative random deletion procedure that enabled the exploitation of multiple genome streamlining trajectories and involved the automatic selection of the fittest variants in the population. By doing this, they were able to show that the elimination of certain genomic segments could improve competitive fitness and biomass yield, but the choice of truly beneficial deletions is limited to a few genomic regions. The deleted region found in the case of *T. viridans* Δ*1* is from an extrachromosomal region that is currently suspected to be a chromid (Pheiffer et al., 2023).

This observed difference in optical density measurements across the wild-type and mutant strains could also be attributed to a variation in the ratio of planktonic to biofilm cells found between the two strains. Although not specifically measured, no significant differences in the appearance of the different cultures were observed and so this is not thought to be the case.

With regards to siderophore production, as determined by the CAS-Shuttle assay (Section 2.5.4) and then converted to DFOB µM equivalents (Section 6), no significant differences were seen between the two *T. viridans* strains in the corresponding iron conditions (Figure 11). However, clear and significant differences in siderophore production are seen when comparing the strains grown with iron to those grown without. One would expect high levels of siderophore production in iron-limited media but not in iron-containing media, as this can result in cellular iron overload (Section 3.1). This result clearly shows siderophore production by both strains when iron starved. This positive result for siderophore activity in both the *T. viridans* and *T. viridans* Δ*1* strains indicates that the genomic region deleted in *T. viridans* Δ*1* is not responsible for the activity seen. Because of this, the deletion strain (*T. viridans* Δ*1*) was selected to be used exclusively for the remainder of this study, which aided in simplifying genome mining studies as it allowed for 1.1 Mb of genetic material to immediately be excluded from being responsible for siderophore synthesis.

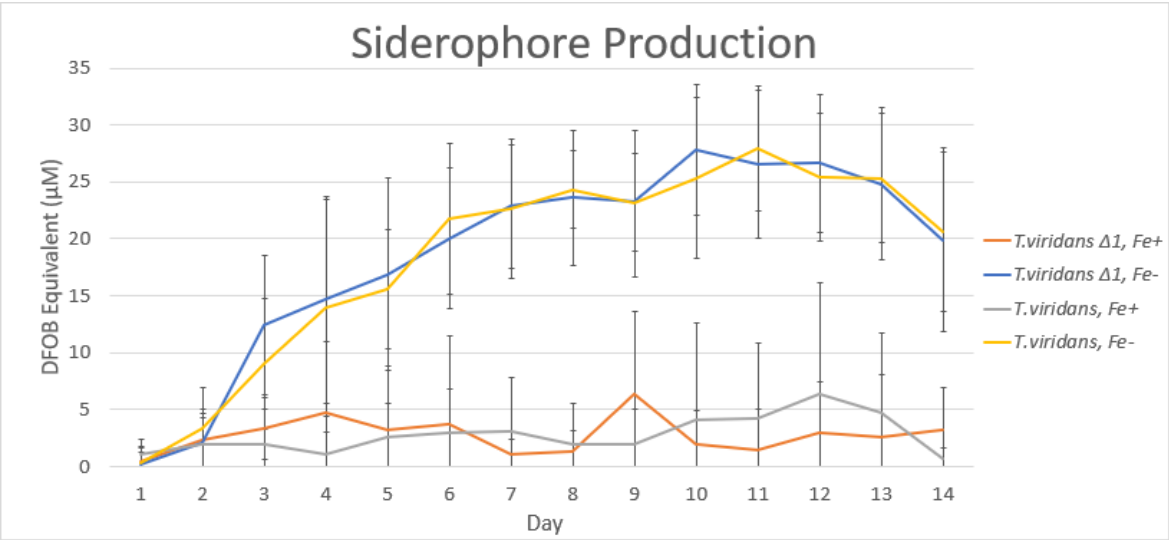

Figure 11: Siderophore production of T. viridans and T. viridans Δ1, both grown with (Fe+) and without (Fe-) iron for a period of 14 days.

3.3 Siderophore Purification

Cultures of *T. viridans Δ1* were grown in either MMM Fe- in the case of siderophore extraction until a %SU of at least 70% was reached, after approximately 8 days. In the case of a negative control for Mass Spectrometry (MS) data, extraction was performed in the same way, except those cultures were grown in MMM Fe+ for 8 days. After cultures were grown, like cultures were pooled together, centrifuged, and their supernatants filtered at 0.22 µm.

Filtered supernatants were then purified using SEPABEADS® SP207 resin as described in Section 2.10.1. Each of the flow-through fractions was collected, labelled, and tested for siderophore activity using the CAS-shuttle assay to determine in which fraction the siderophore activity was eluted from the beads.

Very little activity was seen in the first fraction (Figure 12), indicating that majority of the iron-binding molecules had bound to the resin. The highest activity was found in the 25% acetone fraction, with gradually less activity being seen in the 50%, 75%, and 100% acetone fractions. The final water wash fraction showed no activity.

SEPABEADS® SP207 is a styrene-based, highly porous adsorbent resin containing bromine groups chemically bonded to a cross-linked polystyrene matrix. This bromination makes it superior to styrene-divinylbenzene polymers. It is strongly hydrophobic, has a high density,

and has a large capacity. This type of adsorbent is suitable for adsorption of very low concentrations of organic substances or highly hydrophilic substances. (Yavuz et al., 2013)

As of date, most of the known marine siderophores have been seen to be produced as families of amphiphiles, consisting of an iron (III)-binding headgroup and a fatty acid tail (Chiu et al., 2020; Alok et al., 2020; Kramer et al., 2020; Malviya et al., 2020; Van Doan et al., 2020; Kour et al., 2020). These amphiphilic siderophores have been seen to range from being hydrophobic, such as the amphibactins and ochrobactins, to hydrophilic, such as the loihichelins (Kour et al., 2020). The observed binding of the siderophore produced by *T. viridans* Δ*1* to the SEPABEADS® SP207 resin indicates that this is a hydrophilic siderophore.

The variation in hydrophobicity seen in amphiphilic siderophores is due to differences in the headgroup composition relative to fatty acid chain length. Significant variations in hydrophobicity are also seen with single families of amphiphilic siderophores. This is caused by variations in the length of fatty acid chains on a constant headgroup. An example of this is seen by the marinobactins, that with six amino acids in the headgroup, are ligated predominantly with $C_{16:1}$ and $C_{16:0}$ fatty acids (marinobactin D and E, respectively). Marinobactin F with a $C_{18:1}$ fatty acid tail is noticeably more hydrophobic (Xue et al., 2019). Such a variation in fatty acid chain length could explain why, as shown in Figure 12, siderophore activity was detected in multiple acetone concentration elutions rather than just one.

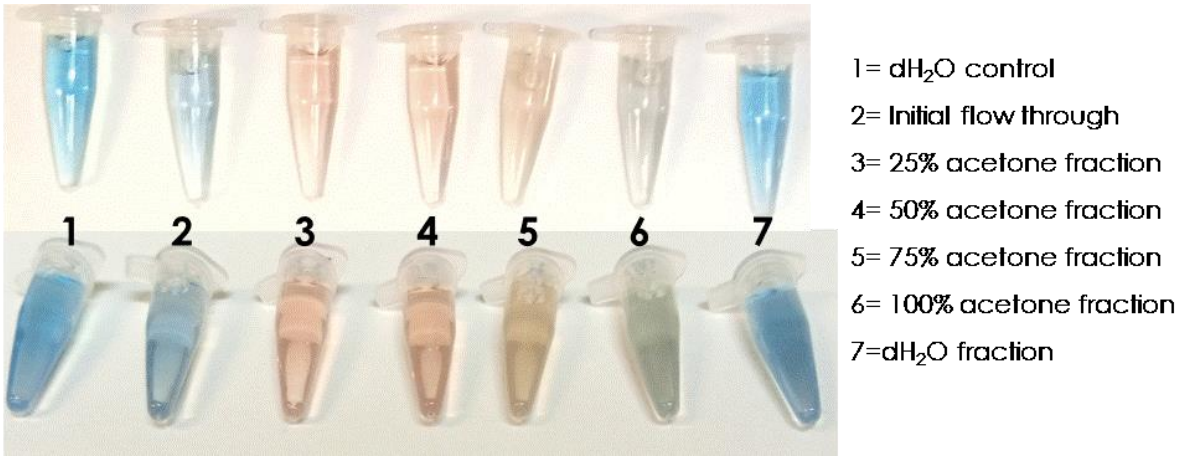

Figure 12: Siderophore activity detection of various SEPABEADS® SP207 extraction fractions as determined via the CAS-shuttle assay. Activity can be seen in the following fractions: 25% acetone, 50% acetone, 75% acetone, and 100% acetone.

Fractions that tested positive for siderophore activity (25, 50, 75 and 100% acetone) were pooled together, dried, resuspended in 3 ml dH20, and then further fractionated through size exclusion. The CAS-shuttle assay was performed at each step of this process to track the siderophore activity. The activity was found in the supernatant and was able to pass through both size filters (Figure 13). This indicated that the molecule responsible for the activity is less than 3 kDa in size which correlates with the statement that siderophores are low-molecular-mass (500-1000 Da) free ligands with a high affinity for iron (Neilands, 1984).

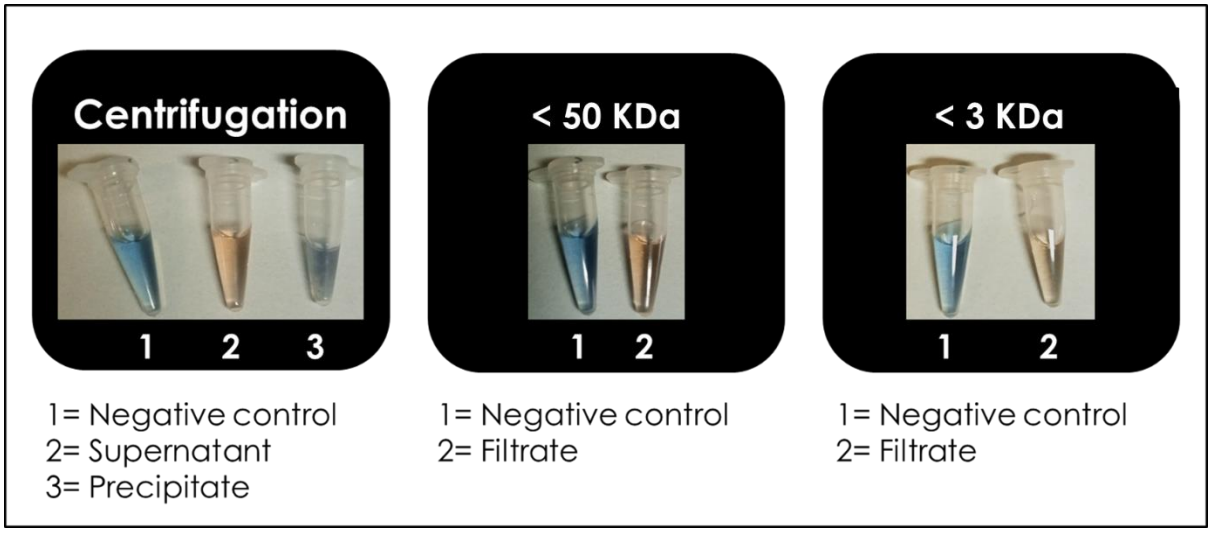

Figure 13: Siderophore activity tests at various steps of size exclusion filtration performed using the CAS-shuttle assay.

3.4 Antimicrobial Assays

Previous studies (Rogers et al., 1982; Shah et al., 1992; Wang et al., 2009; Chowdappa et al., 2020) have shown that certain siderophores display antimicrobial activity. This activity can be due to two possibilities: (a) antibiotic-like activity and (b) iron chelation, resulting in its unavailability to test organisms.

Initially, an agar well diffusion antimicrobial activity test, in which wells were loaded with siderophore extract that had been purified up until the point of HPLC, showed very promising results. Antimicrobial activity was detected against all test strains (Appendix A). Unfortunately, this could not be repeated. In an attempt to repeat this result, an additional 6 extractions were performed. All of the additional extractions showed high siderophore activity, but the original level of antimicrobial activity could not be recovered. This indicates that the original activity observed could not have been caused by the siderophore.

T. viridans has shown antimicrobial activity in past studies (Adams, 2019) against various test strains (*S. epidermidis, B. cereus, E. coli* 1699 and *P. putida*). Currently, the nature of the compound responsible remains unknown. It is possible that the initial antimicrobial activity detected was due to this uncharacterised bioactive. It is not immediately clear as to why activity was detected initially, but not in subsequent extractions that had been performed with no intended changes. This could be due to many possible reasons such as highly sensitive induction conditions for this bioactive under iron-limited conditions which could have resulted in vastly different concentrations of the bioactive molecule, an undetected contaminant producing the activity in the first sample, or even a faulty filter allowing larger compounds, to enter the first sample.

3.5 Chemical Characterisation

Siderophores can be classified into different groups based on their functional groups and hydrophobicity. These include α-hydroxycarboxylates, hydroxamates, catecholates, and mixed-type siderophores (Neilands, 1990). To determine to which group a particular siderophore belongs, various assays are used to test for each type of functional group (carboxylate, hydroxamate, and catecholate).

The tetrazolium salt test (Snow, 1954) for hydroxamates is based on the ability of hydroxamic acid to reduce tetrazolium salt by hydrolysis of hydroxamate groups using a strong alkali, which results in the instant appearance of a deep red colour. When this test was performed on purified siderophore extracts (post size exclusion filtration), no colour change was seen (Figure 14). This suggests that the extract and thus the siderophore under investigation does not contain a hydroxamate functional group.

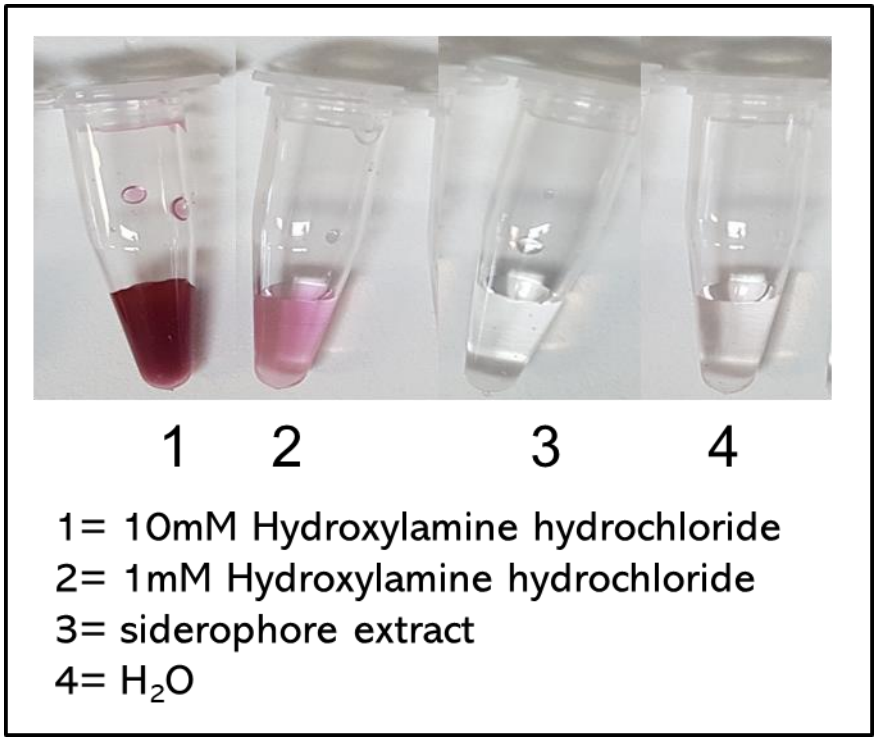

Figure 14: Results of tetrazolium salt test for hydroxamates.

Arnow's method for detecting catecholates is based on the reaction between catechol and nitrite-molybdate reagent in acidic conditions, originating in a yellow colour. The colour then changes to an intense orange-red in alkaline conditions, with the colour intensity being dependent on the amount of catechol present (Arnow, 1937). No colour change was seen when testing the post size exclusion filtration siderophore extract from this study (Figure 15). This indicates that in addition to not containing hydroxamate groups, it does not contain catecholate groups.

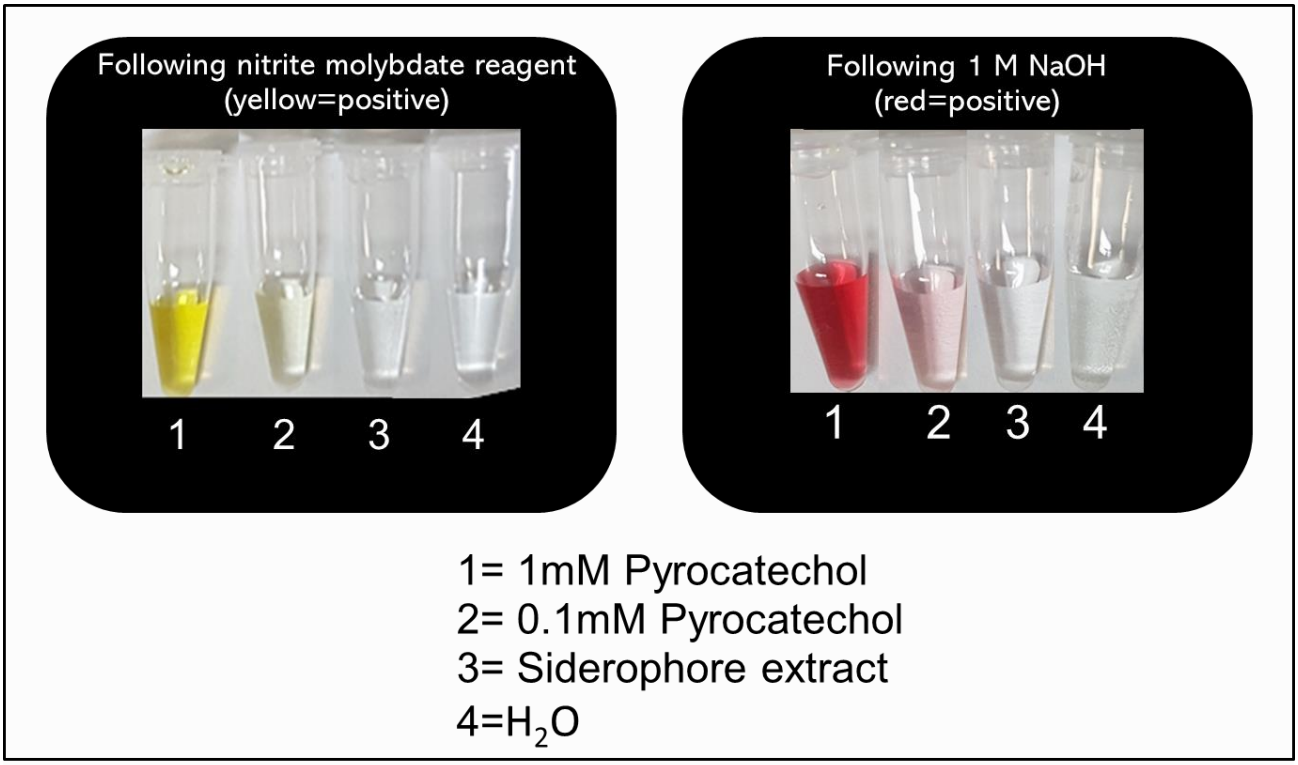

Figure 15: Results of Arnow's method of catecholate detection.

Vogel's test for carboxylates was then performed. This test is a titration-based assay that uses phenolphthalein as an indicator. In general, the choice of an indicator for titration is dictated by the acid to be determined, i.e., the colour change interval of the indicator must include the equivalence point. In this case, as described by Vogel (1987), phenolphthalein is a suitable indicator for detecting carboxylic acids. A positive result for carboxylate groups was seen when testing the post size exclusion filtered siderophore extract (Figure 16). This, combined with the negative results seen for the other two functional groups, strongly indicated that the siderophore in question falls under the carboxylate group of siderophores.

Figure 16: Results of Vogel's test for carboxylates.

In the case of mixed-type siderophores one would expect to see positive results for more than one of the tests described above. This has been seen in many studies including that by Ferreira et al. (2019), in which a catechol/hydroxamate siderophore tested positive in tests for both of these classes. Similarly, studies by Amsaveni et al. (2016), Maheshwari et al. (2019) and Nabila and Kasiamdari (2021) have all demonstrated that in the case of mixed-type siderophores that positive results are seen in the case of all of the included groups within a siderophore.

In addition to the methods described above, spectrophotometric assays were performed to determine the nature of the siderophore produced. To check for hydroxamate and catecholate types, the $FeCl_3$ test (Neilands, 1981) was used. The method of (Shenker et al., 1992) was used to investigate the possibility of a carboxylate siderophore. No peaks were seen for the expected wavelengths for either hydroxamates or catecholates in the $FeCl_3$ test (Neilands, 1981). When performing the method of (Shenker et al., 1992), a peak was seen at approximately 240 nm. In this test, a peak seen anywhere within the range of 190 and 280 nm indicates a carboxylate, and therefore, this confirms the results obtained from the Vogel's test.

3.6 Chelation of Other Metals

To investigate the extracted siderophores' ability to chelate metals other than iron, the method of (Mehnert et al., 2017) was used. In addition to iron, the siderophore extract was tested for binding activity with aluminium, vanadium, and arsenic (Table 6). Out of the many non-iron metals that have been seen to bind to various known siderophores, aluminium was selected as it is the most common (Braud et al., 2009), arsenic was selected due to the biotechnological potential of an arsenic binding siderophore (Retamal-Morales et al., 2018), and vanadium was selected at random.

Table 6: Summary of metal binding ability of siderophore extract.

Metal Tested	**% Siderophore units measured**	**Result**
Iron	59.5	Positive
Aluminium	50.5	Positive
Vanadium	0	Negative
Arsenite	0	Negative

It was seen that the isolated siderophore was able to bind aluminium at a high level. Siderophores binding aluminium in addition to iron have been commonly seen in other studies (Hernlem et al., 1996; Hu and Boyer., 1996; Neubauer et al., 2000; del Olmo et al., 2003; Braud et al., 2009). In fact, the very first siderophore to be isolated, mycobactin, was isolated as an aluminium complex (Snow, 1965). This phenomenon of siderophores of all classes commonly binding aluminium, which has absolutely no biological function (Schalk et al., 2011), is due to its high similarity with regard to size and charge to Fe (III) (Garrison and Crumbliss, 1987).

Although aluminium has no physiological role in metabolic processes (Exley and House, 2011), if the amount of aluminium taken up by the body exceeds its excretory capacity, the excess is deposited in various tissues, including bone, brain, liver, heart, spleen, and muscle. This accumulation, which frequently occurs in patients with end-stage renal

failure (Malluche et al., 1984), causes morbidity and mortality through various mechanisms (Verstraeten et al.,2008). The discovery of aluminium chelating molecules is thus of clinical significance as they could possibly be used to treat aluminium overload. This has already been done using the chelating agents deferoxamine, ascorbate, and Feralex-G (Ciancioni et al., 1984; Nebeker et al., 1984; Molitoris et al., 1987; Yokel et al., 1996; Kruk et al., 2004).

Vanadium has been previously seen to form complexes with certain siderophores such as pyochelin, putrebactin, pyoverdine, enterobactin, and desferrioxamine B (Lutoretti and Grdinic, 1986; Karpishin et al., 1993; Baysse et al., 2000; Pakchung et al., 2011). In this study, the isolated siderophore was not seen to bind vanadium. Currently, no carboxylate-type siderophores have been observed to bind with vanadium, but both catecholate and hydroxamate types have.

Arsenic is one of the most toxic metals derived from the natural environment. Previous studies have concluded that certain siderophores can bind arsenic and thus could potentially be used as a method of removing arsenic from contaminated environments (Nair et al., 2007; Drewniak et al., 2008; Sultana et al., 2012; Ghosh et al., 2015; Retamal-Morales et al., 2018). No arsenic binding activity by the extracted siderophore was seen in this study.

3.7 Genome Mining of *Thalassomonas viridans*

The genome of *T. viridans* Δ*1* was mined for secondary metabolite-specific pathways using antiSMASH version 6.1.1 and PRISM version 4.4.5. A total of eight pathways were identified within this genome. These eight pathways belonged to seven different classes (Figure 17).

Siderophore biosynthesis is typically carried out by one of two types of enzymatic machinery. These are either non-ribosomal peptide synthetase (NRPS) modular multienzymes or NRPS-independent synthetases (NIS) (Barry and Challis, 2009). No NIS siderophore pathways were identified within this genome, which are usually identified by antiSMASH if present. This suggests that either a NRPS pathway or a highly novel NIS pathway (and therefore, undetected bioinformatically) is responsible for encoding the production of the detected siderophore.

Cluster	Type
Cluster 1	NRPS
Cluster 2	T3PKS
Cluster 3	NRPS
Cluster 4	CDPS
Cluster 5	TfuA-related
Cluster 6	Bacteriocin
Cluster 7	Lanthipeptide
Cluster 8	T1PKS/NRPS

Figure 17: Secondary metabolite pathways identified in the genome of T. viridans Δ1 using antiSMASH version 6.1.1. Clusters are colour coded according to their types.

To narrow down the eight identified clusters, based on the likelihood that they are responsible for siderophore synthesis, each cluster was searched for the presence of siderophore-dependent receptors. This was done since, as explained by Crits-Christoph et al. (2020), it is rare for siderophore-specific transporters to be found in biosynthetic gene clusters that do not have siderophore functions. In the case of Gram-negative siderophore BGCs, the TonB-dependent receptor has been found in almost 80% of siderophore BGCs and never in BGCs with other activities.

Cluster 8 was seen to include a TonB siderophore-dependent receptor gene and so was thought to possibly be the pathway responsible for siderophore synthesis. This cluster contains a single NRPS gene as well as a single T1PKS gene, both orientated in the same direction. The presence of both NRPS and T1PKS components indicates a hybrid T1PKS/NRPS pathway. Figure 18 displays the prediction of open reading frames within cluster 8 as identified by antiSMASH.

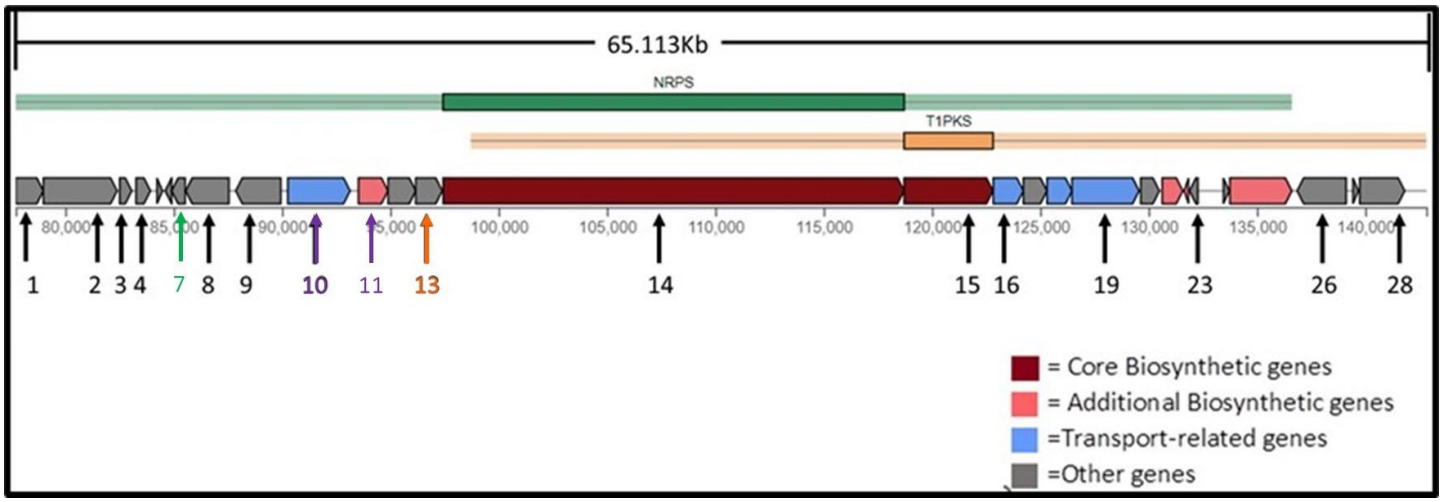

Figure 18: Prediction of ORFs within cluster 8 using antiSMASH 6.1.1. Each ORF is assigned a number and colour coded according to their role as described in the key.

Each of these open reading frames was then looked at in more detail. Table 7 shows the top BLASTp hit and proposed function for each open reading frame.

Table 7: Predicted ORFs within cluster 8, their top BLAST hits, and their putative functions.

ORF	Gene	Top blast hit	Proposed function	Amino acid percent identity	Accession number
1	M13 family peptidase	Peptidase M13 [*Shewanella schlegeliana*]	Metalloendopeptidase involved in Posttranslational modification, protein turnover, and chaperones.	473/694(68%)	WP_202722516.1
2	Hypothetical protein				
3	PD40 domain-containing protein	Winged helix-turn-helix transcriptional regulator [*Colwellia* sp. D2M02]	Transcriptional regulatory protein	311/774(40%)	WP_215980683.1
4	Insulinase family protein	Insulinase family protein [*Pseudoalteromonas porphyrae*]	Insulin degradation	574/952(60%)	WP_054455314.1
5	Hypothetical protein				

6	Winged helix-turn-helix domain-containing protein	Winged helix-turn-helix domain-containing protein [*Pseudoalteromonas piscicida*]	Phosphorelay signal transduction and regulation of transcription.	59/114(52%)	WP_088533097.1
7	MbtH-like protein	MbtH family NRPS accessory protein [*Microbispora triticiradicis*]	NRP Biosynthesis	37/65(57%)	WP_208804395.1
8	CPBP family intramembrane metalloprotease	CPBP family intramembrane metalloprotease [*Pseudoalteromonas* sp. McH1-7]	Cleavage of transmembrane domains of integral membrane proteins	163/275(59%)	WP_176032044.1
9	Cupin-like domain-containing protein	Cupin-like domain-containing protein [*Pseudoalteromonas* sp. PS5]		184/290(63%)	WP_128731648.1
10	AcrB/AcrD/AcrF family protein	Efflux RND transporter permease subunit [*Pseudoalteromonas piscicida*]	Transmembrane transport	555/1020(54%)	WP_099643594.1
11	RND family efflux transporter MFP subunit	Efflux transporter periplasmic adaptor subunit [*Colwelliaceae bacterium*]	Resistance, Nodulation, cell Division, and heavy metal efflux	152/390(39%)	MAG75636.1
12	Hypothetical protein	Hypothetical protein [*Pseudoalteromonas* sp. McH1-7]		148/335(44%)	WP_176032041.1
13	Major facilitator transporter	MFS transporter [*Pseudoalteromonas piscicida*]	Facilitates transmembrane transport	299/425(70%)	WP_099643596.1
14	Beta-ketoacyl synthase	Thioester reductase domain-containing protein [*Pseudoalteromonas piscicida*]	Acyl transferase domain in polyketide synthase (PKS) enzymes	720/1353(53%)	WP_119232723.1
15	Condensation domain-containing protein	Non-ribosomal peptide synthetase [*Pseudoalteromonas piscicida*]	peptide synthase	3767/7030(54%)	WP_099643598.1
16	Aspartyl protease family protein	Aspartyl protease family protein [*Campylobacteraceae*	Cleavage of dipeptide bonds that have hydrophobic residues as well as a beta-	189/400(47%)	NQY93751.1

		bacterium]	methylene group		
17	Aspartate kinase	Hypothetical protein [*Pseudoalteromonas piscicida*]	Catalyzes the phosphorylation of the amino acid aspartate.	164/419(39%)	WP_099643600.1
18	Aminotransferase class-III	Diaminobutyrate--2-oxoglutarate transaminase family protein [*Pseudoalteromonas piscicida*]	Catalyzes the chemical reaction L-2,4-diaminobutanoate + 2-oxoglutarate ←→ L-aspartate 4-semialdehyde + L-glutamate	292/438(67%)	WP_099643601.1
19	TonB-dependent siderophore receptor family	TonB-dependent receptor [*Thalassomonas actiniarum*]	Outer membrane receptor protein, mostly Fe transport	870/957(91%)	WP_044835227.1
20	Hypothetical protein	Hypothetical protein [*Thalassomonas actiniarum*]		638/692(92%)	WP_152646779.1
21	tssI	Type VI secretion system tip protein VgrG [*Thalassomonas actiniarum*]	Putative auto-transporter adhesion	626/664(94%)	WP_044835225.1
22	Hypothetical protein	Hypothetical protein [*Thalassomonas actiniarum*]		178/205(87%)	WP_044835224.1
23	PAAR domain-containing protein	PAAR domain-containing protein [*Thalassomonas actiniarum*]	Involved in TypeVI secretion (Intracellular trafficking, secretion, and vesicular transport)	91/99(92%)	WP_044835223.1
24	Type I addiction module toxin, SymE family	SymE family type I addiction module toxin [*Thalassomonas actiniarum*]	SOS-induced toxin involved in RNA binding, cytoplasm, RNA metabolic processes, and hydrolase of ester bonds	60/82(73%)	WP_044834333.1
25	PEP-CTERM	PEP-CTERM sorting	Protein export sorting	185/217(85%)	WP_044835222.1

	sorting domain-containing protein	domain-containing protein [*Thalassomonas actiniarum*]	system		
26	Hypothetical protein	Hypothetical protein [*Thalassomonas actiniarum*]		128/181(71%)	WP_044835221.1
27	Type VI secretion system membrane subunit TssM	Type VI secretion system membrane subunit TssM [*Thalassomonas actiniarum*]	Transport of proteins from the interior of a bacterial cell across the cellular envelope into an adjacent target cell	1030/1138(91%).	WP_084692937.1
28	DotU family type IV/VI secretion system protein	Type IVB secretion system protein IcmH/DotU [*Thalassomonas actiniarum*]	Periplasmic protein involved in septation, Cell cycle control, cell division, and chromosome partitioning.	345/433(80%)	WP_053043346.1

When looking more closely at the various identified ORFs, several further indicated that this is a putative siderophore pathway and are described below.

3.7.1 Cluster 8 Open Reading Frames with Possible Siderophore-Related Activity

3.7.1.1 ORF 7

Highlighted in green in Table 7 and in Figure 18, this was predicted to represent a MbtH-like protein. Studies have shown that MbtH-like proteins are commonly encoded by NRPS clusters that are responsible for the synthesis of either antibiotics or siderophores. Although they play important roles in secondary metabolite biosynthesis, MbtH-like proteins do not act directly as catalysts but rather as facilitators or chaperones (Baltz, 2011). A specific example of the linkage of these proteins in siderophore synthesis pertains to the production of the non-ribosomal peptide siderophore coelichelin by *S. coelicolor* (Lautru et al., 2007). One of the two genes (*cdaX* and *cchK*) encode MbtH-like proteins and is required for the biosynthesis of coelichelin.

3.7.1.2 ORFs' 10 and 11

These two ORF's, highlighted in purple in Table 7 and Figure 18, were predicted to encode a RND family efflux transporter. RND efflux pumps are known to be involved in heavy metal export and transport various drugs, lipids, pigments, and siderophores (Miethke and Marahiel, 2007). Examples of RND efflux pumps involved in siderophore export include AcrAB, AcrAD, and MdtABC in *E. coli*, which export enterobactin, ApeX in *Bacillus anthracis*, which exports petrobactin, VexGH in *Vibrio cholerae* which exports vibriobactin, and as MmpL4 and MmpL5 in *Mycobacterium tuberculosis* which exports both mycobactin and carboxymycobactin (Horiyama and Nishino, 2014; Hagan et al., 2017; Kunkle et al., 2017; Sandhu and Akhter, 2017).

3.7.1.3 ORF 13

This ORF, highlighted in orange in Table 7 and Figure 18, was identified as encoding for a MFS transporter. In addition to the ABC superfamily and the RND superfamily, MFS transporters are known to facilitate the transport of siderophores across bacterial membranes. (Alav et al., 2021). MFS siderophores that have been previously characterised include EntS of *E. coli*, NorA of *Staphylococcus aureus*, CsbX of *Azotobacter vinelandii*, and AlcS of both *Bordetella pertussis* and *Bordetella bronchiseptica* (Furrer et al., 2002; Page et al., 2003; Brickman and Armstrong, 2005; Deng et al., 2012).

3.7.2 Modular Organisation of Cluster 8

For an NRPS enzyme to be able to synthesise a non-ribosomal peptide, it must contain at least three core domains, including a condensation domain (C), an adenylation domain (A), and a thiolation (T) domain (Martínez-Núñez and López López, 2016). The NRPS gene in cluster 8 contains six sets of these core domains and an additional group that contains A and T domains but no C domain (Figure 19). This group that does not contain a C domain is the first module of the NRPS. As described by Lautru and Challis (2004), it is a common occurrence for the first module of an NRPS to not contain a C domain, and so it can be said that this NRPS, in fact, contains seven sets of core domains.

Usually, the number and order of modules in NRPS systems determine the number and order of amino acids in the peptide product. Therefore, a prediction as to the number of amino acids that are incorporated can be made based on the number of A domains seen. Exceptions to this

have, however, been seen in the synthesis of some molecules such as coelichelin and fusachelin A.

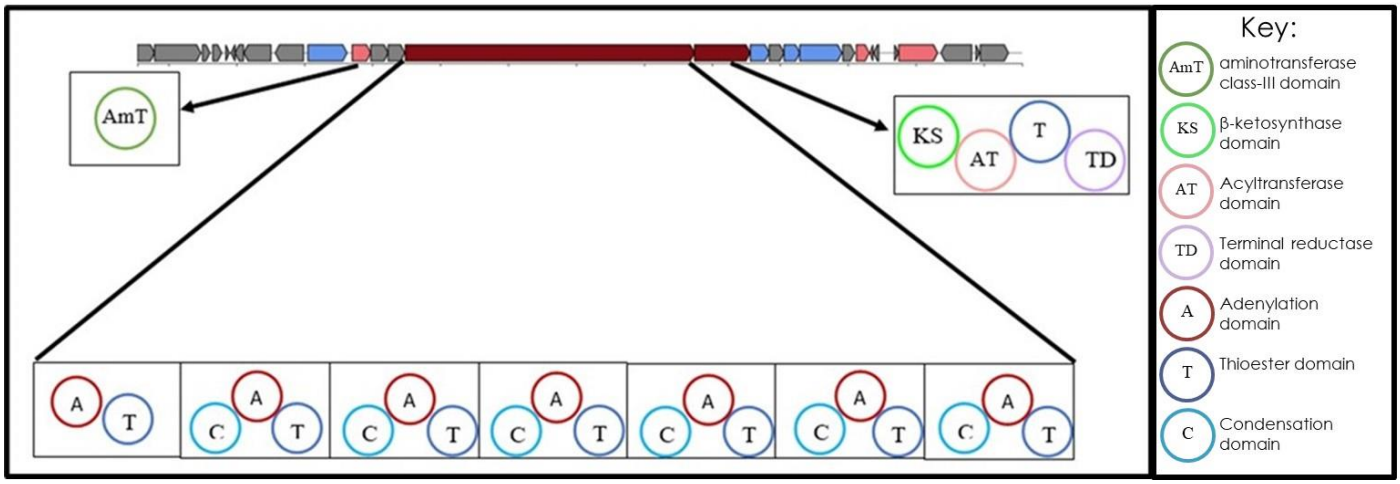

Figure 19: Modular organisation of cluster 8 in T. viridans as detected by antiSMASH version 6.1.1.

Upstream of the NRPS/T1pks, an ORF predicted to be encoding an aminotransferase class-III (AMT) was observed. The top BLASTp hit for this ORF corresponds to a diaminobutyrate-2-oxoglutarate transaminase family protein of *Pseudoalteromonas piscicida*, which catalyses the reaction shown below:

L-2,4-diaminobutanoate + 2-oxoglutarate ←→ L-aspartate 4-semialdehyde + L-glutamate

A similar essential class III AMT is involved in the synthesis of the pyoverdine siderophore by *Pseudomonas aeruginosa* PAO1; PvdH. It is required for the formation of L-2,4-diaminobutyrate, an important component of the final siderophore (Vandenende et al., 2004).

Downstream and directly adjacent to the NRPS cluster, a T1PKS cluster is seen. As previously mentioned, the close proximity of these two elements indicates a hybrid NRPS/PKS pathway. T1PKSs are large protein complexes that contain multiple modules of covalently linked catalytic domains (Keatinge-Clay, 2012). They function to construct polyketides (chain-like molecules consisting of alternating ketone (or reduced ketone) and methylene groups from simple carboxylic acid-derived components. Each PKS must contain a minimum of three functional domains: a β-ketosynthase (KS), an acyltransferase (AT), and an acyl carrier protein (ACP) (Keatinge-Clay, 2012). In the case of the T1PKS identified here, both KS and AT domains were identified; however, no ACP domain was seen.

Interestingly, a thiolation domain was seen in the place of the missing ACP domain. ACP and T domains share a similar carrier function (Weber et al., 2000), with ACP domains usually found in PKS systems and T domains in NRPS systems. This crossover of domains further motivates the conclusion that this is a hybrid NRPS/T1PKS pathway rather than two separate pathways. In addition, a terminal reductase (TD) domain was detected within the T1PKS pathway. TDs are again typically found in NRPS pathways rather than PKS pathways. They facilitate the 2-electron reduction of an enzyme-bound thioester, releasing the generated peptides as C-terminal aldehydes (Tietze et al., 2020).

3.7.3 Prediction of A-domain Amino Acid Specificity of Cluster 8 NRPS Domain

A built-in feature of antiSMASH version 6.1.1 is the prediction of A-domain amino acid specificity, powered by NRPSpredictor2. NRPSpredictor2 was designed to predict the putative substrate specificity for bacterial A-domains on four hierarchical levels. These levels include the gross physicochemical properties of the substrate, large clusters, small clusters, and a single amino acid level. Predictions of higher hierarchical levels are regarded as the best performing, with the prediction confidence decreasing as the level decreases up until the single amino acid prediction (Röttig et al., 2011).

As shown in Table 8, The predicted amino acids for the seven A-domains found in cluster 8 by antiSMASH included hydrophobic-aliphatic amino acids in modules 1, 3, 5, and 6, hydrophilic amino acids in modules 2 and 4, and a hydrophobic-aromatic amino acid in module 7. Only one of the modules showed a strong Stachelhaus prediction score, this being module 6 with a 100% score for Thr. The remaining modules all displayed week scores of 70% or less. These low levels of similarity to known active site sequence signatures could result from A-domains with specificity to substrates that are not yet represented by the available NRPSpredictor2 reference database. Alternatively, the low identification levels could be due to the degeneracy of amino acid specificity signatures or enzyme promiscuity whereby enzymes can incorporate more than one specific amino acid. An example of enzyme promiscuity is seen in the case of tyrocidine biosynthesis by *Bacillus brevis*, were the A domain TycB_m3 activates L -tryptophan with 100% relative activity but is also able to activate L -phenylalanine with 48% relative activity (Rausch et al., 2005).

Table 8: Prediction of A-domain amino acid specificity in T. viridans cluster 8 using NRPSpredictor2.

Module	Predicted physicochemical class	Large clusters prediction	Small clusters prediction	Single AA prediction	Nearest Stachelhaus code	Stachelhaus code match
1	Hydrophobic-aliphatic	Gly, Ala, Val, Leu, Ile, Abu, Iva	Val, Leu, Ile, Abu, Iva	N/A	Ile	70% (weak)
2	Hydrophilic	Asp, Asn, Glu, Gln, Aad	N/A	N/A	Arg	60% (weak)
3	Hydrophobic-aliphatic	Gly, Ala, Val, Leu, Ile, Abu, Iva	Val, Leu, Ile, Abu, Iva	Val	Val	70% (weak)
4	Hydrophilic	Asp, Asn, Glu, Gln, Aad	N/A	N/A	Arg	60% (weak)
5	Hydrophobic-aliphatic	Gly, Ala, Val, Lue, Ile, Abu, Iva	Val, Leu, Ile, Abu, Iva	N/A	Ile	70% (weak)
6	Hydrophobic-aliphatic	Ser, Thr, Dhpg, Hpg	Thr	Thr	Thr	100% (strong)
7	Hydrophobic-aromatic	Phe, Trp, Phg, Tyr, Bht	N/A	Tyr	Phe	60% (weak)

When using PRISM to perform the same analysis of predicting A-domain amino acid specificity within cluster 8, variations were seen when compared to that supplied by antiSMASH's NRPSpredictor2. PRISM predictions (Table 9) were similar to NRPSpredictor2 predictions in that they both predict module 7 to be specific to Thr with a relatively high degree of confidence. This phenomena of different bioinformatic tools displaying different results highlights the fact that these are merely predictions and that these tools are not able to give the exact results. Currently, the chemistry prediction accuracies of the latest versions of antiSMASH and PRISM have yet to be compared and thus it would be appropriate to consider both predictions.

Table 9: Prediction of A-domain amino acid specificity in T. viridans cluster 8 using PRISM.

Module	Top three predictions	Top prediction	Top prediction score
1	Val, Leu, Ile	Val	356.6
2	2,3-DAP, Ser, Phe	2,3-DAP	414.1
3	Val, Ile, Phe	Val	403.6
4	2,3-DAP, Ser, Phe	2,3-DAP	415.9
5	Val, Ile, Leu	Val	389
6	Thr, Thr, Thr	Thr	650.5
7	Phe, Trp, Leu	Phe	430.1

3.7.4 Specificity Prediction of A-domain Amino Acid Specificity of Cluster 8 T1PKS Domain

Built into antiSMASH is the algorithm described by Minowa et al. (2007) which uses an HMM based approach to predict the specificities of NRPS adenylation domains and PKS AT domains. This tool predicted that the T1PKS of cluster 8 is most likely to be specific for malonyl-CoA. In this case, the same prediction was seen through the use of PRISM.

Malonyl-CoA is an important central metabolite serving as the basic building block for the microbial synthesis of many polyketides and fatty acid-derived compounds (Milke and Marienhagen, 2020). Most PKSs select malonyl-CoA molecules as extender units, which are successively added to growing β-ketoacyl chains (Chan et al., 2009). Yersiniabactin is an example of a siderophore that is synthesized by a mixed PKS-NRPS strategy that features modular assembly of the siderophore from salicylate, a group derived from malonyl-CoA, three molecules of cysteine, and three methyl groups (Crosa and Walsh, 2002).

3.7.5 Cluster 8 C-domain Classification

During NRP biosynthesis, the C-domain plays an important role in peptide-bond formation between amino acids (Samel et al., 2007). C-domains can be classified based on the

stereochemistry of the amino acids between which they catalyse peptide-bond formation and their functions. Table 10 explains these subcategories of C-domains.

Table 10: Summary of NRPS C-domain subcategories.

Classification	Description	Reference
LcL domains	catalyse the peptide-bond formation between L-amino acids	(Rausch et al., 2007)
DcL domains	catalyse peptide-bond formation between a D and L-amino acids	(Rausch et al., 2007)
Heterocyclization (Cyc) domains	catalysing peptide-bond formation and plays a role in cyclization of the peptide product	(Rausch et al., 2007).
Dual E/C domains	both epimerization and peptide-bond formation	(Balibar et al., 2005)
Starter C domains	acylation of the first amino acid with a fatty acid or polyketide moiety	(Miao et al., 2006).

The Natural Product Domain Seeker (NaPDos) server, built into antiSMASH, was used to classify the NRPS C-domains, and the KS domain of the T1PKS region in cluster 8 into their respective sub-types. As shown in Table 11, it was found that all of the C domains within this cluster belong to the LcL domain, and thus it is predicted that all amino acids incorporated by the NRPS pathway are L-amino acids. The KS domain was seen to belong to the class of hybrid KS.

In addition to functional classification, the NaPDos server identifies potential pathways from which the C-domain in question originates. C-domains in cluster 8 were predicted to originate from seven different pathways (Table 11). C-domains with 85% or higher amino acid identities are likely to belong to pathways that produce similar or identical compounds to those of the reference pathway (Gongtang et al., 2010). In this case, all domains showed amino acid identities of no higher than 45% to their respective predicted pathways. These low scores indicate that it is likely that cluster 8 codes for the biosynthesis of a novel compound.

Table 11: C-domain subtypes as determined by the NaPDos server

Module	Class	Pathway	Identity (%)
2	LCL	Mycosubtilin	30
3	LCL	Syringomycin	31
4	LCL	Tyrocidin	30
5	LCL	Surfactin	34
6	LCL	Syringomycin	43
7	LCL	Lychenicin	34
T1PKS	Hybrid KS	Epothilone	45

3.7.6 Gene Cluster Comparison

When comparing cluster 8's architecture to clusters found in other genomes, a high degree of similarity was seen to a cluster found in *Pseudoalteromonas piscicida* (Figure 20). When looking at the BLAST hits for each open reading frame within cluster 8, it was also seen that 11 out of 28 reading frames showed a top hit corresponding to *Pseudoalteromonas* genes (Table 7). These top hits ranged in similarity percentages from 39 to 70% between *T. viridans* and *Pseudoalteromonas* species; and the pathways share a very high degree of synteny. When comparing the predicted A-domain amino acid specificities of cluster 8 and the similar pathway seen in *Pseudoalteromonas piscicida*, it was seen that the predictions, at least at the large cluster level, were identical between the two pathways. This degree of similarity between these two pathways indicates that it is possible that they will result in similar or related products.

Figure 20: Comparison of cluster 8 of T. viridans and similar cluster found in Pseudoalteromonas piscicida.

Pseudoalteromonas piscicida is a Gram-negative gammaproteobacterium found in the marine environment (Richards et al., 2017). This organism has been seen to produce the siderophores Pseudoalteropeptide A (Ueoka et al., 2020) and Pseudochelin A (Sonnenschein et al., 2017). In the case of Pseudochelin A, the pathway responsible for synthesis has been identified in *Pseudoalteromonas piscicida* S2040 (Korp et al., 2018) and is not the same pathway showing homology to cluster 8. The genetic pathway responsible for the synthesis of Pseudoalteropeptide A has yet to be identified, and its genome is not available. It is therefore not possible to rule out the possibility that Pseudoalteropeptide A is produced via the pathway showing similarities to cluster 8 in *T. viridans*. The structures of these two *P. piscicida* siderophores are shown in Figure 21.

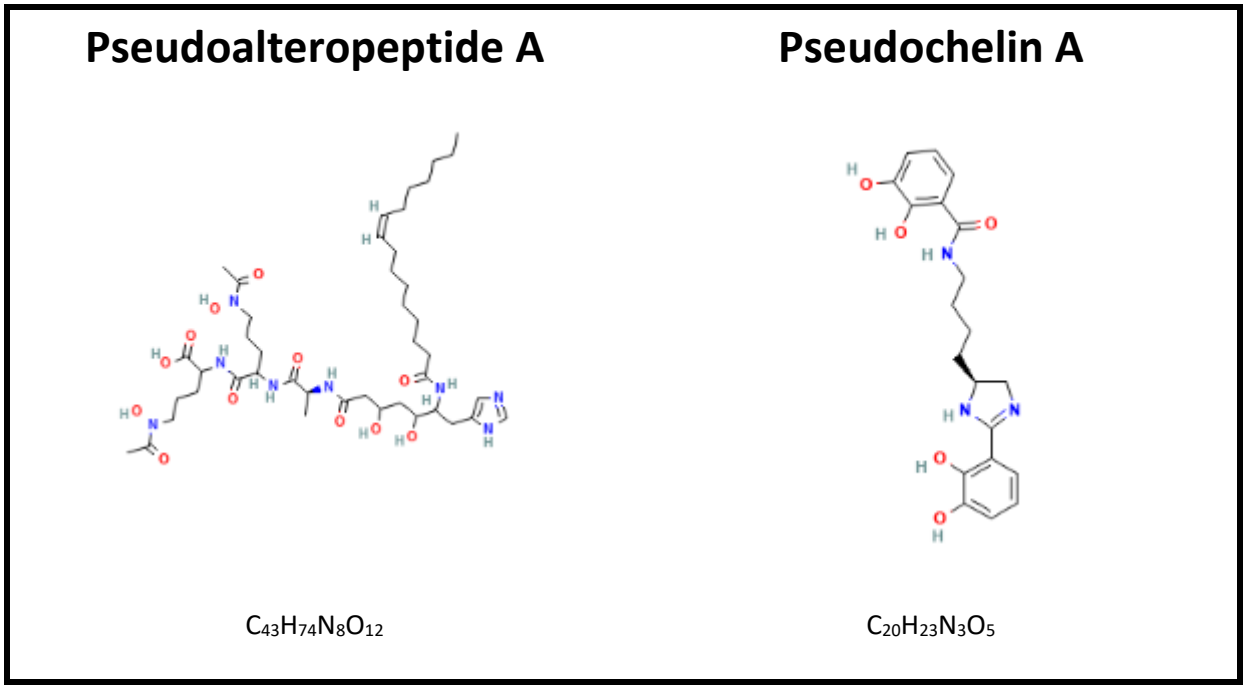

Figure 21: Structures of Pseudoalteropeptide A and Pseudochelin A.

3.7.7 Structure Prediction

An additional feature of both antiSMASH and PRISM is their built-in structure prediction capabilities. This function aims to predict the compound's chemical structure produced by a particular pathway. Unfortunately, these predictions do not consider tailoring reactions and assume PKS/NRPS collinearity. Thus, this feature can only provide a rough prediction of the core scaffold of a molecule, and it is highly likely that the structure of the actual molecule will differ from the prediction (antiSMASH bacterial version, 2022). This feature cannot

accurately predict the structure of the final molecule but is useful in giving a rough idea what it may look like.

The structure predictions provided by antiSMASH and PRISM for cluster 8 in *T. viridans* and the similar pathway in *P. piscicida* are shown in Figure 22. These two structure predictions are similar, with the main difference being the presence of a hydroxy-benzene moiety seen in the case of *T. viridans.*

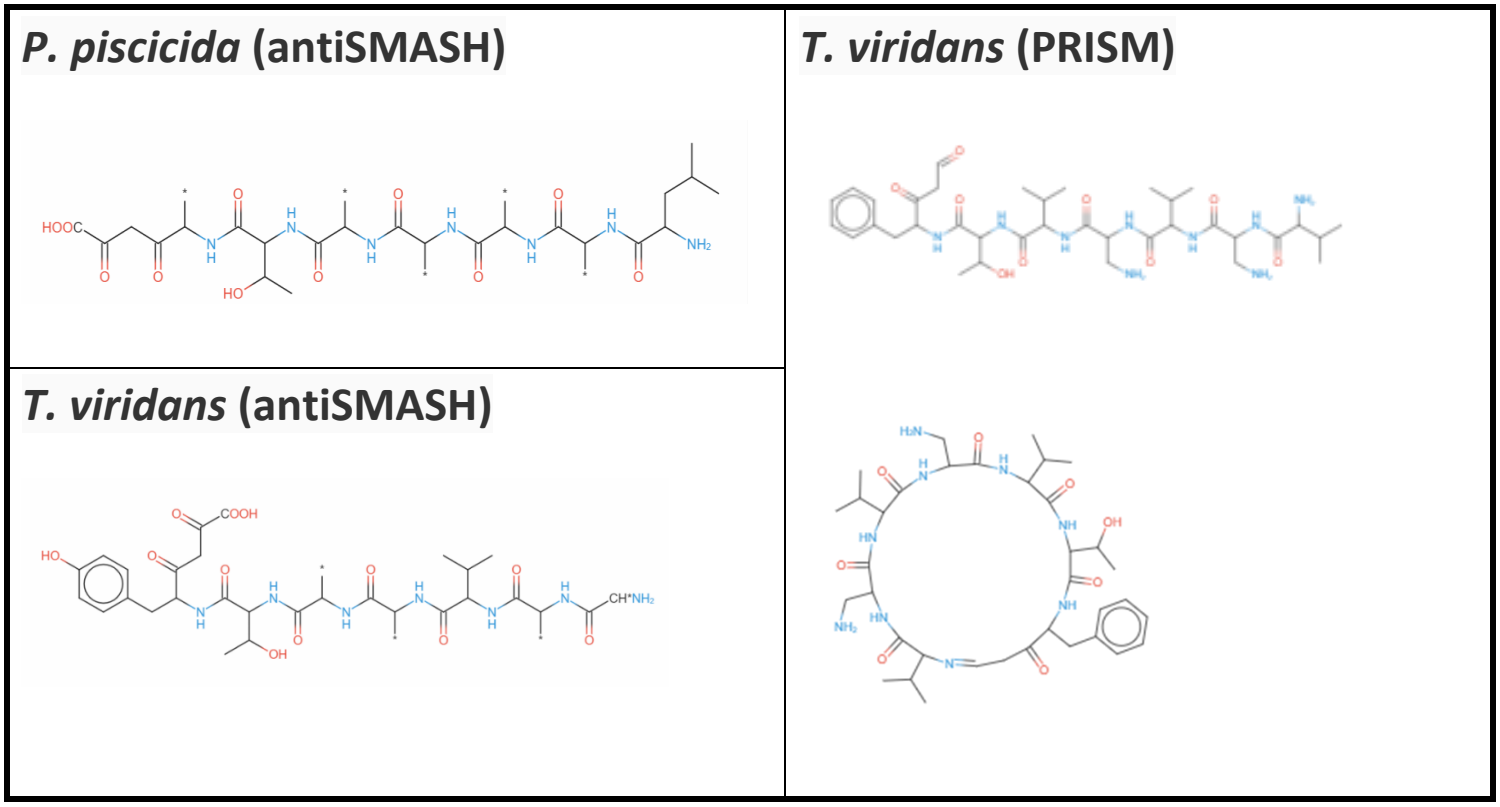

Figure 22: antiSMASH predicted structures of T. viridans cluster 8 and similar P. piscicida cluster.

When comparing the predicted structure for the *P. piscicida* pathway (Figure 22) to that of the structures of the known siderophore, pseudoalteropeptide A (Figure 21), they do not appear similar. This could be because, as previously mentioned, the structure prediction provided by antiSMASH represents only a rough estimation of the core scaffold and is unlikely to be the same as the actual structure. Even so, some degree of similarity between prediction and actual structure should be seen. It is thus more likely that the metabolite being produced by this *P. piscicida* pathway is not pseudoalteropeptide A. Moreover, no similarity is seen between the known structures of pseudoalteropeptide A and that predicted by either anstiSMASH or PRISM for *T. viridans* cluster 8. This lack of similarity between the known structure of pseudoalteropeptide A and the structural predictions seen here indicates that the *P. piscicida* pathway showing similarities to *T. viridans* cluster 8 may not be the pathway

responsible for pseudoalteropeptide A synthesis. Through genome mining alone this cannot be definitively determined as antiSMASH is not known to accurately predict structures of NRPS-T1PKS hybrid molecules and rather focuses only on the peptide section of molecules. If we were, however, to assume that the structure predicted here for cluster 8 is not the same as pseudoalteropeptide A, this then raises the question of is it the case that the siderophore produced by *T. viridans* does not show any resemblance to pseudoalteropeptide A, or that a pathway other than the proposed cluster 8 is responsible for siderophore synthesis?

3.8 Mass Spectrometry

Following siderophore extraction and size exclusion filtration (Section 2.10), the resulting siderophore-containing extract was assessed through mass spectrometry (MS) analysis. For comparison, an extract was prepared under identical conditions except that the culture did contain iron and which displayed no siderophore activity. This was done as a negative control in order to identify which MS peaks were linked to siderophore activity.

Figure 23 shows the MS chromatograms of the two samples run in positive mode, and Figure 24 shows the same two samples run in negative mode. As seen in these two figures, much clearer peaks were seen when run in negative mode. A study by (Liigand et al., 2017), in which they investigate which ionisation modes are best for different analytes, explains that negative mode ionisation is better suited for compounds containing oxygen bases, such as carboxylic acids. This, combined with the previously presented result (Section 3.5) that the siderophore in question can be categorised as a carboxylate, could possibly explain why much clearer peaks were seen in negative ionisation mode compared to the positive ionisation mode.

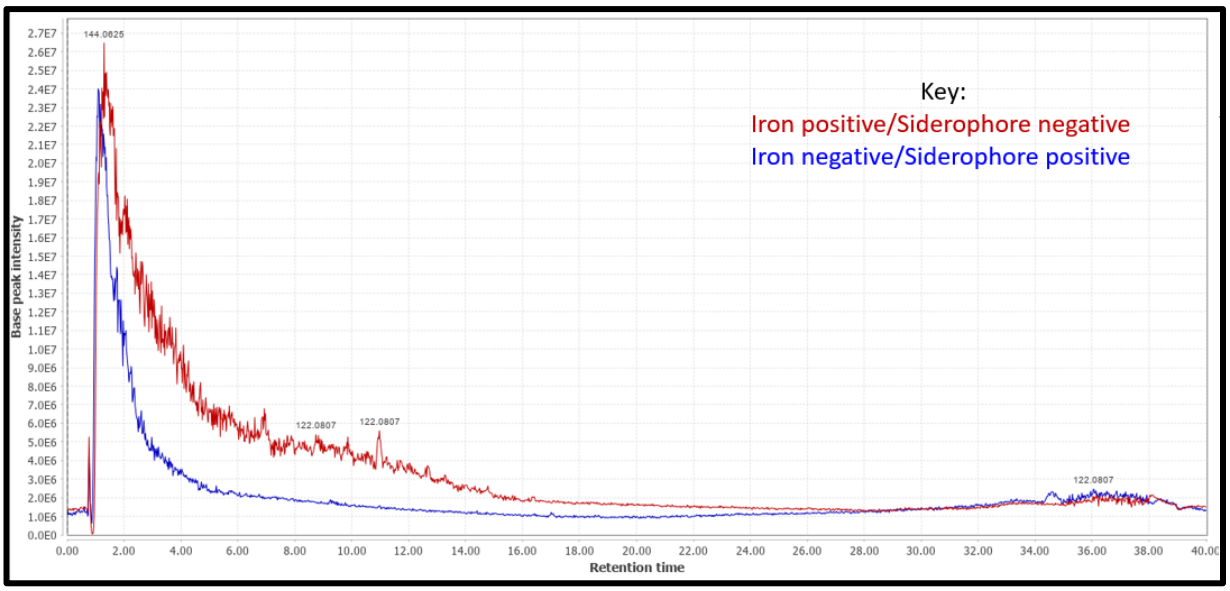

Figure 23: MS1 chromatograms of siderophore positive and siderophore negative samples run in positive mode.

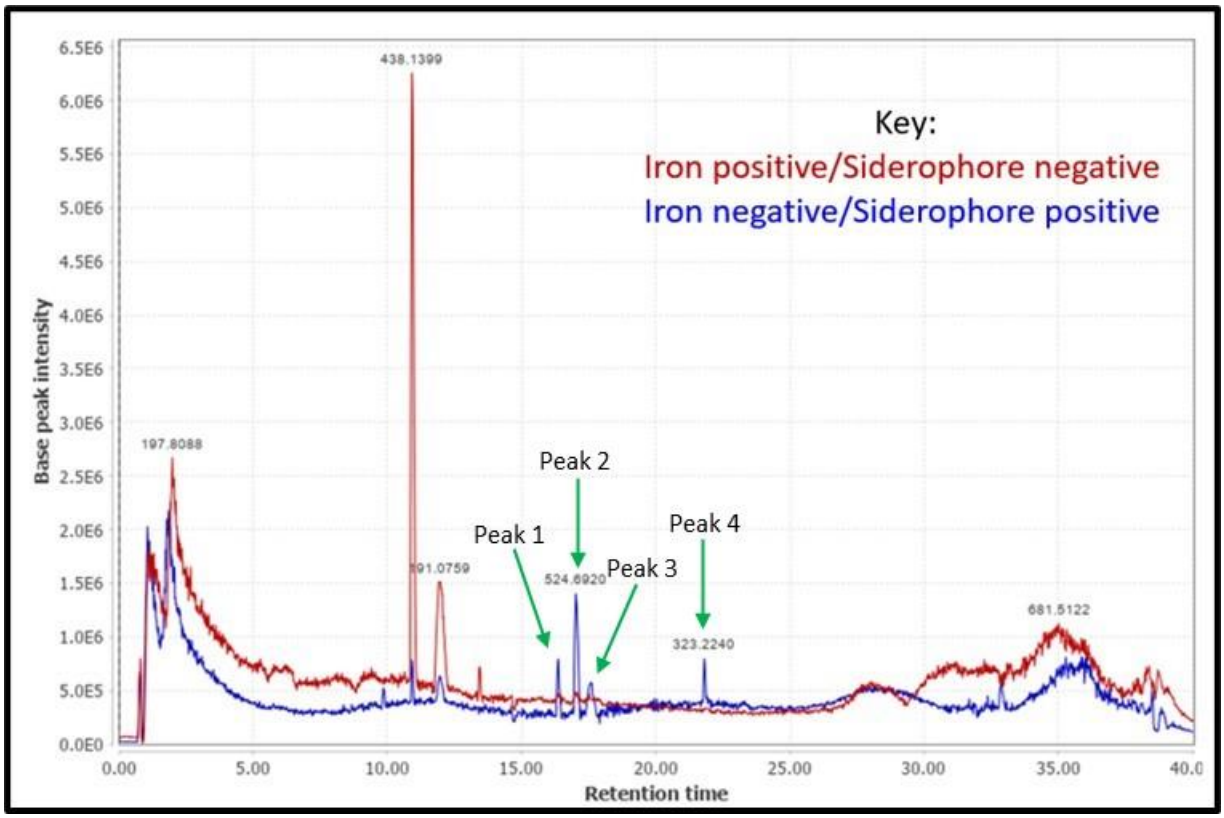

Figure 24:MS1 chromatograms of siderophore positive and siderophore negative samples run in negative mode.

As seen in Figure 24 above, four peaks were present in the siderophore-containing sample that were absent in the control sample. These peaks were thus labelled as peaks 1-4 and were the target of further analysis.

When looking at the results obtained through the use of the SIRIUS software, summaries of results were prepared and grouped based on retention times correlating to each of the four identified peaks. This was done since various compounds were detected within each of the peaks and so that all of these compounds, rather than only the most abundant, could be considered. Results showed several compounds with masses lower than 1000 Da (Tables 11-14) and three with masses larger than 1000 Da. Known siderophores range in size from 138.03 Da (Salicyclic acid) to 1229.61 Da (Ferrocin B). Since three compounds with masses over 1000 Da were found in the siderophore-positive sample but not in the siderophore-negative sample, it is possible that the siderophore in question has a mass of over 1000 Da and that the various smaller compounds detected represent precursors and building blocks of the final iron-chelating molecule.

3.8.1 SIRIUS Analysis of Compounds Less Than 1000 Da

When looking at the compounds detected by SIRIUS that were assigned masses of less than 1000 Da, several predictions were made. Summaries of these predictions were grouped based on retention times corresponding to peaks. Table 12 depicts a summary of predictions for compounds less than 1000 Da under the time frame of peak 1, Table 13 shows the same under the time frame of peak 2, Table 14 shows that for peak 3 and Table 15 for peak 4. None of the SIRIUS provided structural predictions provided for these compounds correspond to that of known siderophores.

Table 12: Summary of SIRIUS results for compounds less than 1000 Da under the time frame of Peak 1.

Precursor (Da)	**Predicted molecular formulas**	**Isotope score**	**Tree score**	**Total explained**	**Median mass error (ppm)**	**Top structure prediction**	**Structure similarity**	**Structure score**
250.15	$C_{14}H_{21}NO_3$	2.651	72.132	92.953	5.792	3-(1-Adamantyl)-4-amino-4-oxobutanoic acid	56.46	-151.6

	$C_{14}H_{23}NO_4$	2.651	72.132	92.953	5.792	1-Amino-2-cyclohexylcyclohexane-1,3-dicarboxylic acid	56.48	-179.3
268.16	$C_{14}H_{25}NO_5$	5.408	34.369	91.267	4.752	3-Cyclohexyl-3-[(2-methylpropan-2-yl)oxycarbonylamino] oxypropanoic acid	49.79	-171.9
	$C_{14}H_{23}NO_4$	5.408	34.369	91.267	4.752	(1S)-2-[(1R)-1-amino-1-carboxy-3-cyclohexylpropyl]cyclopropane-1-carboxylic acid	58.48	-161.5

Table 13: Summary of SIRIUS results for compounds less than 1000 Da under the time frame of Peak 2.

Precursor (Da)	**Predicted molecular formulas**	**Isotope score**	**Tree score**	**Total explained**	**Median mass error (ppm)**	**Top structure prediction**	**Structure similarity**	**Structure score**
371.16	$C_{12}H_{30}N_4O_8S$	0	17.338	82.155	-7.418			
	$C_{12}H_{28}N_4O_7S$	0	17.338	82.155	-7.418			
	$C_{15}H_{32}O_6S_2$	0	17.271	82.155	4.894	1,15-Pentadecanedisulfonic acid	37.78	-209.4
	$C_{15}H_{34}O_7S_2$	0	17.271	82.155	4.894			
	$C_8H_{26}N_{10}O_6S$	0	16.7	82.155	1.02			
	$C_8H_{24}N_{10}O_5S$	0	16.7	82.155	1.02			
393.14	$C_{19}H_{32}FeO_3S$	0	29.724	64.476	3.185			
	$C_{19}H_{34}FeO_4S$	0	29.724	64.476	3.185			
	$C_{10}H24N_{10}O_6S$		28.501	60.489	-3.403			

	$C_{10}H22N_{10}O_5S$	0	28.501	60.489	-3.403			
	$C_{17}H_{32}O_7S_2$	0	26.083	59.378	-0.753	1-[6-Hydroxy-11-(1-sulfocyclopropyl)undecyl]cyclopropane-1-sulfonic acid	52.55	-175.02
	$C_{17}H_{30}O_6S_2$	0	26.083	59.378	-0.753	[(1R,2R,3S,4S)-3-(4-methylpent-3-enyl)-3-(methylsulfonyloxymethyl)-2-bicyclo[2.2.1]heptanyl] methyl methanesulfonate	38.08	-342.88
240.95	$C_9H_6O_3$	0	17.234	82.493	5.807			
	$C_4H_2N_2O_8$	0	14.077	84.647	1.422	dinitro (Z)-but-2-enedioate	35.94	-183.966
	$C_4H_4FeN_4O_5$	0	11.903	84.647	1.488			
	$C_4H_4FeN_4O_6$	0	11.903	84.647	1.488			
287.15	$C_{14}H_{26}O_7$	3.258	44.552	96.488	5.098	Decanedioic acid 1-(2,3,4-trihydroxybutyl) ester	50.99	-107.037
	$C_{14}H_{24}O_6$	3.258	44.552	96.488	5.098	(E)-3,10-dihydroxy-4,9-dimethyldodec-6-enedioic acid	98.51	-34.472

Table 14: Summary of SIRIUS results for compounds less than 1000 Da under the time frame of Peak 3.

Precursor (Da)	**Predicted molecular formulas**	**Isotope score**	**Tree score**	**Total explained**	**Median mass error (ppm)**	**Top structure prediction**	**Structure similarity**	**Structure score**
333.18	$C_{18}H_{28}N_2O_5$	5,432	45.938	97.646	5.993	4-[[1-Hydroxypropan-2-yl(2-hydroxypropyl)carbamoyl]amino]-5-phenylpentanoic	62.38	-176,766

						acid		
	$C_{18}H_{26}N_2O_4$	5,432	45.938	97.646	5.993	(2S)-2-[[(2S)-2-acetamido-4-phenylbutanoyl]amino]-4-methylpentanoic acid	83.81	-117,539

Table 15: Summary of SIRIUS results for compounds less than 1000 Da under the time frame of Peak 4.

Precursor (Da)	**Predicted molecular formulas**	**Isotope score**	**Tree score**	**Total explained**	**Median mass error (ppm)**	**Top structure prediction**	**Structure similarity**	**Structure score**
305.21	$C_{19}H_{32}O_4$	5,381	96,614	96,952	5,817	8-[2-(3-Hydroxyhex-1-enyl)-5-oxocyclopentyl]octanoic acid	82,09	-67,305
	$C_{19}H_{30}O_3$	5,381	96,614	96,952	5,817	Havardic Acid F	77,52	-61,971

3.8.2 SIRIUS Analysis of Compounds Larger Than 1000 Da

SIRIUS was able to detect three compounds with masses above 1000 Da that were present in the siderophore containing sample yet absent in the siderophore negative sample. These three compounds had masses of 1050.39 Da, 1032.38 Da and 1034.40 Da and corresponded to the retention times of peaks 2, 1 and 3 respectively (Figure 24).

It was seen that MS1 spectra had assigned an m/z values of 516.19 and 525.19 to peaks 1 and 2 respectively. When comparing these values to the masses detected by SIRIUS in each case (1032.38 Da and 1050.39 Da) it was seen that the SIRIUS masses were exactly double that assigned to the peaks in the MS1 spectra. This is indicative that the MS1 values represent doubly charged versions of the larger molecules (Margolin Eren et al., 2019).

When looking at the MS2 spectra of these the compounds (Figure 25) similar patterns can be seen across all three, indicating that they may be closely related compounds. Although one might expect these compounds to be the siderophore in question due to them being present in the sample showing siderophore activity and not in the sample with no activity, one cannot say unequivocally that they are the siderophore. In order to do so, one would have to test a sample of these compound containing no other compounds for iron-chelating activity. For the case of this study, the current available evidence suggests that these are the most likely candidate compounds to represent the siderophore and thus are analysed as such.

1050.39 Da Compound

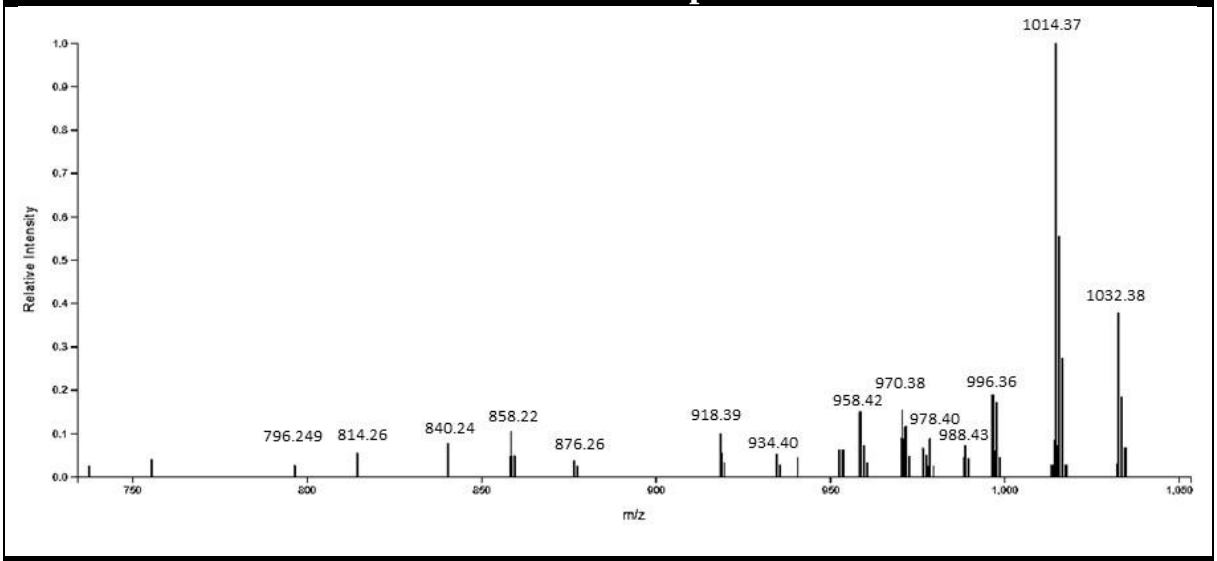

1032.38 Da Compound

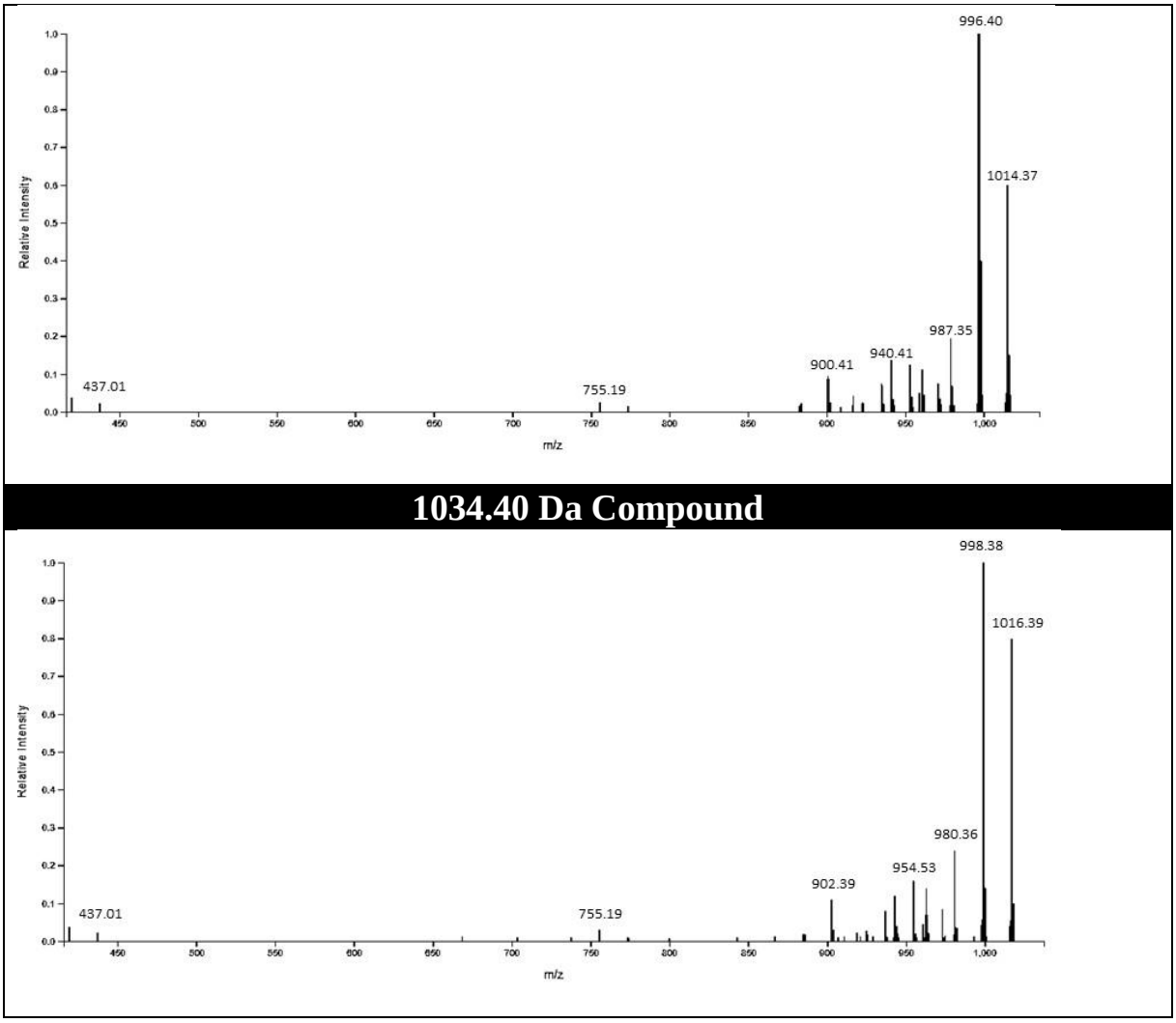

Figure 25: MS2 chromatograms for three compounds with masses larger than 1000 Da as detected by SIRIUS.

When comparing various fragmentation patterns across the three compounds, a pattern was seen to emerge. Peaks found in the MS2 spectra for the 1050.39 Da compound were seen to consistently be found in the corresponding MS2 data for the 1032.38 Da compound with a mass loss of 18 Da. Similarly, peaks found in the 1034.40 Da compound corresponded to those of the 1050.39 Da compound, with a mass loss of 16 Da in this case. A summary of corresponding peaks and mass losses across compounds can be seen in Table 16, which includes peaks with intensities of 0.1 and above.

Table 16: Masses of MS2 peaks with intensities of 0.1 and above for the compounds of 1050.39 Da, 1032.38 Da and 1034.40 Da. Mass losses of 18 Da are indicated by green arrows. Mass losses of 16 Da are indicated by blue arrows.

1034.40		1050.39		1032.38
		858.22		
902.39	-16	918.39		
942.39	-16	958.42	-18	940.41
954.42	-16	970.38	-18	952.41
		971.42		
962.39				960.38
980.36	-16	996.4	-18	978.35
		997.4		
998.38	-16	1014.37	-18	996.4
999.37	-16	1015.37	-18	997.1
		1016.37		
1016.39	-16	1032.38	-18	1014.37
1017.38	-16	1033.38	-18	1015.37

This pattern of mass losses is indicative that the compound with a mass of 1050.39 Da represents a parent compound, the compound of 1034.40 Da represents the parent compound with the loss of an oxygen molecule (Mw=16 Da), and that the compound of 1032.38 Da represents the parent compound with the loss of an H_2O molecule (Mw=18 Da).

Previous experiments (Section 3.5) indicated that the siderophore in question is a carboxylate-type siderophore and thus, if the compounds in question do in fact represent the siderophore it would be expected that their mass spectrums show fragmentation patterns

associated with carboxyl groups. Common mass losses found in carboxylate molecules include losses of 17 Da which represents the loss of an OH, losses of 45 Da which represent the loss on an CO_2H, and losses of 60 Da which represent the loss of $C_2H_4O_2$. Multiple mass losses corresponding to these values were seen in the case of each of the three detected compounds (Appendix B) indicating that the detected molecule may contain carboxylate groups. Additionally, multiple peaks showed similar or identical masses across the three compounds (Appendix B) further indicating that all three compounds are related.

3.8.2.1 SIRIUS Analysis of Compounds with Masses of 1050.39 Da and 1032.38 Da

Within the top 5 prediction results provided by SIRIUS for the compounds with masses of 1050.39 Da (Table 17) and 1032.38 Da (Table 18) one predicted formula stood out. This was $C_{45}H_{57}N_{13}O_{17}$ and was seen to be predicted for both compounds. In the case of the m/z 1032.38 compound this predicted formula was assigned an adduct of $[M-H_2O-H]^-$ which corresponds to the previous assumption that these are in fact the same compound with an H_2O loss in the case of the 1032.38 Da compound.

Table 17: Summary of top five SIRIUS predictions for the compound with a mass of 1050.39 Da.

Molecular formula	Isotope score	Tree score	Total explained intensity	Median mass error (ppm)	Median absolute mass error (ppm)
$C_{45}H_{59}N_{13}O_{18}$	4.332	116.831	67.163	-0.080	1.744
$C_{45}H_{57}N_{13}O_{17}$	4.332	116.831	67.163	-0.080	1.744
$C_{44}H_{61}N_9O_{21}$	4.039	116.846	67.163	1.315	3.030
$C_{44}H_{63}N_9O_{22}$	4.039	116.846	67.163	1.315	3.030
$C_{41}H_{55}N_{19}O_{16}$	3.785	116.011	67.163	2.985	3.641

Table 18: Summary of top five SIRIUS predictions for the compound with a mass of 1032.38 Da.

Molecular formula	Isotope score	Tree score	Total explained intensity	Median mass error (ppm)	Median absolute mass error (ppm)
$C_{46}H_{53}N_{17}O_{13}$	2.773	102.779	50.625	-1.480	1.792
$C_{46}H_{51}N_{17}O_{12}$	2.773	102.779	50.625	-1.480	1.792
$C_{45}H_{57}N_{13}O_{17}$	5.663	102.987	50.625	-0.105	0.981
$C_{45}H_{55}N_{13}O_{16}$	2.511	102.779	50.625	-0.105	0.981
$C_{55}H_{61}N_{3}O_{18}$	2.496	102.779	50.625	4,600	4,600

In the case of both compounds SIRUIS predicted the same molecular structure (Figure 26), Ala-Asn-Asp-His-Gly-Tyr-Asp-Asn-Phe. The highest structure prediction scores and substructure peak matching were seen in the case of the m/z 1050.39; however, these predictions were still not significant enough to say that this is in fact the structure of the compound in question. It can be said that the detected compound is likely to share a degree of structural similarity but is not identical to the compound predicted.

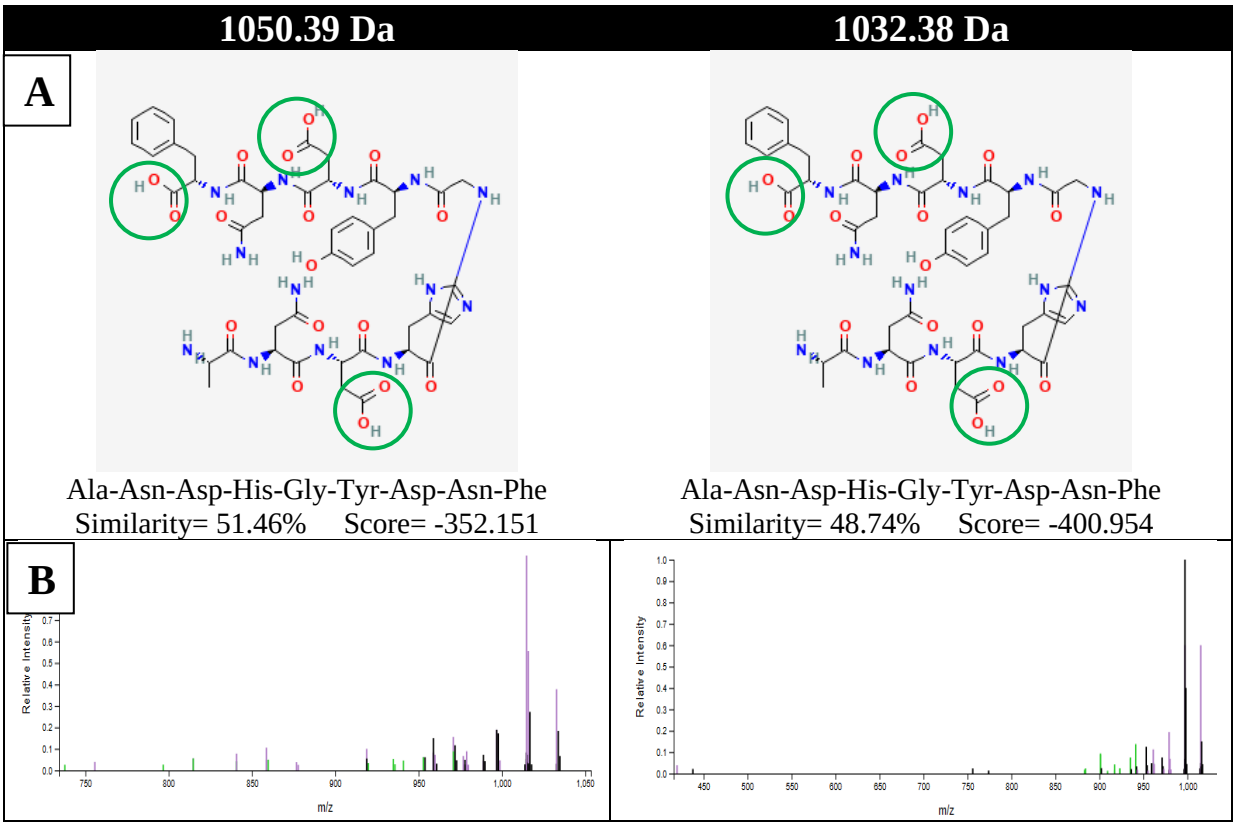

Figure 26:SIRIUS structure prediction results (A) and substructure peak matching results(B) for the predicted formula $C_{45}H_{57}N_{13}O_{17}$ for the detected compounds of 1050.39 Da and 1032.38 Da.

The predicted structure is seen to include three carboxyl groups (Figure 26, circled in green). Most siderophores, except for vibriobactin (Li et al., 2012), contain three iron binding groups and thus six donor oxygen atoms that form an octahedral structure to encapsulate the iron, producing a hexadentate centre (Hider and Kong, 2010). This stable tri- or tetradentate complex permits interaction with the siderophore-specific receptor.

When comparing the above predicted structure to the structures predicted by antiSMASH and PRISM, a lack of similarity can be observed. The predicted structures for cluster 8 include seven amino acids and PRISM structure predictions were assigned masses of either 761.44 or 743.43 Da. Here, much larger masses are seen as well as an additional two amino acids. These PRISM provided mass predictions do not account for all types of modifications and rather normally just represent the scaffold structure and therefore it is not intended to match an observed m/z to the predicted one, but rather is used as a guide as to whether a detected m/z could be considered being a product of a particular pathway. Additionally, the structure predictions here do not show any Thr residues, whereas a Thr residue was predicted with relatively high confidence in the structure predictions provided by antiSMASH and PRISM for cluster 8. This could indicate that the compound produced by cluster 8 is not the same

compound that was detected through the MS of the siderophore extract. This could be explained by three possibilities; that the biosynthetic pathway analysed is not in fact responsible for siderophore synthesis; that the extra compounds in the extract do not represent the siderophore; or a combination of both. It is possible that the peaks observed in the extract do represent the siderophore and that cluster 8 is responsible for its synthesis, however analysis of the MS data with SIRIUS does not lead to the correct compound structure identification and analysis of the pathway with antiSMASH or PRISM do not correctly predict the compound structure leading to a mismatch between the bioinformatic predictions and chemical analysis. In the scenario that the biosynthetic pathway analysed, and the compounds detected by SIRIUS are in fact the correct ones, this lack of similarity could be attributed to limitations of the software used. Neither the genome analysis tools, or SIRIUS were able to provide indisputable structure predictions and so it is possible that one or both predictions are incorrect. It is, however, unlikely that all elements of these predictions are completely wrong. If both predictions did in fact correspond to the same product, it would be expected that at least some degree of similarity would be observed.

If one were to make the biased assumption that these compounds with masses above 1000 Da detected do in fact represent siderophore rather than other iron-regulated biomolecules, then it could be said that the identified cluster 8 is in fact not likely to be the pathway responsible for siderophore synthesis. When looking at other pathways found in *T. viridans* Δ*1* identified by antiSMASH and PRISM, none of the detected clusters show predictions that are highly similar to that seen by SIRIUS. This could be explained by the biosynthetic pathway not being detected by the genome mining tools. As explained by (Blin et al., 2019), both antiSMASH and PRISM use a rule-based approach to determine what is annotated as a secondary metabolite biosynthetic gene cluster. These rules are based on existing knowledge regarding key biosynthetic steps and principles, which require the activity of individual or combinations of specific enzymes. These ‘core’ genes are used as anchors or probes to screen the genomic data of interest. This method is highly sensitive and precise for identifying biosynthesis genes for many classes of secondary metabolites, however it is only able detect pathways that follow the rules implemented by the software. It is possible that the siderophore of *T. viridans* is produced by a pathway that uses unknown or unrelated alternative enzymes and thus is not detected by genome mining tools, or that it is produced through the collaboration of more than one pathway.

Despite the fact that none of the antiSMASH detected clusters showed structure predictions with high degrees of similarity to SIRIUS predictions, each cluster was looked at more closely in an attempt to identify additional clusters that could potentially be better matched to SIRIUS predictions. Cluster 3 represents a NRPS gene cluster containing a total of five NRPS moieties. This particular cluster has not yet been assigned to a particular product and so it is possible that this cluster, cluster 3, is in fact responsible for the synthesis of siderophore in *T. viridans*. As explained in Section 3.7 and as explained by Crits-Christoph et al. (2020), it is rare for siderophore-specific transporters to be found in biosynthetic gene clusters that do not have siderophore functions. The presence of a TonB-dependent (TBD) siderophore receptor gene within cluster 8 thus provided the rationale for it being the primarily suspected pathway for siderophore synthesis. A closer look at cluster 3, however, revealed the presence of a TonB-dependent (TBD) receptor gene. Although not specifically detected as a TBD siderophore receptor gene by antiSMASH, no further classification was given and thus the possibility of this being a siderophore related TBD receptor gene cannot be excluded. It therefore would be unjust to exclude cluster 3 as an alternative possibility for the pathway responsible for siderophore synthesis.

When looking at the antiSMASH and PRISM predicted A-domain specificities for cluster 3 (Table 19), again variations are seen between the two software's. Also shown in Table 19 is the SIRIUS predicted amino acid residues found within the detected compounds with masses of 1050.39 and 1032.38. It can be seen that although a significant number of differences are found between the genomic predictions and SIRIUS predictions, four out of the nine amino acids predicted by SIRUS can be correlated to antiSMASH/PRISM predictions for cluster 3 (highlighted in Table 19). This represents a higher degree of similarity when compared to cluster 8.

Table 19:A-domain amino acid specificity in T. viridans cluster 3 using NRPSpredictor2 and PRISM. Amino acids predicted to be incorporated in the compounds of 1050.39 Da and 1032.38 Da also shown.

Module	**antiSMASH predicted physicochemical class**	**antiSMASH large clusters prediction**	**antiSMASH nearest Stachelhaus code and score**	**PRISM top three predictions**	Prism top prediction and score	Amino acids predicted by SIRIUS
						Ala
1	hydrophobic-aliphatic	N/A	Orn - 60% (weak)	Long-chain fatty acid, β-aminoalaninamide, Short-chain fatty acid	Long-chain fatty acid - 309.2	Asn
2	Hydrophilic	Asp, Asn, Glu, Gln, Aad	Asp - 90% (moderate)	Asp, Phe, (2S,6R)-diamino-(5R,7)-dihydroxy-heptanoic acid	Asp - 323.4	Asp
3	Hydrophilic	Asp, Asn, Glu, Gln, Aad	Lys - 70% (weak)	Arg, Phe, Lys	Arg - 509.8	His
4	Hydrophilic	Asp, Asn, Glu, Gln, Aad	Glu - 70% (weak)	Phe, Gly, Ser	Phe - 506.7	Gly
5	Hydrophobic-aliphatic	Ser, Thr, Dhpg, Hpg	Ser - 80% (moderate)	Ser, Ala, Arg	Ser - 631.3	Tyr
6	Hydrophilic	Asp, Asn, Glu, Gln, Aad	Asp - 90% (moderate)	Asp, Val, His	Asp - 295.4	Asp
7	Hydrophobic-aliphatic	Gly, Ala, Val, Leu, Ile, Abu, Iva	Gly - 90% (moderate)	Gly, Gly, Phe	Gly - 426.4	Asn
8	Hydrophilic	Asp, Asn, Glu, Gln, Aad	Asp - 100% (strong)	Phe, Asp, Arg	Phe - 332.4	Phe

The antiSMASH and PRISM structure predictions for the compound resulting from cluster 3 are all seen to contain carboxylate groups (Figure 27). When compared to the structure predicted by SIRIUS, again no high degree of similarity is seen. As discussed in Section 3.8.2.2, this could be due to the pathway and compound not being related or due to limitations of the software used. The predicted structures provided by PRISM for cluster 3 were assigned the predicted molecular weights of 996.5 and 978.5 Da. These molecular weights are closer to those predicted by SIRIUS than the PRISM predicted weights for cluster 8 (761.44 and 743.43 Da). The PRISM structure predictions for cluster 3 are both seen to

include hydrocarbon tails, a common feature of marine amphiphilic siderophores (Martinez and Butler, 2011).

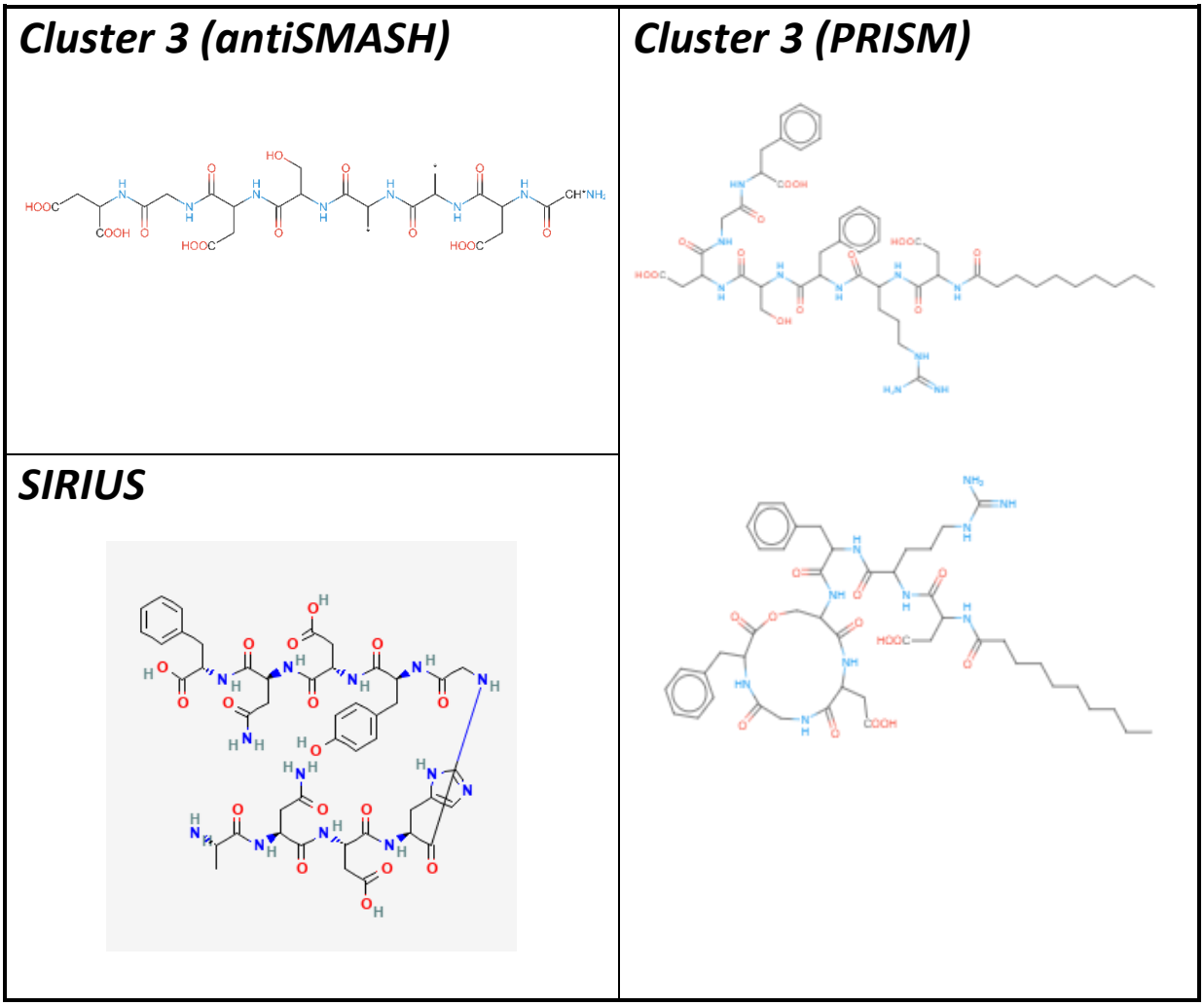

Figure 27: antiSMASH and PRISM predicted structures of T. viridans cluster 3 and SIRIUS predicted structure of compounds with masses of 1050.39 Ds and 1032.38 Da.

This analysis of cluster 3 indicates not only that it is possible that cluster 3, rather than cluster 8 is responsible for siderophore synthesis, but that it actually represents a stronger candidate for the production of the compounds detected by SIRIUS.

An additional feature of SIRIUS software is the CANOPUS tool which provides compound class predictions. In the cases of both the 1050.39 Da and the 1032.38 Da compounds a probability of 100% was assigned to the prediction that the molecule in question contains a carboxylic acid group or a derivative thereof and a probability of 99% was assigned to the molecules containing a carboxylic acid group (not a derivative). Although one still cannot say with absolute certainty that these molecules are the siderophore, there is some evidence to suggest that they could be.

3.8.2.2 SIRIUS Analysis of Compound with Mass of 1034.40 Da

The top 5 predictions provided by SIRIUS for the compound with a mass of 1034.40 Da (Table 20) did not show any formula that appeared to be related to the previously discussed formula of $C_{45}H_{57}N_{13}O_{17}$. One of the molecular formula predicions was however seen to be related (Table 20). This predicted formula was $C_{45}H_{57}N_{13}O_{16}$ which is exactly what would be expected if the previous assumptions that this molecule would represent $C_{45}H_{57}N_{13}O_{17}$ with the loss of an oxygen molecule were correct.

Table 20: Summary of top five SIRIUS predictions, as well as the eighth prediction (highlighted in green) for the compound with a mass of 1034.40 Da

Molecular formula	Isotope score	Tree score	Total explained intensity	Median mass error (ppm)	Median absolute mass error (ppm)
$C_{53}H_{63}N_7O_{14}S$	0	114.663	83.273	-0.214	0.846
$C_{52}H_{61}N_7O_{13}S$	0	114.663	83.273	-0.214	0.846
$C_{65}H_{59}N_5O_7S$	0	114.522	83.273	1.592	1.592
$C_{65}H_{57}N_5O_6S$	0	114.522	83.273	1.592	1.592
$C_{50}H_{55}N_{17}O_8S$	0	114.372	83.273	1.033	1.149
$C_{45}H_{57}N_{13}O_{16}$	0	114.256	73.554	-0.093	0.787

Unfortunately, no structure predictions were available for this predicted formula. CANOPUS results showed a 100% probability of this compound containing a carboxylic acid group.

The top 5 formula predictions for this compound all contained a sulphur atom, with the software assigning a probability of 99.972% that the compound contains at least 1 sulphur group. This was not seen in the case of the predictions for the other two compounds. Although not predicted, it is not impossible that all three compounds do in fact contain sulphur, which could account for the relatively low prediction scores seen in Section 3.8.2.1. The presence of sulphur atoms was also seen in several of the previous predictions discussed in Section 3.8.1. It should be noted that when looking at the given MS2 peaks, a pattern of

mass difference corresponding to the mass of sulphur (32.06 Da) was not seen, neither was the expected pattern of peak differences relating to the isotope ratio of sulphur. Additionally, if the compound in question did contain a sulphur, it would be expected that this would be predicted in the case of the largest related molecule, which is not seen in this case. This prediction of sulphur in the case of the 1034.40 Da compound should thus not be assigned a high degree of certainty, although a possibility, the data does not strongly point to the molecule in question including sulphur. Most known siderophores do not contain sulphur atoms, however, a select few have been described. Currently, there are seven known siderophores that contain sulphur atoms, which are shown in Table 21.

Table 21: Currently known sulphur-containing siderophores

Name	Organism	Formula	Structure
Aeruginic acid	*Pseudomonas aeruginosa*	$C_{10}H_{10}N_2O_3S_1$	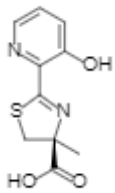
Albomycin δ1	*Actinomyces subtropicus*	$C_{36}H_{58}N_{10}O_{18}S_1$	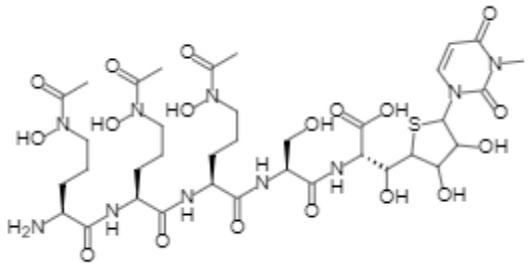
Albomycin δ2	*Actinomyces subtropicus*	$C_{37}H_{60}N_{12}O_{18}S_1$	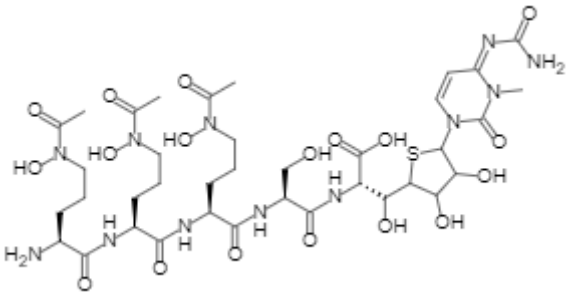

Albomycin ε	*Actinomyces subtropicus*	$C_{36}H_{59}N_{11}O_{17}S_1$	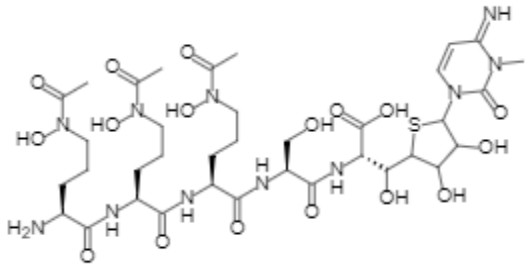
Anguibactin	*Vibrio anguillarum* *Vibrio cholerae* *Vibrio* sp. DS40M4	$C_{15}H_{16}N_4O_4S_1$	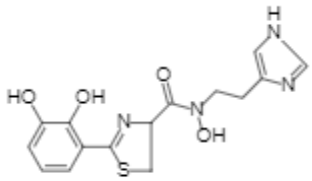
Desferrithiocin (ferrithiocin)	*Streptomyces antibioticus*	$C_{10}H_{10}N_2O_3S_1$	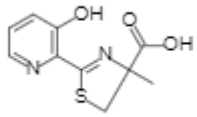
Petrobactin sulfate (petrobactin sulphonate)	*Marinobacter hydrocarbonoclasticus*	$C_{34}H_{46}N_6O_{14}S_1$	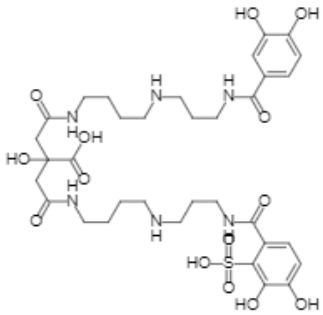
Pseudoalterobactin A	*Pseudoalteromonas* sp. KP20-4	$C_{42}H_{61}N_{11}O_{21}S_1$	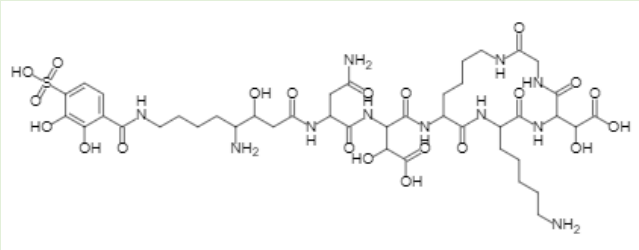
Pseudoalterobactin B	*Pseudoalteromonas* sp. KP20-4	$C_{41}H_{59}N_{13}O_{21}S_1$	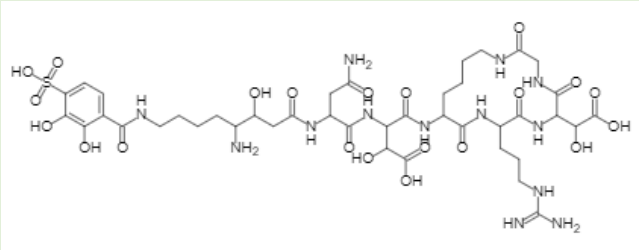

Thio-quinolobactin	*Pseudomonas fluorescens*	$C_{11}H_9N_1O_3S_1$	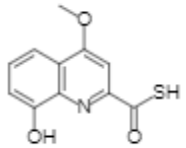
Enantio-pyochelin	*Pseudomonas fluorescens*	$C_{14}H_{16}N_2O_3S_2$	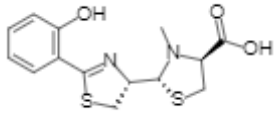
Petrobactin disulphonate	*Marinobacter aquaeolei*	$C_{32}H_{38}N_6O_{17}S_2$	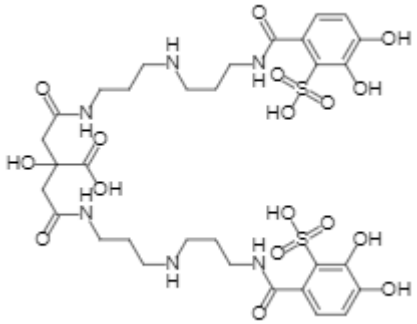
Pyochelin	*Burkholderia cepacia* *Pseudomonas aeruginosa* *Pseudomonas fluorescens* *Streptomyces scabies*	$C_{14}H_{16}N_2O_3S_2$	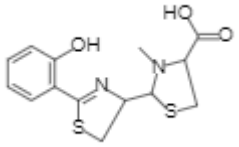
Pyridine-2,6-bis(thiocarboxylic acid)	*Pseudomonas putida* *Pseudomonas stutzeri*	$C_7H_5N_1O_2S_2$	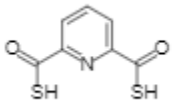
Thiazostatin	*Streptomyces tolurosus*	$C_{15}H_{18}N_2O_3S_2$	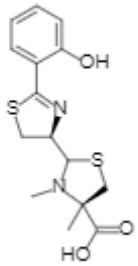

Micacocidin	*Ralstonia solanacearum*	$C_{27}H_{39}N_3O_4S_3$	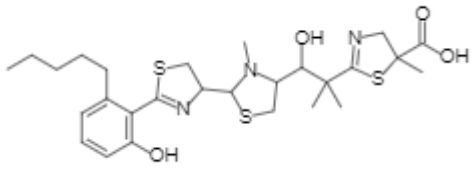
Yersiniabactin	*Pseudomonas syringae* *Salmonella enterica* *Yersinia enterocolitica* *Yersinia pestis*	$C_{21}H_{27}N_3O_4S_3$	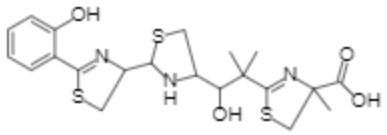

Interestingly, two known sulphur-containing siderophores (as highlighted in green in Table 19) are pseudoalterobactin A and pseudoalterobactin B, both produced by a marine *Pseudoalteromonas* sp. KP20-4 (Kanoh et al., 2003). The genomic region found within *T. viridans* Δ*1*, cluster 8, was seen to show some similarities to a pathway seen in a different *Pseudoalteromonas* strain (Section 3.7.6) Although slightly larger than the molecules detected to be produced by *T. viridans*, at 1087.4 Da for pseudoalterobactin A and 1101.4 Da for pseudoalterobactin B, these siderophores are seen to be of a similar size to the molecules detected here. A study by Chau et al. (2021) identified a putative genetic pathway responsible for preudoalterobactin synthesis in *Pseudoalteromonas* strain HM-SA03. When comparing this pathway to those found within *T. viridans*, no similarity is seen. No enzymes required for the addition of sulphur to a biomolecule are seen with cluster 8 of *T. viridans*, however in the case of the pseudoalterobactins there are also no obvious sulphur adding enzymes encoded by putative gene cluster. It is hypothesised that either a proposed cysteine desulfurase, located 10 kb downstream from the last NRPS gene, may provide sulphur to the pseudoalterobactins, or that an enzyme acting in trans and therefore not clustered with the NRPS/PKS genes, may be involved in the sulfonation of pseudoalterobactins (Chau et al., 2021). The known structures of the pseudoalterobactins additionally do not show similarity to those predicted by SIRIUS for the compounds with masses of above 1000 Da produced by *T. viridans*. There is thus no evidence that the pathway or compounds identified in this study are related to the pseudoalterobactins.

The SIRIUS software can provide structural predictions based on MS data. It does this by comparing the obtained MS spectrum with all the compounds found within an extensive list of databases. If the spectrum of the unknown fully coincides with one of the database

spectrums, it means that the structural formula of the unknown is identical to that of the reference, thus the unknown compound structure can be identified. If no complete match is found, the problem of structure elucidation arises (Pauli et al., 2014). In this case, no complete structural matches were found, indicating that the compound in question is novel and thus not found in any available databases. Through the use of the SIRIUS software, we can get clues into what the structure may look like, but to know for sure, further studies are required.

NMR is the most widely used technique for characterising the structure of novel organic molecules. NMR spectra encode the local environments of the atoms that make up a molecule, providing molecular "fingerprints" that can be used to deduce connectivity and relative stereochemistry (Huang et al., 2021). Unfortunately, NMR studies were outside the scope of this study, so the structure of this compound produced by *T. viridans* (which is possibly a novel siderophore) remains unknown. MS data analysed with SIRIUS software has, however, indicated that it is likely to have a molecular weight of 1050.39 Da, contain carboxylate groups, and be of novel peptide structure.

3.10 Proteomic Analysis

Towards identifying the metabolic pathway responsible for siderophore synthesis in *T. viridans*, total protein extracts were prepared from cultures grown with iron (where low levels of siderophore synthesis proteins are expected) and without iron (where high levels of these proteins would be expected). Following the total protein extractions (Section 2.13), extracts were analysed by SDS-PAGE to assess their quality before being subjected to proteomic analysis. As shown in Figure 28, the protein extractions were successful and thus proteomic analysis was performed on these samples.

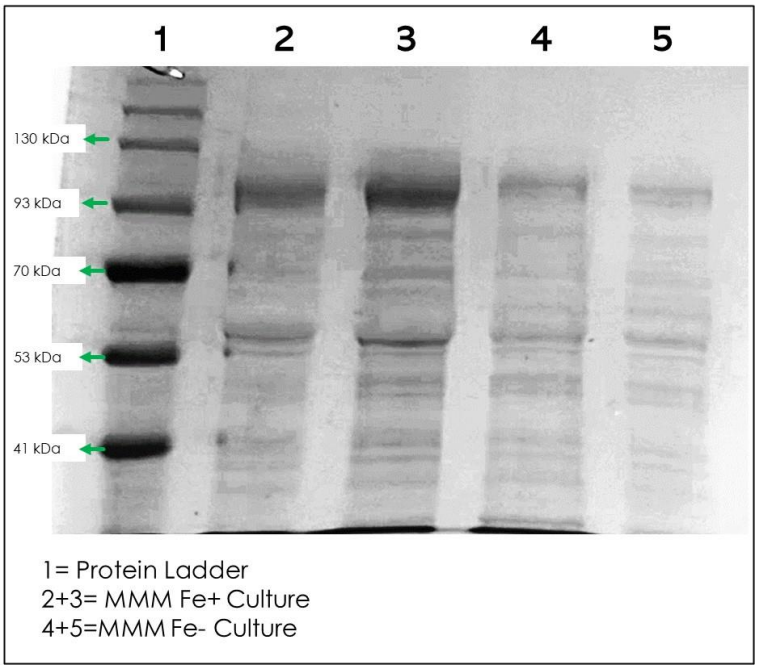

Figure 28: SDS-PAGE of total protein extracts from T. viridans cultures grown with and without iron to assess extraction quality prior to proteomic analysis.

If the hypothesis that cluster 8 (Figure 18) is responsible for synthesis of the siderophore detected through the various assays was correct, it would be expected that the biosynthesis proteins for this cluster would be found in the sample extracted from iron-starved cultures and that they would be absent or found in much lower quantities in the case of the culture grown with sufficient iron. Examples of studies following this same rationale include that by Teng et al. (2018) in which comparative transcriptomic and proteomic analyses revealed the upregulated expression of virulence and iron transport factors of *Aeromonas hydrophila* under iron limitation.

Results were analysed using MaxQuant version 2.1.3.0 and Perseus version 2.0.6.0 according to the developers' instructions (Tyanova et al., 2016). Since the proteins of interest were expected to be found in higher amounts in the case of the iron-starved sample, the proteins identified for each sample were compared, and those found exclusively or in higher amounts in the case of the iron-starved culture were selected for further analysis. Ten peptides were identified in higher amounts in the case of the iron starved culture (Figure 29) and thus were looked at in more detail (Table 22).

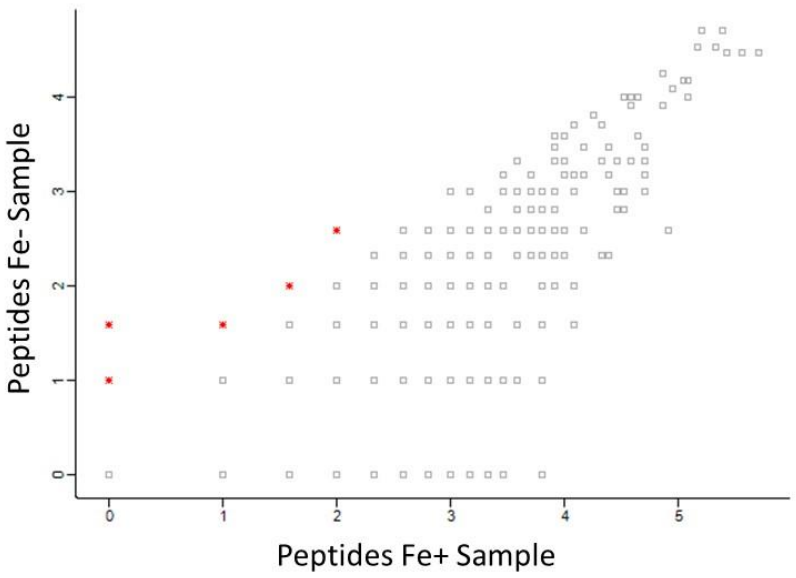

Figure 28: Graph displaying relative amounts of the peptides identified in the iron-starved (Fe-) and iron-sufficient (Fe+) protein extracts of T. viridans. Axes represent the log of the number of unique peptides found in each sample.

Table 22: Table Summarising peptides that were found in higher amounts in the case of the iron-starved protein sample when compared to the iron-sufficient protein sample and the corresponding proteins from which the peptides originate.

Protein Precursor ID	Description	Peptides Fe+ Sample*	Peptides Fe- Sample*
TVIR_01940	50S ribosomal protein L16	2	3
TVIR_10215	hypothetical protein	1	2
TVIR_16330	50S ribosomal protein L20	3	4
TVIR_01920	50S ribosomal protein L2	4	6
TVIR_04055	peptide synthase	2	3
TVIR_27270	50S ribosomal protein L21	2	3
TVIR_22480	hypothetical protein	2	3
TVIR_01960	50S ribosomal protein	1	3

	L24		
TVIR_02005	30S ribosomal protein S13	3	4
TVIR_01980	50S ribosomal protein L6	1	2

*Number of peptides detected

Unfortunately, none of these proteins of interest correspond to the biosynthetic pathway, cluster 8. Only one out of the twenty-eight proteins belonging to the suspected pathway was found in either of the samples. This was a Colicin I receptor precursor and was not seen to be upregulated in the iron-starved sample. This did not allow identification of the responsible pathway since it could not be determined whether or not the production of the suspected proteins was upregulated, as no data was provided for most of the proteins of interest.

As explained by both Choong et al. (2015) and Schork et al. (2021), there are several reasons why there may be protein data points missing from proteomic experiments and that it is a fairly common problem. These reasons include the fact that the detection of certain proteins (membrane proteins, hydrophobic proteins, low-abundance proteins, very small proteins, and those without trypsin cleavage sites) is constrained by the detection capability of MS technology (Beck et al., 2011; Farrah et al., 2012; Marko-Varga et al., 2012; Lane et al., 2013; Ezkurdia et al., 2014; Omenn, 2014). Additionally, missing proteins may be caused by the nature of the MS measurement, for example, stochastic selection of precursor ions for fragmentation. Additional data filters, such as requiring at least two unique peptides or normalization steps, may also lead to missing values (Schork et al., 2021). Often for a certain missing value in the data, it is not clear why exactly it is missing (Schork et al., 2021).

In this study total protein extracts were prepared from 5-day old cultures, which in the case of the iron-deprived culture contained low levels of biomass. In order to determine whether or not the lack of detected proteins could be due to the samples containing low concentrations of protein, the data was searched for the presence and amounts of three housekeeping proteins (Table 23).

Table 23: Summary of the presence or absence of three housekeeping proteins seen in both the Iron-starved and iron-sufficient protein extracts.

Protein	Reference	Detected in Fe+ Sample	Detected in Fe- Sample
DNA gyrase subunit A	Rocha et al., 2015	No	No
DNA gyrase subunit B	Rocha et al., 2015	Yes	No
RpoB RNA polymerase subunit B	Ogier et al., 2019	Yes (higher amount)	Yes (lower amount)

As described by Ogier et al. (2019) and Rocha et al. (2015) one would expect these housekeeping proteins to be constantly found in similar amounts. The fact that this was not seen indicates problems with the protein samples that were analysed. It appears that the samples analysed did not contain high enough concentrations for successful proteomic analysis.

Despite low protein levels and missing data points, it was seen that a peptide synthase protein was found in slightly higher amounts in the iron-starved sample (Table 22). This particular peptide synthase corresponds to cluster 3 (Figure 17).

Cluster 3, as previously discussed in Section 3.8.2.1, represents a NRPS gene cluster containing a total of five NRPS moieties. The analysis of cluster 3 indicates not only that it is possible that cluster 3, rather than cluster 8 is responsible for siderophore synthesis, but that it actually could represent a stronger candidate. This, combined with a higher amount of a peptide synthase linked to cluster 3 being found in the iron-starved sample protein extract, indicates that it is possible that the siderophore synthesis is carried out by cluster 3. As a result of the low protein levels and missing data points seen here, this cannot however be confirmed and remains as just a possibility.

There are various other methods of linking a particular gene to a specific metabolite. Alternative proteomic-based methods include SDS-PAGE, MALDI-TOF, and Yeast two-hybrid systems (Bouchez and Hofte, 1998). Non-proteomic-based methods include Targeting

Induced Local Lesions In Genomes (TILLING) (Henikoff et al., 2004), map-based cloning (Sun et al., 2004), and methods involving the suppression or over-expression of genes. (Matzke and Matzke, 1995). RNA based methods include the use of RT PCR which can be used to track gene expression (Jalali et al., 2017). In this case, it is recommended that one of these alternative methods be attempted to identify the genome region responsible for synthesizing a siderophore by *T. viridans*.

Chapter 4: General Discussion and Conclusion

Natural products produced by bacteria, fungi, plants, and marine animals represent a large group of diverse chemical entities that display a broad range of biological activities. These

molecules have been used by humans since ancient times and in folklore for the treatment of many diseases and illnesses. Today, their uses are both widespread and diverse, particularly in the fields of agriculture and medicine (Bhanot et al., 2011; Demain, 2014). In recent years the focus of NP discovery has shifted away from those produced solely by terrestrial organisms, and scientists have begun to also search the oceans for novel compounds (Montaser and Leusch, 2011). The search for novel marine NPs has already resulted in the isolation of tens of thousands of metabolites (Fusetani, 2000) with diverse biological activities, including antibiotic, antifungal, toxic, cytotoxic, neurotoxic, antimitotic, antiviral, antineoplastic, and immunosuppression activities (Kelecom, 1999). One such NP is siderophores, which are secondary metabolites produced by various microorganisms to scavenge iron from the environment.

Thalassomonas viridans is a strictly aerobic, halophilic, chemo-organotrophic marine bacterium that was first isolated from cultivated oysters off the Mediterranean coast of Spain near Valencia (Macián et al., 2001). Various tests for siderophore production showed that *T. viridans* produces siderophores when grown under iron-limited conditions.

Growth and siderophore production comparisons showed that a deletion strain of *T. viridans* had a faster growth rate and unchanged rate of siderophore production when compared to the original strain. As a result, and in order to simplify genome mining studies, the deletion strain (*T. viridans* $\Delta 1$) was selected to be used exclusively for the remainder of this study. This was helpful since it allowed for 1.1 Mb of genetic material to immediately be excluded from being potentially responsible for siderophore synthesis.

Since the start of the genome sequencing of microorganisms, treasures of previously unseen natural product biosynthetic genes have been revealed (Leal et al., 2012; Chaudhary et al., 2013). Genome sequencing gives clues to understanding the biosynthesis of novel drug molecules and unlocking novel chemistry (Rutledge and Challis, 2015). It also provides direct access to the genome, allowing researchers to “mine” for a wide range of novel compounds at a nucleotide level. In this study, despite it being seen that *T. viridans* clearly does produce siderophores, neither antiSMASH nor PRISM were able to identify any *T. viridans* gene clusters as siderophore producing. This is likely due to the pathway responsible being novel and thus not detectable by these programs. It is recommended that when using these programs that care be taken. If a particular secondary metabolite is not predicted to be encoded by a genome, one cannot say that it is not produced by the organism in question.

antiSMASH analysis was able to identify a TonB siderophore-dependent receptor gene within cluster 8 of *T. viridans* Δ*1*. A study by Crits-Christoph et al. (2020) has shown that it is rare for siderophore-specific transporters to be found in biosynthetic gene clusters that do not have siderophore functions. This resulted in cluster 8 being presented as a pathway potentially responsible for siderophore synthesis. It was seen that A-domain amino acid specificity predictions and structure predictions for *T. viridans* Cluster 8 varied across the two genome-mining tools used (antiSMASH and PRISM). This variation across platforms displays another limitation to these tools and highlights the fact that these are merely predictions and that these tools are not able to give the exact results.

During siderophore purification steps it was seen that siderophore produced by *T. viridans* Δ*1* bound to SEPABEADS® SP207 resin, indicating that it is a hydrophilic siderophore. As of date, most of the known marine siderophores have been seen to be produced as families of amphiphiles, consisting of an iron (III)-binding headgroup and a fatty acid tail (Chiu et al., 2020; Alok et al., 2020; Kramer et al., 2020; Malviya et al., 2020; Van Doan et al., 2020; Kour et al., 2020). These amphiphilic siderophores have been seen to range from being hydrophobic, such as the amphibactins and ochrobactins, to hydrophilic, such as the loihichelins (Kour et al., 2020). It was also seen that siderophore activity was detected in multiple acetone concentration elutions rather than just one which could be explained by the fact that variations in hydrophobicity are often seen within single families of amphiphilic siderophores, due to variations in the length of fatty acid chains on a constant headgroup.

Siderophores can be classified into different groups based on their functional groups and hydrophobicity. These include α-hydroxycarboxylates (carboxylates), hydroxamates, catecholates, and mixed-type siderophores (Neilands, 1990). In order to determine to which group the siderophore produced by *T. viridans* belong, various chemical tests were performed. The results of these tests indicated that the siderophore in question is a carboxylate, which was confirmed using the spectrometric tests of Neilands (1981) and Shenker et al. (1992). Carboxylate siderophores are known to be produced by various organisms including *Rhizobium*, *Staphylococcus*, *Zygomycota*, and various marine bacteria species (Butler and Theisen, 2010).

Siderophores have been seen to be involved in various processes besides iron acquisition. These processes include heavy metal biosorption, iron overload disease treatment, antibiosis, quorum sensing, and plant growth promotion (Aravinth, 2012). The siderophore in question

was tested for antimicrobial activity using the agar well diffusion assay but no activity that could be linked to the siderophore was seen. The siderophore was tested for binding activity with aluminium, vanadium, and arsenic and it was seen to have a high binding affinity for aluminium. The siderophore produced by *T. viridans* could thus be a potential treatment agent for aluminium overload disease as has been done previously with other aluminium chelating agents such as; deferoxamine, ascorbate, and Feralex-G (Ciancioni et al., 1984; Nebeker et al., 1984; Molitoris et al., 1987; Yokel et al., 1996; Kruk et al., 2004).

MS analysis of the purified siderophore extract was performed with the goal of identifying the structure of the unknown siderophore. MS data analysed with SIRIUS software detected three seemingly related compounds with masses of 1032.38 Da, 1034.40 Da and 1050.39 Da. Numerous losses that would be expected in the case of carboxylate molecules were seen and the CANOPUS tool (built into SIRIUS) assigned a 100% probability of all three compounds containing a carboxylic acid or a derivative thereof. Currently, it cannot be said with absolute confidence that these compounds represent siderophores rather than other iron-regulated biomolecules. In order to do so, samples containing these compounds exclusively would need to be checked for siderophore activity. It is recommended that in future studies mass-directed fractionation is performed.

Molecular structure predictions generated by SIRIUS for the compounds in question showed the same prediction for both the 1050.39 Da and the 1032.38 compounds. This structure corresponds to Ala-Asn-Asp-His-Gly-Tyr-Asp-Asn-Phe. No structural predictions were able to be generated for the 1034.40 Da compound. The fact that the structure predictions given here were assigned relatively low similarity and confidence score is highly indicative that these molecules are novel and thus cannot be found in any databases. When dealing with the structural elucidation of a novel compound, rather than the identification of a known one, the methods used in this study are not sufficient to provide an answer. NMR is the most widely used technique for characterising the structure of novel organic molecules. NMR spectra encode the local environments of the atoms that make up a molecule, providing molecular “fingerprints” that can be used to deduce connectivity and relative stereochemistry (Huang et al., 2021). Unfortunately, NMR studies were outside this study's scope, so the structure of the novel siderophore produced by *T. viridans* remains unknown. It is recommended that future studied make use of NMR techniques in order to elucidate the structure of the novel siderophore produced by *T. viridans*.

When comparing the SIRIUS predicted structure to those predicted by antiSMASH and PRISM, a low degree of similarity was seen in the case of cluster 8. This resulted in other clusters being looked at more closely. It was seen that antiSMASH/PRISM predictions for cluster 3 showed a higher degree of similarity to SIRIUS predictions than cluster 8. While still no complete matches are seen between genome mining and MS analysis predictions, it was seen that cluster 3 represents an alternative candidate for being responsible for the synthesis of the detected compounds to cluster 8.

Since the advent of high throughput DNA sequencing, the ability to identify genes has extensively surpassed the ability to determine the functions of these genes. Numerous complete genome sequences are now available, and so the focus of many researchers across the world has been directed towards functional genomics and assigning functions to newly identified DNA sequences (Srinivasan et al., 2005). In this study, the approach of proteomic MS was selected in attempt to confirm whether or not the suspected genomic pathway was responsible for siderophore synthesis in *T. viridans*. Unfortunately, in the case of the originally suspected cluster 8, MS results showed no detection of the majority of the proteins of interest in either the test or control samples. This was likely due to the protein samples that were analysed not being of high enough concentrations for successful proteomic analysis. This highlights the importance of the quality of samples being subjected to MS analysis.

Irrespective of low protein levels, it was seen that a peptide synthase protein belonging to the proposed alternative pathway, cluster 3, was found in slightly higher amounts in the iron-starved sample. This further indicated that it is possible that siderophore synthesis is carried out by cluster 3. As a result of the low protein levels and missing data points seen here, this cannot however be confirmed and remains as just a possibility. It is recommended that further studies include alternative methods of functional genomics in order to link a specific pathway to the production of siderophore in *T. viridans.* One such method is the use of gene knock-out systems. This approach, which involves the disruption of genes for the acquisition of knock-out mutants provides a direct route to determining function as opposed to most other approaches of determining gene function that are correlative (Srinivasan et al., 2005).

This study once again highlights the importance of the marine environment as sources of novel natural products. It is the first study to show siderophore production by *T. viridans.* Through the use of a combination of both culture dependent and culture independent strategies it has been shown that this marine organism produces a novel carboxylate-type

siderophore. Although the chemical structure and genomic region responsible for the synthesis of this siderophore remain unknown, this study serves as the foundation for future studies investigating this novel NP.

References

Abergel, R.J., Moore, E.G., Strong, R.K. and Raymond, K.N., 2006. Microbial evasion of the immune system: structural modifications of enterobactin impair siderocalin recognition. *J. Am. Chem. Soc*., 128, pp.10998-10999.

Adams, S., 2019. *Bioactivity-and-genome guided isolation of a novel antimicrobial protein from Thalassomonas viridans.* MSc. The University of the Western Cape.

Alanjary, M., Kronmiller, B., Adamek, M., Blin, K., Weber, T., Huson, D., Philmus, B. and Ziemert, N., 2017. The Antibiotic Resistant Target Seeker (ARTS), an exploration engine for antibiotic cluster prioritization and novel drug target discovery. *Nucleic Acids Res*., 45, pp.42-48.

Alav, I., Kobylka, J., Kuth, M., Pos, K., Picard, M., Blair, J. and Bavro, V., 2021. Structure, Assembly, and Function of Tripartite Efflux and Type 1 Secretion Systems in Gram-Negative Bacteria. *Chemical Reviews*, 121(9), pp.5479-5596.

Amsaveni, R., Sureshkumar, M., Aravinth, A., Mary, J.R. and Vivekanandhan, G., 2016. Production of Non-Ribosomal Peptide Synthetase (NRPS)- Dependent Siderophore by Aeromonas Isolates. *Iran Biomed J.*, 20(4), pp.235-240.

Andrews, S.C., Robinson, A.K. and Quinones, F.R., 2003. Bacterial iron homeostasis. *FEMS Microbiol. Rev*., 27, pp.215-237.

Antismash.secondarymetabolites.org. 2022. *antiSMASH bacterial version*. [online] Available at: <https://antismash.secondarymetabolites.org/> [Accessed 3 May 2022].

Aravinth, A., 2012. *Screening and characterization of siderophores produced by marine bacteria.* PhD. Madurai Kamraj University.

Arnow, L., 1937. Colorimetric determination of the components of 3,4-dihydroxyphenylalaninetyrosine mixtures. *Journal of Biological Chemistry*, 118(2), pp.531-537.

Azpiroz-Leehan, R. and Feldmann, K.A., 1997. T-DNA insertion mutagenesis in Arabidopsis: going back and forth. *Trends in Genetics*, 13(4), pp.152-156.

Baars, O., Morel, F.M.M. and Perlman, D.H., 2014. ChelomEx: Isotope-Assisted Discovery of Metal Chelates in Complex Media Using High-Resolution LC-MS. *Anal. Chem*, 86(22), pp.11298–11305.

Baars, O., Zhang, X., Morel, F.M.M. and Seyedsayamdost, M.R., 2015. The Siderophore Metabolome of Azotobacter vinelandii. *Appl. Environ. Microbiol.*

Balado, M., Benzekri, H., Labella, A., Claros, M., Manchado, M., Borrego, J., Osorio, C. and Lemos, M., 2017. Genomic analysis of the marine fish pathogen Photobacterium damselae subsp. piscicida: Insertion sequences proliferation is associated with chromosomal reorganisations and rampant gene decay. *Infection, Genetics and Evolution*, 54, pp.221-229.

Balado, M., Lages, M., Fuentes-Monteverde, J., Martínez-Matamoros, D., Rodríguez, J., Jiménez, C. and Lemos, M., 2018. The Siderophore Piscibactin Is a Relevant Virulence Factor for Vibrio anguillarum Favored at Low Temperatures. *Frontiers in Microbiology*, 9.

Balado, M., Osorio, C. and Lemos, M., 2008. Biosynthetic and regulatory elements involved in the production of the siderophore vanchrobactin in Vibrio anguillarum. *Microbiology*, 154(5), pp.1400-1413.

Balibar, C., Vaillancourt, F. and Walsh, C., 2005. Generation of D Amino Acid Residues in Assembly of Arthrofactin by Dual Condensation/Epimerization Domains. *Chemistry & Biology*, 12(11), pp.1189-1200.

Baltz, R., 2011. Function of MbtH homologs in nonribosomal peptide biosynthesis and applications in secondary metabolite discovery. *Journal of Industrial Microbiology & Biotechnology*, 38(11), pp.1747-1760.

Banin, E., Vasil, M.L. and Greenberg, E.P., 2005. Iron and Pseudomonas aeruginosa biofilm formation. *Proc. Natl. Acad. Sci. USA*, 102, pp.11076– 11081.

Barry, S.M. and Challis, G.L., 2009. Recent advances in siderophore biosynthesis. *Curr. Opin. Chem. Biol.*, 13, pp.205-215.

Baysse, C., De Vos, D., Naudet, Y., Vandermonde, A., Ochsner, U., Meyer, J., Budzikiewicz, H., Schäfer, M., Fuchs, R. and Cornelis, P., 2000. Vanadium interferes with siderophore-mediated iron uptake in Pseudomonas aeruginosa. *Microbiology*, 146(10), pp.2425-2434.

Beasley, F.C., Marolda, C.L., Cheung, J., Buac, S. and Heinrichs, D.E., 2011. Staphylococcus aureus transporters Hts, Sir, and Sst capture iron liberated from human transferrin by staphyloferrin A, staphyloferrin B, and catecholamine stress hormones, respectively, and contribute to virulence. *Infect. Immun.*, 79, pp.2345-2355.

Beck, M., Claassen, M. and Aebersold, R., 2011. Comprehensive proteomics. *Current Opinion in Biotechnology*, 22(1), pp.3-8.

Bell, M., 2001. Biofilms: A clinical perspective. *Curr. Infect. Dis. R.*, 3, pp.483-486.

Bennett, J. W., 1997. White paper: genomics for filamentous fungi. *Fungal Genet. Biol.*, 21(1), pp.3-7.

Bérdy, J., 2012. Thoughts and facts about antibiotics: Where we are now and where we are heading. *Journal of Antibiotics*, 65(8), pp.385-395.

Bhanot, A., Sharma, R. and Noolvi, M.N., 2011. Natural sources as potential anti-cancer agents: a review. *Int J Phytomed*, 3, pp.9-26.

Blast.ncbi.nlm.nih.gov. 2022. *BLAST: Basic Local Alignment Search Tool*. [online] Available at: <https://blast.ncbi.nlm.nih.gov/Blast.cgi> [Accessed 7 April 2022].

Bleuel, C., Große, C., Taudte, N., Scherer, J., 2005. TolC is involved in enterobactin efflux across the outer membrane of Escherichia coli. *J. Bacteriol.* 187, pp.6701-6707.

Blin, K., Pedersen, L.E., Weber, T. and Lee, S.Y., 2016. CRISPy-web: An online resource to design sgRNAs for CRISPR applications. *Synth. Syst. Biotechnol.*, 1, pp.118-121.

Blin, K., Shaw, S., Steinke, K., Villebro, R., Ziemert, N., Lee, S., Medema, M. and Weber, T., 2019. antiSMASH 5.0: updates to the secondary metabolite genome mining pipeline. *Nucleic Acids Research*, 47(W1), pp.W81-W87.

Blunt, J.W., Carroll, A.R., Copp, B.R., Davis, R.A., Keyzers, R.A., and Prinsep, M.R., 2018. Marine Natural Products. *Natural Product Reports*, 35(1), pp.8-53.

Böcker, S. and Dührkop, K., 2016. Fragmentation trees reloaded. *Journal of Cheminformatics*, 8(1).

Böcker, S., Letzel, M., Lipták, Z. and Pervukhin, A., 2008. SIRIUS: decomposing isotope patterns for metabolite identification†. *Bioinformatics*, 25(2), pp.218-224.

Bouchez, D. and Hofte, H., 1998. Functional genomics in plants. *Plant Physiology*, 118(3), pp.725-732.

Boukhalfa, H. and Crumbliss, A.L., 2002. Chemical aspects of siderophore mediated iron transport. *BioMetals*, 15, pp.325-339.

Braud, A., Jézéquel, K., Bazot, S. and Lebeau, T., 2009. Enhanced phytoextraction of an agricultural cr- and pb-contaminated soil by bioaugmentation with siderophore-producing bacteria. *Chemosphere*, 74, pp.280-286.

Braun, V. and Braun, M., 2002. Iron transport and signalling in Escherichia coli. *FEBS Lett*., 529, pp.78-85.

Braun, V. and Killmann, H., 1999. Bacterial solutions to the iron supply problem. *Trends Biochem. Sci*., 24, pp.104-109.

Braun, V., Pramanik, A., Gwinner, T., Koberle, M. and Bohn, E., 2009. Sideromycins: tools and antibiotics. *BioMetals*, 22, pp.3-13.

Brickman, T. and Armstrong, S., 2005. Bordetella AlcS Transporter Functions in Alcaligin Siderophore Export and Is Central to Inducer Sensing in Positive Regulation of Alcaligin System Gene Expression. *Journal of Bacteriology*, 187(11), pp.3650-3661.

Bsat, N., Herbig, A., Casillas-Martinez, L., Setlow, P. and Helmann, J.D., 1998. Bacillus subtilis contains multiple Fur homologues: identification of the iron uptake (Fur) and peroxide regulon (PerR) repressors. *Mol. Microbiol*., 29, pp.189-198.

Butler, A., 2005. Marine Siderophores and Microbial Iron Mobilization. *BioMetals*, 18(4), pp.369-374.

Butler, A., and Theisen, R.M. 2010. Iron(III)–Siderophore coordination chemistry: Reactivity of marine siderophores. *Coordination Chemistry Reviews*, 254(3-4), pp.288-296.

Castellani, A. and Chalmers, A., 1919. *Manual of tropical medicine*. 3rd ed. William Wood and Co., New York.

Caza, M., Lépine, F. and Dozois, C.M., 2011. Secretion, but not overall synthesis, of catecholate siderophores contributes to virulence of extraintestinal pathogenic Escherichia coli. *Mol. Microbiol*., 80, pp.266-282.

Chakraborty, R., Lemke, E., Cao, Z., Klebba, P.E. and van der Helm, D., 2003. Identification and mutational studies of conserved amino acids in the outer membrane receptor protein, FepA, which affect transport but not binding of ferricenterobactin in Escherichia coli. *Biometals*, 16, pp.507-518.

Challis, G.L., 2005. A widely distributed bacterial pathway for siderophore biosynthesis independent of nonribosomal peptide synthetases. *Chembiochem*., 6, pp.601-11.

Challis, G.L., Ravel, J. and Townsend, C.A., 2000. Predictive, structure-based model of amino acid recognition by nonribosomal peptide synthetase adenylation domains. *Chemistry and Biology*, 7(3), pp.211-223.

Chan, Y.A., Podevels, A.M., Kevany, B.M. and Thomas, M.G., 2009. Biosynthesis of polyketide synthase extender units. *Nat. Prod. Rep.*, 26(1), pp.90–114.

Chau, R., Pearson, L., Cain, J., Kalaitzis, J. and Neilan, B., 2021. A pseudoalteromonas clade with remarkable biosynthetic potential. *Applied and Environmental Microbiology*, 87(6).

Chaudhary, A.K., Dhakal, D. and Sohng, J.K., 2013. An insight into the '-omics' based engineering of Streptomycetes for secondary metabolite overproduction. *BioMed Research International*, 2013, pp1-16.

Chen, J., Guo, Y., Lu, Y., Wang, B., Sun, J., Zhang, H., and Wang, H., 2019. Chemistry and biology of siderophores from marine microbes. *Marine Drugs*, 17(10), p.562.

Chi, Z., Wang, X., Ma, Z., Buzdar, M. and Chi, Z., 2011. The unique role of siderophore in marine-derived Aureobasidium pullulans HN6.2. *BioMetals*, 25(1), pp.219-230.

Chim, N., Habel, J.E., Johnston, J.M., Krieger, I., 2011. The TB structural genomics consortium: a decade of progress. *Tuberculosis*, 91, pp.155-172.

Chiu, C., Jheng, T., Peng, B., Chung, W. and Mong, K., 2020. Convergent Synthesis of Macrocyclic and Linear Desferrioxamines. *European Journal of Organic Chemistry*, 2020(24), pp.3650-3659.

Choong, W., Chang, H., Chen, C., Tsai, C., Hsu, W., Chen, Y. and Sung, T., 2015. Informatics View on the Challenges of Identifying Missing Proteins from Shotgun Proteomics. *Journal of Proteome Research*, 14(12), pp.5396-5407.

Chowdappa, S., Jagannath, S., Konappa, N., Udayashankar, A. and Jogaiah, S., 2020. Detection and Characterization of Antibacterial Siderophores Secreted by Endophytic Fungi from Cymbidium aloifolium. *Biomolecules*, 10(10), p.1412.

Ciancioni, C., Poignet, J., Narel, C., Delons, S., Mauras, Y., Allain, P. and Man, N., 1984. Plasma aluminum and iron kinetics in hemodialyzed patients after i.v. infusion of desferrioxamine. *Transactions - American Society for Artificial Internal Organs*, 30, pp.479-482.

Cooke, R., Raynal, M., Laudie, M., Grellet, F., Delseny, M., Morris, P.C., Guerrier, D., Giraudat, J., Quigley, F., Clabault, G., Li, Y.F., Mache, R., Krivitzky, M., Gy, I.J., Kreis, M., Lecharny, A., Parmentier, Y., Marbach, J., Fleck, J., Clement, B., Philipps, G., Herve, C., Bardet, C., Tremousaygue, D. and Hofte, H., 1996. Further progress towards a catalogue of all Arabidopsis genes: analysis of a set of 5000 non-redundant ESTs. *The Plant Journal*, 9(1), pp.101-124.

Cordero, O.X., Ventouras, L.A., DeLong, E.F. and Polz, M.F., 2012. Public good dynamics drive evolution of iron acquisition strategies in natural bacterioplankton populations. *Proc. Natl. Acad. Sci*., pp.1-6.

Costerton, J.W., Stewart, P.S. and Greenberg, E.P., 1999. Bacterial biofilms: A common cause of persistent infections. *Science*, 284, pp.1318-1322.

Cox, C.D. and Graham, R., 1979. Isolation of an iron-binding compound from Pseudomonas aeruginosa. *J. Bacteriol*., 137, pp.357-64.

Cox, C.D., 1982. Effect of pyochelin on the virulence of Pseudomonas aeruginosa. *Infect. Immun*., 36, pp.17-23.

Crits-Christoph, A., Bhattacharya, N., Olm, M., Song, Y. and Banfield, J., 2020. Transporter genes in biosynthetic gene clusters predict metabolite characteristics and siderophore activity. *Genome Research*, 31(2), pp.239-250.

Crosa, J. and Walsh, C., 2002. Genetics and assembly line enzymology of siderophore biosynthesis in bacteria. *Microbiology and Molecular Biology Reviews*, 66(2), pp.223-249.

Crouch, M-L.V., Castor, M., Karlinsey, J.E., Kalhorn, T. and Fang, F.C., 2008. Biosynthesis and IroC-dependent export of the siderophore salmochelin are essential for virulence of Salmonella enterica serovar Typhimurium. *Mol. Microbiol.*, 67, pp.971-983.

Crowley, D. and Kraemer, S., 2007. Function of siderophores in the plant rhizosphere. In: R. Pinton, Z. Varanini and P. Nannipieri, ed., *The Rhizosphere, Biochemistry and Organic Substances at the Soil–Plant Interface*. Boca Raton: CRC Press.

de Brito, A., Gagne, S. and Antoun, H., 1995. Effect of compost on rhizosphere microflora of the tomato and on the incidence of plant growth-promoting rhizobacteria. *Applied and Environmental Microbiology*, 61(1), pp.194-199.

del Olmo, A., Caramelo, C. and SanJose, C., 2003. Fluorescent complex of pyoverdin with aluminum. *Journal of Inorganic Biochemistry*, 97(4), pp.384-387.

Dell'Anno, F., Vitale, G.A., Buonocore, C., Vitale, L., Palma Esposito, F., Coppola, D., Della Sala, G., Tedesco, P., and de Pascale, D., 2022. Novel insights on Pyoverdine: From biosynthesis to biotechnological application. *International Journal of Molecular Sciences*, 23(19), p.11507.

Demain, A.L., 2014. Importance of microbial natural products and the need to revitalize their discovery. *J Ind Microbiol Biotechnol*, 4, pp.185–201.

Demange, P., Wendenbaum, S., Linget, C., Mertz, C., Cung, M.T., Dell, A., and Abdallah, M.A., 1990. Bacterial siderophores : Structure and NMR assignment of pyoverdins PA, siderophores ofpseudomonas aeruginosa ATCC 15692. *Biology of Metals*, 3(3-4), pp.155-170.

Demir, M. and Kaleli, I., 2004. Production by Escherichia coli isolates of siderophore and other virulence factors and their pathogenic role in a cutaneous infection model. *Clin Microbiol. Infec.*, 10, pp.1011-1014.

Deng, X., Sun, F., Ji, Q., Liang, H., Missiakas, D., Lan, L. and He, C., 2012. Expression of Multidrug Resistance Efflux Pump Gene norA Is Iron Responsive in Staphylococcus aureus. *Journal of Bacteriology*, 194(7), pp.1753-1762.

Dertz, E.A., Stintzi, A. and Raymond, K.N., 2006. Siderophore-mediated iron transport in Bacillus subtilis and Corynebacterium glutamicum. *J. Biol. Inorg. Chem.*, 11, pp.1087-1097.

Dimkpa, C., Merten, D., Svatos, A., Buchel, G. and Kothe, E., 2009a. Metal-induced oxidative stress impacting plant growth in contaminated soil is alleviated by microbial siderophores. *Soil Biology and Biochemistry*, 41, pp.154-162.

Dimkpa, C., Merten, D., Svatos, A., Büchel, G. and Kothe, E., 2009b. Siderophores mediate reduced and increased uptake of cadmium by Streptomyces tendae F4 and sunflower (Helianthus annuus) respectively. *Journal of Applied Microbiology*, 107, pp.1687-1696.

Dimkpa, C., Svatos, A., Dabrowska, P., Schmidt, A., Boland, W., Kothe, E., 2008a. Involvement of siderophores in the reduction of metal-induced inhibition of auxin synthesis in Streptomyces spp. *Chemosphere*, 74, pp.19-25.

Dimkpa, C., Svatos, A., Merten, D., Büchel, G. and Kothe, E., 2008b. Hydroxamate siderophores produced by Streptomyces acidiscabies E13 bind nickel and promote growth in cowpea (Vigna unguiculata L.) under nickel stress. *Canadian Journal of Microbiology*, 54, pp.163-172.

Dittmar, T., Koch, B., Hertkorn, N. and Kattner, G., 2008. A simple and efficient method for the solid-phase extraction of dissolved organic matter (SPE-DOM) from seawater. *Limnol. Ocean. Methods*, 6, pp.230-235.

Djoumbou Feunang, Y., Eisner, R., Knox, C., Chepelev, L., Hastings, J., Owen, G., Fahy, E., Steinbeck, C., Subramanian, S., Bolton, E., Greiner, R. and Wishart, D., 2016. ClassyFire: automated chemical classification with a comprehensive, computable taxonomy. *Journal of Cheminformatics*, 8(1).

Donlan, R.M., 2001. Biofilm formation: A clinically relevant microbiological process. *Clin. Infect. Dis.*, 33, pp.1387-1392.

D'Onofrio, A., Crawford, J.M., Stewart, E.J., Witt, K., 2010. Siderophores from neighboring organisms promote the growth of uncultured bacteria. *Chemistry & Biology* 17, 254–264.

Drechsel, H. and Jung, G., 1998. Peptide siderophores. *J. Peptide Sci*., 4, pp.147-181

Drewniak, L., Styczek, A., Majder-Lopatka, M. and Sklodowska, A., 2008. Bacteria, hypertolerant to arsenic in the rocks of an ancient gold mine, and their potential role in dissemination of arsenic pollution. *Environmental Pollution*, 156(3), pp.1069-1074.

Du, X., Creed, I., Sorichetti, R. and Trick, C., 2019. Cyanobacteria biomass in shallow eutrophic lakes is linked to the presence of iron-binding ligands. *Canadian Journal of Fisheries and Aquatic Sciences*, 76(10), pp.1728-1739.

Duhme, A.K., Hider, R., Naldrett, M. and Pau, R., 1998. The stability of the molybdenum-azotochelin complex and its effect on siderophore production in Azotobacter vinelandii. *J. Biol. Inorg. Chem*., 3, pp.520-526.

Dührkop, K., Fleischauer, M., Ludwig, M., Aksenov, A., Melnik, A., Meusel, M., Dorrestein, P., Rousu, J. and Böcker, S., 2019. SIRIUS 4: a rapid tool for turning tandem mass spectra into metabolite structure information. *Nature Methods*, 16(4), pp.299-302.

Dührkop, K., Nothias, L., Fleischauer, M., Reher, R., Ludwig, M., Hoffmann, M., Petras, D., Gerwick, W., Rousu, J., Dorrestein, P. and Böcker, S., 2020. Systematic classification of unknown metabolites using high-resolution fragmentation mass spectra. *Nature Biotechnology*, 39(4), pp.462-471.

Dührkop, K., Shen, H., Meusel, M., Rousu, J. and Böcker, S., 2015. Searching molecular structure databases with tandem mass spectra using CSI:FingerID. *Proceedings of the National Academy of Sciences*, 112(41), pp.12580-12585.

Escolar, L., Pérez-Martín, J. and De Lorenzo, V., 1999. Opening the iron box: transcriptional metalloregulation by the Fur protein. *J. Bacteriol*., 181, pp.6223-6229.

Esmaeel, Q., Pupin, M., Kieu, N., Chataigné, G., Béchet, M., Deravel, J., Krier, F., Höfte, M., Jacques, P. and Leclère, V., 2016. Burkholderia genome mining for nonribosomal peptide synthetases reveals a great potential for novel siderophores and lipopeptides synthesis. *MicrobiologyOpen*, 5(3), pp.512-526.

Exley, C. and House, E., 2011. Aluminium in the human brain. *Monatshefte für Chemie - Chemical Monthly*, 142(4), pp.357-363.

Ezkurdia, I., Juan, D., Rodriguez, J., Frankish, A., Diekhans, M., Harrow, J., Vazquez, J., Valencia, A. and Tress, M., 2014. Multiple evidence strands suggest that there may be as few as 19 000 human protein-coding genes. *Human Molecular Genetics*, 23(22), pp.5866-5878.

Fadeev, E.A., Luo, M. and Groves, J.T., 2004. Synthesis, structure and molecular dynamics of gallium complexes of schizokinen and the amphiphilic siderophore acinetoferrin. *J. Am. Chem. Soc*., 126, pp.12065-12075.

Farhana, A., Kumar, S., Rathore, S.S., Ghosh, P.C., 2008. Mechanistic insights into a novel exporter-importer system of Mycobacterium tuberculosis unravel its role in trafficking of iron. *PLoS One* 3, e2087.

Farrah, T., Deutsch, E., Hoopmann, M., Hallows, J., Sun, Z., Huang, C. and Moritz, R., 2012. The State of the Human Proteome in 2012 as Viewed through PeptideAtlas. *Journal of Proteome Research*, 12(1), pp.162-171.

Ferguson, A.D. and Deisenhofer, J., 2004. Metal import through microbial membranes. *Cell*, 116, pp.15-24.

Ferreira, C.M., Vilas-Boas, Â., Sousa, C.A., Soares, H.M. and Soares, E.V., 2019. Comparison of five bacterial strains producing siderophores with ability to chelate iron under alkaline conditions. *AMB Express*, 9(1).

Fetherston, J.D., Kirillina, O., Bobrov, A.G., Paulley, J.T. and Perry, R.D., 2010. The yersiniabactin transports system is critical for the pathogenesis of bubonic and pneumonic Plague. *Infect. Immun*., 78, pp.2045-2052.

Finn, R., Tate, J., Mistry, J., Coggill, P., Sammut, S., Hotz, H., Ceric, G., Forslund, K., Eddy, S., Sonnhammer, E. and Bateman, A., 2007. The Pfam protein families database. *Nucleic Acids Research*, 36(Database), pp.D281-D288.

Friedlaender, C., 1882. Ueber die Schizomyceten bei der acuten fibrösen Pneumonie. *Archiv für Pathologische Anatomie und Physiologie und für Klinische Medicin*, 87(2), pp.319-324.

Fuchs, R., Schafer, M., Geoffroy, V. and Meyer, J.M., 2001. Siderotyping a powerful tool for the characterization of pyoverdines. *Curr. Top. Med. Chem.*, 1, pp.31-57.

Furrer, J.L., Sanders, D.N., Hook-Barnard, I.G. and Mcintosh, M.A., 2002. Export of the siderophore enterobactin in *Escherichia coli*: involvement of a 43 kDa membrane exporter. *Mol. Microbiol.*, 44, pp.1225-1234.

Fusetani, N., 2000. Introduction. In: N. Fusetani, ed., *Drugs from the Sea*. Basel: Karger, pp. 1-5.

Gauglitz, J. M. and Butler, A., 2013. Amino acid variability in the peptide composition of a suite of amphiphilic peptide siderophores from an open ocean Vibrio species. *J. Biol. Inorg. Chem.*, 18(5), pp.489-97.

Geider, R.J., 1999. Complex lessons of iron uptake. *Nature*, 400, pp.815-816.

Gerea, A.L., Branscum, K.M., King, J.B., You, J., Powell, D.R., Miller, A.N., Spear, J.R. and Cichewicz, R.H., 2012. Secondary metabolites produced by fungi derived from a microbial mat encountered in an iron-rich natural spring. *Tetrahedron Lett*, 53, pp. 4202-4205

Gessard, C., 1882. Sur les colorations bleue et verte des linges a pansements. *CR Acad. Sci. Hebd. Seances Acad. Sci.*, 94, pp.536-538.

Ghosh, s., Pal, s. and Chakraborty, n., 2015. The qualitative and quantitative assay of siderophore production by some microorganisms and effect of different media on its production. *Int. J. Chem. Sci.*, 13(4), pp.1621-1629.

Gledhill, M. and Buck, K.N., 2012. The organic complexation of iron in the marine environment: a review. *Front. Microbiol.*, 3, pp.1-17.

Gledhill, M. and van den Berg, C.M.G., 1994. Determination of complexation of iron (III) with natural organic complexing ligands in seawater using cathodic stripping voltammetry. *Mar. Chem.*, 47(1), pp.41-54.

Gledhill, M., McCormack, P., Ussher, S., Achterberg, E.P., Mantoura, R.F.C and Worsfold, P.J., 2004. Production of siderophore type chelates by mixed bacterioplankton populations in nutrient enriched seawater incubations. *Mar. Chem.,* 88(1-2), pp.75-83.

Glick, B.R., 2003. Phytoremediation: Synergistic use of plants and bacteria to clean up the environment. *Biotechnol. Advances,* 21, pp.383-393.

Gontang, E., Gaudêncio, S., Fenical, W. and Jensen, P., 2010. Sequence-Based Analysis of Secondary-Metabolite Biosynthesis in Marine Actinobacteria. *Applied and Environmental Microbiology,* 76(8), pp.2487-2499.

Granger, J. and Price, N.M., 1999. Importance of siderophores in iron nutrition of heterotrophic marine bacteria. *Limnol. Oceanogr.,* 44, pp.541-555.

Greenwald, J., Zeder-Lutz, G., Hagege, A., Celia, H. and Pattus, F., 2008. The metal dependence of pyoverdine interactions with its outer membrane receptor FpvA. *J. Bacteriol.,* 190, pp.6548-6558.

Grigg, J.C., Cooper, J.D., Cheung, J., Heinrichs, D.E. and Murphy, M.E.P., 2010. The Staphylococcus aureus siderophore receptor HtsA undergoes localized conformational changes to enclose staphyloferrin A in an arginine-rich binding pocket. *J. Biol. Chem.,* 285, pp.11162-11171.

Grunewald, J. and Marahiel, M.A., 2006. Chemoenzymatic and template-directed synthesis of bioactive macrocyclic peptides. *Microbiol. Mol. Biol. Rev.,* 70, pp.121-146.

Guan, L., Kanoh, K. and Kamino, K., 2001. Effect of Exogenous Siderophores on Iron Uptake Activity of Marine Bacteria under Iron-Limited Conditions. *Applied and Environmental Microbiology,* 67(4), pp.1710-1717.

Guan, L.L. and Kamino, K., 2001. Bacterial response to siderophore and quorum sensing chemical signals in the seawater community. *BMC Microbiol*., 1, pp.27.

Guerinot, M.L., 1994. Microbial iron transport. *Ann. Rev. Microbiol*., 48, pp.743-772.

Haefner, B., 2003. Drugs from the deep: marine natural products as drug candidates. *Drug Discov Today,* 8, pp.536-544.

Hagan, A., Tripathi, A., Berger, D., Sherman, D. and Hanna, P., 2017. Petrobactin Is Exported from Bacillus anthracis by the RND-Type Exporter ApeX. *mBio*, 8(5).

Hannauer, M., Barda, Y., Mislin, G.L.A., Shanzer, A. and Schalk, I.J., 2010. The ferrichrome uptake pathway in Pseudomonas aeruginosa involves an iron release mechanism with acylation of the siderophore and recycling of the modified desferrichrome. *J. Bacteriol*., 192, pp.1212-1220.

Hantke, K., 1981. Regulation of ferric iron transport in Escherichia coli K12: Isolation of a constitutive mutant. *Mol. Gen. Genet*., 182, pp.288-292.

Hantke, K., 2001. Iron and metal regulation in bacteria. *Curr. Opin. Microbiol*., 4, pp.172-177.

Hashimoto, M., Ichimura, T., Mizoguchi, H., Tanaka, K., Fujimitsu, K., Keyamura, K., Ote, T., Yamakawa, T., Yamazaki, Y., Mori, H., Katayama, T. and Kato, J., 2004. Cell size and nucleoid organization of engineered Escherichia coli cells with a reduced genome. *Molecular Microbiology*, 55(1), pp.137-149.

Haynes, S.W. and Challis, G.L., 2007. Non-linear enzymatic logic in natural product modular mega-synthases and -synthetases. *Curr. Opin. Drug Discov. Devel*., 10, pp.203-218.

Heinisch, L., Wittmann, S., Stoiber, T. and Scherlitz-Hofmann, I., 2003. Synthesis and biological activity of tris-and tetrakiscatecholate siderophores based on poly-aza alkanoic acids or alkylbenzoic acids and their conjugates with beta-lactam antibiotics. *Arzneimittel-Forschung.* 53, pp.188.

Henikoff, S., Till, B.J. and Comai, L.T., 2004. Traditional mutagenesis meets functional genomics. *Plant Physiology*, 135, pp.630-636.

Hernlem, B., Vane, L. and Sayles, G., 1996. Stability constants for complexes of the siderophore desferrioxamine B with selected heavy metal cations. *Inorganica Chimica Acta*, 244(2), pp.179-184.

Hider, R. and Kong, X., 2010. Chemistry and biology of siderophores. *Natural Product Reports*, 27(5), p.637.

Hider, R.C., 1984. Siderophore mediated absorption of iron. *Structure and Bonding*, 58, pp. 25-87.

Higgs, P.I., Myers, P.S. and Postle, K., 1998. Interactions in the TonB-Dependent Energy Transduction Complex: ExbB and ExbD Form Homomultimers. *J. Bacteriol.*, 180, pp.6031-6038

Hoffmann, M., Nothias, L., Ludwig, M., Fleischauer, M., Gentry, E., Witting, M., Dorrestein, P., Dührkop, K. and Böcker, S., 2021. Assigning confidence to structural annotations from mass spectra with COSMIC.

Hofte, M., 1993. Classes of microbial siderophores. In: L.L. Barton and B.C. Hemming, eds., Iron chelation in plants and soil microorganisms. San Diego: *Academic Press*, pp.3-26.

Holt, P.D., Reid, R.R., Lewis, B.L., Luther, G.W. and Butler, A., 2005. Iron(III) coordination chemistry of alterobactin A: a siderophore from the marine bacterium Alteromonas luteoviolacea. *Inorg. Chem*., 44(21), pp.7671-7677.

Homann, V. V., Edwards, K. J., Webb, E. A., and Butler, A., 2009a. Siderophores of Marinobacter aquaeolei: petrobactin and its sulfonated derivatives. *Biometals*, 22, pp.565-571.

Homann, V. V., Sandy, M., Tincu, J. A., Templeton, A. S., Tebo, B. M., and Butler, A., 2009b. Loihichelins A-F, a suite of amphiphilic siderophores produced by the marine bacterium Halomonas LOB-5. *J. Nat. Prod.*, 72, pp.884-888.

Hopkinson, B.M. and Barbeau, K.A., 2012. Iron transporters in marine prokaryotic genomes and metagenomes. *Environ. Microbiol.*, 14(1), pp.114-28.

Horiyama, T. and Nishino, K., 2014. AcrB, AcrD, and MdtABC Multidrug Efflux Systems Are Involved in Enterobactin Export in Escherichia coli. *PLoS ONE*, 9(9), p.e108642.

Hormaeche, E. and Edwards, P.R., 1960. A proposed genus *Enterobacter*. *Int. Bull. Bacteriol. Nomen. Taxon*, 10, pp.71-74.

Hu, X. and Boyer, G.L., 1996. Siderophore-mediated aluminum uptake by Bacillus megaterium ATCC 19213. *Appl. Environ. Microbiol*., 62, pp.4044-4048.

Huang, Z., Chen, M., Woroch, C., Markland, T. and Kanan, M., 2021. A framework for automated structure elucidation from routine NMR spectra. *Chemical Science*, 12(46), pp.15329-15338.

Ito, Y. and Butler, A., 2005. Structure of synechobactins, new siderophores of the marine cyanobacterium Synechococcus sp. PCC 7002. *Limnol. Oceanogr.*, 50(6), pp.1918-1923.

Jalali, M., Zaborowska, J., and Jalali, M., 2016. Chapter 1 - The Polymerase Chain Reaction: PCR, qPCR, and RT-PCR. In: *Basic Science Methods for Clinical Researchers*. Academic Press, pp.1-12.

Jimenez, P.N., Koch, G., Papaioannou, E. and Wahjudi, M., 2010. Role of PvdQ in Pseudomonas aeruginosa virulence under iron-limiting conditions. *Microbiology*, 156, pp.49-59.

Jin, B., Newton, S.M.C., Shao, Y., and Jiang, X., 2006. Iron acquisition systems for ferric hydroxamates, haemin and haemoglobin in Listeria monocytogenes. *Mol. Microbiol.* 59, pp.1185-1198.

Johnson, L., 2008. Iron and siderophores in fungal–host interactions. *Mycological Research*, 112(2), pp.170-183.

Johnstone, T. and Nolan, E., 2015. Beyond iron: non-classical biological functions of bacterial siderophores. *Dalton Transactions*, 44(14), pp.6320-6339.

Kanoh, K., Kamino, K., Leleo, G., Adachi, K. and Shizuri, Y., 2003. Pseudoalterobactin A and B, new siderophores excreted by marine bacterium pseudoalteromonas sp.. KP20-4. *The Journal of Antibiotics*, 56(10), pp.871-875.

Karpishin, T., Dewey, T. and Raymond, K., 1993. Coordination chemistry of microbial iron transport. 49. The vanadium(IV) enterobactin complex: structural, spectroscopic, and electrochemical characterization. *Journal of the American Chemical Society*, 115(5), pp.1842-1851.

Karunarathna, M., Ayodele, M., Giammanco, G., Brugh, A., Muizzi, D., Bauman, M., Torelli, A., Alabanza, A., Forbes, M. and Ostrowski, A., 2021. Fe(III)-polyuronic acid

photochemistry: radical chemistry in natural polysaccharide. *Photochemical & Photobiological Sciences*, 20(2), pp.255-263.

Keatinge-Clay, A., 2012. The structures of type I polyketide synthases. *Natural Product Reports*, 29(10), p.1050.

Kelecom, A., 1999. Chemistry of Marine Natural Products: Yesterday, Today and Tomorrow. *An Acad Bras Cienc*, 71, pp.249-263.

Khodr, H.H., Hider, R.C. and Duhme-Klair, A.K., 2002. The iron-binding properties of aminochelin, the mono(catecholamide) siderophore of Azotobacter vinelandii. *J. Biol. Inorg. Chem*., 7, pp.891-896.

Kim, H., Wang, M., Leber, C., Nothias, L., Reher, R., Kang, K., van der Hooft, J., Dorrestein, P., Gerwick, W. and Cottrell, G., 2021. NPClassifier: A Deep Neural Network-Based Structural Classification Tool for Natural Products. *Journal of Natural Products*, 84(11), pp.2795-2807.

Kiss, T. and Farkas, E., 1998. Metal-binding ability of desferrioxamine B. J. Inclusion Phenomena. *Mol. Recog. Chem*., 32, pp.385-403.

Kohli, R.M., Trauger, J.W., Schwarzer, D., Marahiel, M.A. and Walsh, C.T., 2001. Generality of peptide cyclization catalyzed by isolated thioesterase domains of nonribosomal peptide synthetases. *Biochemistry*, 40, pp.7099-7108.

Korp, J., Winandi, L., Sester, A. and Nett, M., 2018. Engineering Pseudochelin Production in *Myxococcus xanthus*. *ASM Journals*, 84(22).

Kour, D., Kaur, T., Devi, R., Rana, K., Yadav, N., Rastegari, A. and Yadav, A., 2020. Biotechnological applications of beneficial microbiomes for evergreen agriculture and human health. *New and Future Developments in Microbial Biotechnology and Bioengineering*, pp.255-279.

Kramer, J., Özkaya, Ö. and Kümmerli, R., 2019. Bacterial siderophores in community and host interactions. *Nature Reviews Microbiology*, 18(3), pp.152-163.

Kreutzer, M.F. and Nett, M., 2012. Genomics-driven discovery of Taiwachelin, a lipopeptide siderophore from Cupriavidus taiwanensis. *Organic & Biomolecular Chemistry*, 10(47), p.9338.

Krewulak, K. and Vogel, H., 2008. Structural biology of bacterial iron uptake. Biochimica et Biophysica Acta (BBA) - *Biomembranes*, 1778(9), pp.1781-1804.

Kruck, T., Cui, J., Percy, M. and Lukiw, W., 2004. Molecular Shuttle Chelation: The Use of Ascorbate, Desferrioxamine and Feralex-G in Combination to Remove Nuclear Bound Aluminum. *Cellular and Molecular Neurobiology*, 24(3), pp.443-459.

Kunkle, D., Bina, X. and Bina, J., 2017. The Vibrio cholerae VexGH RND Efflux System Maintains Cellular Homeostasis by Effluxing Vibriobactin. *mBio*, 8(3).

Kupper, F.C., Carrano. C.J., Kuhn, J.U. and Butler, A., 2006. Photoreactivity of iron(III)-aerobactin: photoproduct structure and iron(III) coordination. *Inorg. Chem.*, 45, pp.6028-6033.

Kurokawa, M., Seno, S., Matsuda, H. and Ying, B., 2016. Correlation between genome reduction and bacterial growth. *DNA Research*, 23(6), pp.517-525.

Kurth, C., Schieferdecker, S., Athanasopoulou, K., Seccareccia, I. and Nett, M., 2016. Variochelins, Lipopeptide Siderophores from Variovorax boronicumulans Discovered by Genome Mining. *Journal of Natural Products*, 79(4), pp.865-872.

Kyung Kim, T. and Fuerst, J.A., 2006. Diversity of polyketide synthase genes from bacteria associated with the marine sponge Pseudoceratina clavata: Culture-dependent and culture-independent approaches. *Environmental Microbiology*, 8(8), pp.1460-1470.

Lam, K., 2006. Discovery of novel metabolites from marine actinomycetes. *Current Opinion in Microbiology*, 9(3), pp.245-251.

Lamont, I.L., Beare, P.A., Ochsner, U., Vasil, A.I., asil, M.L., 2002. Siderophore-mediated signaling regulates virulence factor production in Pseudomonas aeruginosa. *Proc. Natl. Acad. Sci*. 99, pp.7072-7077.

Lane, A.L. and Moore, B.S., 2012. A sea of biosynthesis: marine natural products meet the molecular age. *Natural product reports*, 28(2), pp.411-428

Lane, L., Bairoch, A., Beavis, R., Deutsch, E., Gaudet, P., Lundberg, E. and Omenn, G., 2013. Metrics for the Human Proteome Project 2013–2014 and Strategies for Finding Missing Proteins. *Journal of Proteome Research*, 13(1), pp.15-20.

Lane, S.J., Marshall, P.S., Upton, R.J., Ratledge, C. and Ewing, M., 1995. Novel extracellular mycobactins, the carboxymycobactins from Mycobacterium avium. *Tetrahedron Lett*., 36, pp.4129-4132.

Lankford, C., 1973. Bacterial Assimilation of iron. *CRC Critical Reviews in Microbiology*, 2(3), pp.273-331.

Larsen, R.A., Thomas, M.G., Wood, G.E. and Postle, K., 1994. Partial suppression of an Escherichia coli TonB transmembrane domain mutation (DV17) by a missense mutation in ExbB. *Mol. Microbiol*., 13, pp.627-640.

Lautru, S. and Challis, G., 2004. Substrate recognition by nonribosomal peptide synthetase multi-enzymes. *Microbiology*, 150(6), pp.1629-1636.

Lautru, S., Deeth, R.J., Bailey, L.M. and Challis, G.L., 2005. Discovery of a new peptide natural product by Streptomyces coelicolor genome mining. *Nat. Chem. Biol.*, (1), pp.265-269.

Lautru, S., Oves-Costales, D., Pernodet, J. and Challis, G., 2007. MbtH-like protein-mediated cross-talk between non-ribosomal peptide antibiotic and siderophore biosynthetic pathways in Streptomyces coelicolor M145. *Microbiology*, 153(5), pp.1405-1412.

Lawlor, M.S., O'connor, C. and Miller, V.L., 2007. Yersiniabactin is a virulence factor for Klebsiella pneumoniae during pulmonary infection. *Infect. Immun*., 75, pp.1463.

Leal, M.C., Madeira, C., Brandão, C.A., Puga, J. and Calado, R., 2012. Bioprospecting of marine invertebrates for new natural products - A chemical and zoogeographical perspective. *Molecules*, 17(8), pp.9842-9854.

Lehner, S.M., Atanasova, L., Neumann, N.K.N., Krska, R., Lemmens, M., Druzhinina, I.S. and Schuhmacher, R., 2013. Isotope-assisted screening for iron-containing metabolites reveals a high degree of diversity among known and unknown siderophores produced by Trichoderma spp. *Appl. Environ. Microbiol.*, 79(1), pp.18-31.

Li, J.W. and Vederas, J.C., 2009. Drug discovery and natural products: end of an era or an endless frontier? *Science*, 325, pp. 161-165.

Li, N., Zhang, C., Li, B., Liu, X., Huang, Y., Xu, S. and Gu, L., 2012. Unique Iron Coordination in Iron-chelating Molecule Vibriobactin Helps Vibrio cholerae Evade Mammalian Siderocalin-mediated Immune Response. *Journal of Biological Chemistry*, 287(12), pp.8912-8919.

Liigand, J., Laaniste, A. and Kruve, A., 2016. pH Effects on Electrospray Ionization Efficiency. *Journal of the American Society for Mass Spectrometry*, 28(3), pp.461-469.

Litwin, C.M. and Calderwood, S.B., 1993. Role of iron in the regulation of virulence genes. *Clin. Microbiol. Rev.*, 6, pp.137-149.

Liu, N., Shang, F., Xi, L. and Huang, Y., 2013. Tetroazolemycins A and B, Two New Oxazole-Thiazole Siderophores from Deep-Sea Streptomyces olivaceus FXJ8.012. *Marine Drugs*, 11(5), pp.1524-1533.

Lobiński, R., Schaumlöffel, D. and Szpunar, J., 2006. Mass spectrometry in bioinorganic analytical chemistry. *Mass Spectrom. Rev.*, 25(2), pp.255-289.

Loomis, L.D. and Raymond, K.N., 1991. Solution Equilibria of Enterobactin and Metal Enterobactin Complexes. *Inorg. Chem.*, 30(1), pp.906–911.

Louvel, H., Bommezzadri, S., Zidane, N., Boursaux-Eude, C., Creno, S., Magnier, A., Rouy, Z., Médigue, C., Girons, I., Bouchier, C. and Picardeau, M., 2006. Comparative and Functional Genomic Analyses of Iron Transport and Regulation in Leptospira spp. *Journal of Bacteriology*, 188(22), pp.7893-7904.

Ludwig, M., Nothias, L., Dührkop, K., Koester, I., Fleischauer, M., Hoffmann, M., Petras, D., Vargas, F., Morsy, M., Aluwihare, L., Dorrestein, P. and Böcker, S., 2019. ZODIAC: database-independent molecular formula annotation using Gibbs sampling reveals unknown small molecules.

Luo, Y., Cobb, R. and Zhao, H., 2014. Recent advances in natural product discovery. *Current Opinion in Biotechnology*, 30, pp.230-237.

Luterotti, S. and Grdini?, V., 1986. Spectrophotometric determination of vanadium(V) with desferrioxamine B. *The Analyst*, 111(10), p.1163.

Lynch, A.S. and Robertson, G.T., 2008. Bacterial and fungal biofilm infections. *Annu. Rev. Med*., 59, pp.415-428.

Mabeza, G.F., Loyevsky, M., Gordeuk, V.R. and Weiss, G., 1999. Iron chelation therapy for malaria: A review. *Pharmacol. Ther*., 81, pp.53-75.

Macián, M., Garay, E., Ludwig, W., Pujalte, M. and Schleifer, K., 2001. Thalassomonas viridans gen. nov., sp. nov., a novel marine gamma-proteobacterium. *International Journal of Systematic and Evolutionary Microbiology*, 51(4), pp.1283-1289.

Maheshwari, R., Suneja, P. and Bhutani, N., 2019. Screening and characterization of siderophore producing endophytic bacteria from Cicer arietinum and Pisum sativum plants. *Journal of Applied Biology & Biotechnology*, 7(5), pp.7-14.

Malluche, H., Smith, A., Abreo, K. and Faugere, M., 1984. The Use of Deferoxamine in the Management of Aluminum Accumulation in Bone in Patients with Renal Failure. *New England Journal of Medicine*, 311(3), pp.140-144.

Malviya, D., Sahu, P., Singh, U., Paul, S., Gupta, A., Gupta, A., Singh, S., Kumar, M., Paul, D., Rai, J., Singh, H. and Brahmaprakash, G., 2020. Lesson from Ecotoxicity: Revisiting the Microbial Lipopeptides for the Management of Emerging Diseases for Crop Protection. *International Journal of Environmental Research and Public Health*, 17(4), pp.1434.

Margolin Eren, K.J., Fialkov, A.B., Keshet, U., Tsizin, S. and Amirav, A., 2019. Doubly charged molecular ions in GC–MS with cold EI. *Journal of the American Society for Mass Spectrometry*, 31(2), pp.347-354.

Mark Garrison, J. and Crumbliss, A., 1987. Kinetics and mechanism of aluminum(III)/siderophore ligand exchange: mono(deferriferrioxamine B)aluminum(III) formation and dissociation in aqueous acid solution. *Inorganica Chimica Acta*, 138(1), pp.61-65.

Marko-Varga, G., Omenn, G., Paik, Y. and Hancock, W., 2012. A First Step Toward Completion of a Genome-Wide Characterization of the Human Proteome. *Journal of Proteome Research*, 12(1), pp.1-5.

Martin, J.D., Ito, Y., Homann, V.V., Haygood, M.G. and Butler, A., 2006. Structure and membrane affinity of new amphiphilic siderophores produced by Ochrobactrum sp. SP18. *J. Biol. Inorg. Chem.*, 11(5), pp.633-641.

Martínez Núñez, M.A. and López, V.E., 2016. Nonribosomal peptides synthetases and their applications in industry. *Sustainable Chemical Processes*, 4(13), pp.1-8.

Martinez, J.S. and Butler, A., 2007. Marine amphiphilic siderophores: Marinobactin structure, uptake, and microbial partitioning. *Journal of Inorganic Biochemistry*, 101(11-12), pp.1692-1698.

Martinez, J.S., Haygood, M.G. and Butler, A., 2001. Identification of a natural desferrioxamine siderophore produced by a marine bacterium. *Limnol. Oceanogr*., 46(2), pp.420-424.

Matzanke, B., Bill, E., Trautwein, A. and Winkelmann, G., 1990. Siderophores as iron storage compounds in the yeasts Rhodotorula minuta and Ustilago sphaerogena detected by in vivo Mössbauer spectroscopy. *Hyperfine Interactions*, 58(1-4), pp.2359-2364.

Matzke, M.A. and Matzke, A.J.M., 1995. How and why do plants inactivate homologues (trans)genes? *Plant Physiology*,107(3), pp.679-685.

Mawji, E., Gledhill, M., Milton, J.A., Tarran, G.A., Ussher, S., Thompson, A., Wolff, G.A., Worsfold, P.J. and Achterberg, E.P., 2008. Hydroxamate siderophores: occurrence and importance in the Atlantic Ocean. *Environ. Sci. Technol.*, 42(23), pp.8675-80.

Mawji, E., Gledhill, M., Milton, J.A., Zubkov, M.V., Thompson, A., Wolff, G.A. and Achterberg, E.P., 2011. Production of siderophore type chelates in Atlantic Ocean waters enriched with different carbon and nitrogen sources. *Mar. Chem.*, 124(1-4), pp.90-99.

McCormack, P., Worsfold, P.J. and Gledhillm, M., 2003. Separation and detection of siderophores produced by marine bacterioplankton using high-performance liquid

chromatography with electrospray ionization mass spectrometry. *Anal. Chem.*, 75(11), pp.2647-2652.

Mchugh, J.P., Rodríguez-Quiñones, F., Abdul-Tehrani, H. and Svistunenko, D.A., 2003. Global iron-dependent gene regulation in Escherichia coli. *J. Biol. Chem.* 278, pp.29478-29486

Medema, M.H., Paalvast, Y., Nguyen, D.D., Melnik, A., Dorrestein, P.C., Takano, E. and Breitling, R., 2014. Pep2Path: automated mass spectrometry-guided genome mining of peptidic natural products. *PLoS Comput. Biol*., 10, pp.e1003822.

Mehnert, M., Retamal-Morales, G., Schwabe, R., Vater, S., Heine, T., Levicán, G., Schlömann, M. and Tischler, D., 2017. Revisiting the Chrome Azurol S Assay for Various Metal Ions. *Solid State Phenomena*, 262, pp.509-512.

Meneely, K., 2007. *The biochemistry of siderophore biosynthesis*. PhD. The University of Kansas.

Meyer, J., 2010. Pyoverdine siderophores as taxonomic markers. In: R. Filloux, ed., Pseudomonas. Netherlands: Springer.

Meyer, J.M., Gruffaz, C., Tulkki, T. and Izard, D., 2007. Taxonomic heterogeneity, as shown by siderotyping, of strains primarily identified as Pseudomonas putida. *Int. J. Syst. Evol. Microbiol*., 57, pp.2543-2556.

Meyer, J-M., Gruffaz, C., Raharinosy, V. and Bezverbnaya, I., 2008. Siderotyping of fluorescent–pseudomonas: molecular mass determination by mass spectrometry as a powerful pyoverdine siderotyping method. *BioMetals* 21, pp.259-271.

Miao, V., Coëffet-Le Gal, M., Nguyen, K., Brian, P., Penn, J., Whiting, A., Steele, J., Kau, D., Martin, S., Ford, R., Gibson, T., Bouchard, M., Wrigley, S. and Baltz, R., 2006. Genetic Engineering in Streptomyces roseosporus to Produce Hybrid Lipopeptide Antibiotics. *Chemistry & Biology*, 13(3), pp.269-276.

Michel, L., González, N., Jagdeep, S., Nguyen-Ngoc, T. and Reimmann, C., 2005. Pchr-box recognition by the Arac-type regulator pchr of Pseudomonas aeruginosa requires the siderophore pyochelin as an effector. *Mol. Microbiol*., 58, pp.495-509.

Miethke, M. and Marahiel, M.A., 2007. Siderophore-Based Iron Acquisition and Pathogen Control. *Microbiol. Mol. Biol. Rev.*, 71, pp.413-451.

Miethke, M., Schmidt, S. and Marahiel, M.A., 2008. The major facilitator superfamily-type transporter YmfE and the multidrug-efflux activator Mta mediate bacillibactin secretion in Bacillus subtilis. *J. Bacteriol.*, 190, pp.5143-5152.

Milke, L. and Marienhagen, J., 2020. Engineering intracellular malonyl-COA availability in microbial hosts and its impact on polyketide and fatty acid synthesis. *Applied Microbiology and Biotechnology*, 104(14), pp.6057-6065.

Minowa, Y., Araki, M. and Kanehisa, M., 2007. Comprehensive analysis of distinctive polyketide and nonribosomal peptide structural motifs encoded in microbial genomes. *Journal of Molecular Biology*, 368(5), pp.1500-1517.

Molitoris, B., Alfrey, P., Miller, N., Hasbargen, J., Kaehney, W., Alfrey, A. and Smith, B., 1987. Efficacy of intramuscular and intraperitoneal deferoxamine for aluminum chelation. *Kidney International*, 31(4), pp.986-991.

Mollmann, U., Heinisch, L., Bauernfeind, A., Köhler, T. and Ankel-Fuchs, D., 2009. Siderophores as drug delivery agents: application of the “Trojan Horse” strategy. *BioMetals*, 22, pp.615-624.

Montaser, R and Leusch, H., 2011. Marine natural products: a new wave of drugs? *Future Medicinal Chemistry*, 3(12), pp.1475-1489.

Mootz, H.D. and Marahiel, M.A., 1997. Biosynthetic systems for nonribosomal peptide antibiotic assembly. *Current Opinion in Chemical Biology*, 1(4), pp.543-551.

Morales, G., 2018. *Characterization of arsenic-binding siderophores from environmental bacteria and evaluation of their role in arsenic tolerance*. PhD. Universidad de Santiago de Chile.

Mounicou, S., Szpunar, J. and Lobinski, R., 2009. Metallomics: the concept and methodology. *Chem. Soc. Rev*., 38(4), pp.1119-1138.

Mulet, M., Gomila, M., Gruffaz, C. and Meyer, J-M., 2007. Phylogenetic analysis and siderotyping as useful tools in the taxonomy of Pseudomonas stutzeri: description of a novel genomovar. *Int. J. Syst. Evol. Microbiol*. 58, pp.2309-2315.

Nabila and Kasiamdari, R.S., 2021. Antagonistic activity of siderophore-producing bacteria from black rice rhizosphere against rice blast fungus *pyricularia oryzae*. *Microbiology and Biotechnology Letters*, 49(2), pp.217-224.

Nair, A., Juwarkar, A. and Singh, S., 2006. Production and Characterization of Siderophores and its Application in Arsenic Removal from Contaminated Soil. *Water, Air, and Soil Pollution*, 180(1-4), pp.199-212.

Navarro-Muñoz, J., Selem-Mojica, N., Mullowney, M., Kautsar, S., Tryon, J., Parkinson, E., De Los Santos, E., Yeong, M., Cruz-Morales, P., Abubucker, S., Roeters, A., Lokhorst, W., Fernandez-Guerra, A., Dias Cappelini, L., Thomson, R., Metcalf, W., Kelleher, N., Barona-Gomez, F. and Medema, M., 2018. A computational framework for systematic exploration of biosynthetic diversity from large-scale genomic data. *BioRxiv*.

Nebeker, H., Milliner, D., Ott, S., Sherrard, D., Alfrey, A., Abuelo, J. and Wasserstein, A., 1984. Aluminum-related osteomalacia - clinical-response to desferrioxamine. *Kidney International*, 25, p.173.

Neilands, J., 1981. Microbial Iron Compounds. *Annual Review of Biochemistry*, 50(1), pp.715-731.

Neilands, J., 1984. Methodology of siderophores. In: A. Chimiak, R. Hider, A. Liu, J. Neilands, K. Nomoto and Y. Sugiura, ed., *Structure and Bonding*. Heildelberg: Springer, pp.1-24.

Neilands, J., 1990. Siderophore systems of bacteria and fungi. *Adv. Iorg. Biochem.*, 8, pp.63-90.

Neubauer, U., Nowack, B., Furrer, G. and Schulin, R., 2000. Heavy Metal Sorption on Clay Minerals Affected by the Siderophore Desferrioxamine B. *Environmental Science & Technology*, 34(13), pp.2749-2755.

Nielsen, A., Mansson, M., Wietz, M., Varming, A., Phipps, R., Larsen, T., Gram, L. and Ingmer, H., 2012. Nigribactin, a Novel Siderophore from Vibrio nigripulchritudo, Modulates Staphylococcus aureus Virulence Gene Expression. *Marine Drugs*, 10(12), pp.2584-2595.

Nikolouli, K. and Mossialos, D., 2012. Bioactive compounds synthesized by non-ribosomal peptide synthetases and type-I polyketide synthases discovered through genomemining and metagenomics. *Biotechnology Letters*, 34(8), pp.1393-1403.

Nishimura, I., Kurokawa, M., Liu, L. and Ying, B., 2017. Coordinated Changes in Mutation and Growth Rates Induced by Genome Reduction. *mBio*, 8(4).

Ogier, J., Pages, S., Galan, M., Barret, M. and Gaudriault, S., 2019. rpoB, a promising marker for analyzing the diversity of bacterial communities by amplicon sequencing. *BMC Microbiology*, 19(171).

Ogston, A., 1984. On Abscesses. *Clinical Infectious Diseases*, 6(1), pp.122-128.

Ojha, A. and Hatfull, G.F., 2007. The role of iron in Mycobacterium smegmatis biofilm formation: The exochelin siderophore is essential in limiting iron conditions for biofilm formation but not for planktonic growth. *Mol. Microbiol.*, 66, pp.468-483.

Ollinger, J., Song, K.B., Antelmann, H., Hecker, M. and Helmann, J.D., 2006. Role of the Fur regulon in iron transport in Bacillus subtilis. *J. Bacteriol.*, 188, pp.3664-3673.

Olonade, I., van Zyl, L. and Trindade, M., 2015. Draft Genome Sequences of Marine Isolates of Thalassomonas viridans and Thalassomonas actiniarum. *Genome Announcements*, 3(2).

Omenn, G., 2014. The strategy, organization, and progress of the HUPO Human Proteome Project. *Journal of Proteomics*, 100, pp.3-7.

Page, M.G., 2013. Siderophore conjugates. *Ann. N. Y. Acad. Sci.*, 1277, pp.115-125.

Page, W., Kwon, E., Cornish, A. and Tindale, A., 2003. The csbX gene of Azotobacter vinelandii encodes an MFS efflux pump required for catecholate siderophore export. *FEMS Microbiology Letters*, 228(2), pp.211-216.

Page, W.J., Collinson, S.K., Demange, P., Dell, A. and Abdallah, M.A., 1991. Azotobacter vinelandii strains of disparate origin produce azotobactin siderophores with identical structure. *BioMetals*, 4, pp.217-222.

Pakchung, A., Soe, C., Lifa, T. and Codd, R., 2011. Complexes Formed in Solution Between Vanadium(IV)/(V) and the Cyclic Dihydroxamic Acid Putrebactin or Linear Suberodihydroxamic Acid. *Inorganic Chemistry*, 50(13), pp.5978-5989.

Passador, L., Cook, J., Gambello, M., Rust, L. and Iglewski, B., 1993. Expression of Pseudomonas aeruginosa Virulence Genes Requires Cell-to-Cell Communication. *Science*, 260(5111), pp.1127-1130.

Pauli, G., Chen, S., Lankin, D., Bisson, J., Case, R., Chadwick, L., Gödecke, T., Inui, T., Krunic, A., Jaki, B., McAlpine, J., Mo, S., Napolitano, J., Orjala, J., Lehtivarjo, J., Korhonen, S. and Niemitz, M., 2014. Essential Parameters for Structural Analysis and Dereplication by 1H NMR Spectroscopy. *Journal of Natural Products*, 77(6), pp.1473-1487.

Pheiffer, F., Schneider, Y., Hansen, E., Andersen, J., Isaksson, J., Busche, T., Rückert, C., Kalinowski, J., Zyl, L., and Trindade, M., 2022. Bioassay-guided fractionation leads to the detection of cholic acid generated by the rare thalassomonas sp.. *Marine Drugs*, 21(1), p.2.

Piampiano, E., Pini, F., Biondi, N., Garcia, C., Decorosi, F., Tomàs-Barberàn, F., Giovannetti, L. and Viti, C., 2020. Tetraselmis suecica F&M-M33 phycosphere: associated bacteria and exo-metabolome characterization. *European Journal of Phycology*, 56(1), pp.61-71.

Pickens, L.B., Tang, Y. and Chooi, Y., 2011. Metabolic engineering for the production of natural products. *Annual Review of Chemical and Biomolecular Engineerin*g, 2, pp.211-236.

Pluskal, T., Castillo, S., Villar-Briones, A. and Orešič, M., 2010. MZmine 2: Modular framework for processing, visualizing, and analyzing mass spectrometry-based molecular profile data. *BMC Bioinformatics*, 11(1).

Poole, K. and McKay, G.A., 2003. Iron acquisition and its control in Pseudomonas aeruginosa: many roads lead to Rome. *Front. Biosci*., 8, pp.661-686.

Poole, K., Neshat, S., Krebes, K. and Heinrichs, D.E., 1993. Cloning and nucleotide sequence analysis of the ferripyoverdine receptor gene fpvA of Pseudomonas aeruginosa. *J. Bacteriol*., 175, pp.4597-4604.

Rajkumar, M., Ae, N., Prasad, M.N.V. and Freitas, H., 2010. Potential of siderophore-producing bacteria for improving heavy metal phytoextraction. *Trends Biotechnol*., 28, pp.142-149.

Ratledge, C. and Dover, L.G., 2000. Iron metabolism in pathogenic bacteria. *Annu. Rev. Microbiol*., 54, pp.881-941.

Rausch, C., Hoof, I., Weber, T., Wohlleben, W. and Huson, D., 2007. Phylogenetic analysis of condensation domains in NRPS sheds light on their functional evolution. *BMC Evolutionary Biology*, 7(1), pp.78.

Rausch, C., Weber, T., Kohlbacher, O., Wohlleben, W., and Huson, D., 2005. Specificity prediction of adenylation domains in nonribosomal peptide synthetases (NRPS) using transductive support Vector Machines (tsvms). *Nucleic Acids Research*, 33(18), pp. 5799-5808.

Raymond, K. and Dertz, E., 2004. Biochemical and Physical Properties of Siderophores. In: J. Cross, A. Mey and S. Payne, ed., Iron Transport in Bacteria. Washington D.C., American Society of Microbiology Press, pp.3-17.

Raymond, K., Dertz, E. and Kim, S.S., 2003. Enterobactin: an archetype for microbial iron transport. *Proc. Natl. Acad. Sci.*, 100, pp.3584-3588.

Richards, G., Watson, M., Needleman, D., Uknalis, J., Boyd, E. and Fay, J., 2017. Mechanisms for Pseudoalteromonas piscicida-Induced Killing of Vibrios and Other Bacterial Pathogens. *Applied and Environmental Microbiology*, 83(11).

Richardson, D.R., Kalinowski, D.S., Lau, S., Jansson, P.J. and Lovejoy, D.B., 2009. Cancer cell iron metabolism and the development of potent iron chelators as anti-tumour agents. *Biochim. Biophy. Acta*. 1790, pp.702-707.

Robertson, A., McCarville, N., MacIntyre, L., Correa, H., Haltli, B., Marchbank, D. and Kerr, R., 2018. Isolation of Imaqobactin, an Amphiphilic Siderophore from the Arctic Marine Bacterium Variovorax Species RKJM285. *Journal of Natural Products*, 81(4), pp.858-865.

Rocha, D.J.P., Santos, C.S. and Pacheco, L.G.C., 2015. Bacterial reference genes for gene expression studies by RT-qPCR: survey and analysis. *Antonie van Leeuwenhoek*, 108, pp.685-693.

Rodriguez, G.M. and Smith, I., 2006. Identification of an ABC transporter required for iron acquisition and virulence in Mycobacterium tuberculosis. *J. Bacteriol*. 188, pp.424-430.

Rogers, H., Woods, V. and Synge, C., 1982. Antibacterial Effect of the Scandium and Indium Complexes of Enterochelin on Escherichia coli. *Microbiology*, 128(10), pp.2389-2394.

Röttig, M., Medema, M., Blin, K., Weber, T., Rausch, C. and Kohlbacher, O., 2011. NRPSpredictor2—a web server for predicting NRPS adenylation domain specificity. *Nucleic Acids Research*, 39(suppl_2), pp.W362-W367.

Rutledge, P.J. & Challis, G.L. 2015. Discovery of microbial natural products by activation of silent biosynthetic gene clusters. *Nature Reviews Microbiology*, 13(8), pp.509-523.

Saha, R., Saha, N., Donofrio, R. and Bestervelt, L., 2012. Microbial siderophores: a mini review. *Journal of Basic Microbiology*, 53(4), pp.303-317.

Samel, S., Schoenafinger, G., Knappe, T., Marahiel, M. and Essen, L., 2007. Structural and Functional Insights into a Peptide Bond-Forming Bidomain from a Nonribosomal Peptide Synthetase. *Structure*, 15(7), pp.781-792.

Sandhu, P. and Akhter, Y., 2017. Siderophore transport by MmpL5-MmpS5 protein complex in Mycobacterium tuberculosis. *Journal of Inorganic Biochemistry*, 170, pp.75-84.

Sandy, M. and Butler, A., 2009. Microbial Iron Acquisition: Marine and Terrestrial Siderophores. *Chemical Reviews*, 109(10), pp.4580-4595.

Sandy, M., A. Han, J. Blunt, M. Munro, M. Haygood, and A. Butler, 2010., Vanchrobactin and anguibactin siderophores produced by Vibrio sp. DS40M4. *J. Nat. Prod*., 73(6), pp.1038-1043.

Sayyed, R.Z., Badgujar, M.D., Sonawane, H.M., Mhaske, M.M. and Chincholkar, S.B., 2005. Production of microbial iron chelators (siderophores) by fluorescent Pseudomonas. *Indian J. Biotechnol*., 4, pp.484-490.

Schalk, I.J., 2018. A trojan-horse strategy including a bacterial suicide action for the efficient use of a specific Gram-positive antibiotic on Gram-negative bacteria. *J. Med. Chem*., 61, pp.3842-3844.

Schalk, I.J., Hannauer, M. and Braud, A., 2011. New roles for bacterial siderophores in metal transport and tolerance. *Environ. Microbiol*., 13, pp.2844-2854.

Scheidegger, K. and Payne, G., 2003. Unlocking the Secrets Behind Secondary Metabolism: A Review of *Aspergillus flavus* from Pathogenicity to Functional Genomics. *Journal of Toxicology: Toxin Reviews*, 22(2-3), pp.423-459.

Schmelz, S., Kadi, N., McMahon, S.A., Song, L., Oves-Costales, D., Oke, M., Liu, H., Johnson, K.A., Carter, L.G., Botting, C.H., White, M.F., Challis, G.L. and Naismith, J.H., 2009. AcsD catalyzes enantioselective citrate desymmetrization in siderophore biosynthesis. *Nat. Chem. Biol*., 5, pp.174-182.

Schork, K., Podwojski, K., Turewicz, M., Stephan, C. and Eisenacher, M., 2021. Important Issues. in: Statistical Considerations of Quantitative Proteomic Data. *Methods in Molecular Biology*, pp.1-20.

Schwyn, B. and Neilands, J., 1987. Universal chemical assay for the detection and determination of siderophores. *Analytical Biochemistry*, 160(1), pp.47-56.

Shah, M., Karkhanis, V. and Desai, A., 1992. *Isolation and Characterization of Siderophore, with Antimicrobial Activity, from Azospirillum lipoferum*. M.S. University of Baroda.

Shenker, M., Oliver, I., Helmann, M., Hadar, Y. and Chen, Y., 1992. Utilization by tomatoes of iron mediated by a siderophore produced byRhizopus arrhizus. *Journal of Plant Nutrition*, 15(10), pp.2173-2182.

Shirley, W., Kelley, B., Potier, Y., Koschwanez, J., Bruccoleri, R. and Tarselli, M., 2018. Unzipping Natural Products: Improved Natural Product Structure Predictions by Ensemble Modeling and Fingerprint Matching. *ChemRxiv*.

Singh, P.K., Parsek, M.R., Greenberg, E.P. and Welsh, M.J., 2002. A component of innate immunity prevents bacterial biofilm development. *Nature*, 417, pp.552-555.

Singh-Gasson, S., Green, R.D., Yue, Y., Nelson, C., Blatter, F., Sussman, M.R. and Cerrina, F., 1999. Maskless fabrication of light-directed oligonucleotide microarrays using a digital micro mirror array. *Nature Biotechnology*, 17(10), pp.974-978.

Sinha, A. and Parli, B., 2020. Siderophore production by bacteria isolated from mangrove sediments: A microcosm study. *Journal of Experimental Marine Biology and Ecology*, 524, p.151290.

Skaar, E.P., 2010. The battle for iron between bacterial pathogens and their vertebrate hosts. *PLoS Pathog*., 6, e1000949.

Skinnider, M., Dejong, C., Rees, P., Johnston, C., Li, H., Webster, A., Wyatt, M. and Magarvey, N., 2015. Genomes to natural products PRediction Informatics for Secondary Metabolomes (PRISM). *Nucleic Acids Research*.

Smith, M.J., Shoolery, J.N., Schwyn, B., Holden, I., and Neilands, J.B., 1985. Rhizobactin, a structurally novel siderophore from Rhizobium Meliloti. *Journal of the American Chemical Society*, 107(6), pp.1739-1743.

Snow, G., 1965. The structure of mycobactin p, a growth factor for mycobacterium johnei, and the significance of its iron complex. *Biochemical Journal*, 94(1), pp.160-165.

Snow, G.A., 1954. Mycobactin, a growth factor for Mycobacterium johnei II: degradation and identification of fragments. *J. Chem. Soc. (Lond.)*, 49, pp.2588-2596.

Soengas, R.G., Anta, C., Espada, A., Paz, V., Ares, I.R., Balado, M., Rodríguez, J., Lemos, M.L. and Jiménez, C., 2006. Structural characterization of vanchrobactin, a new catechol siderophore produced by the fish pathogen Vibrio Anguillarum serotype O2. *Tetrahedron Letters*, 47(39), pp.7113-7116.

Sonnenschein, E., Stierhof, M., Goralczyk, S., Vabre, F., Pellissier, L., Hanssen, K., de la Cruz, M., Díaz, C., de Witte, P., Copmans, D., Andersen, J., Hansen, E., Kristoffersen, V., Tormo, J., Ebel, R., Milne, B., Deng, H., Gram, L., Jaspars, M. and Tabudravu, J.,

2017. Pseudochelin A, a siderophore of Pseudoalteromonas piscicida S2040. *Tetrahedron*, 73(18), pp.2633-2637.

Sorokina, M. and Steinbeck, C., 2020. Review on natural products databases: where to find data in 2020. *J. Cheminform*., 12, pp.20.

Souto, A., Montaos, M., Rivas, A., Balado, M., Osorio, C., Rodríguez, J., Lemos, M. and Jiménez, C., 2012. Structure and Biosynthetic Assembly of Piscibactin, a Siderophore from Photobacterium damselae subsp.piscicida, Predicted from Genome Analysis. *European Journal of Organic Chemistry*, 2012(29), pp.5693-5700.

Souto, A., Montaos, M.A., Balado, M., Osorio, C.R., Rodríguez, J., Lemos, M.L. and Jiménez, C., 2013. Synthesis and antibacterial activity of conjugates between norfloxacin and analogues of the siderophore vanchrobactin. *Bioorg. Med. Chem*., 21, pp.295-302.

Srinivasan, R., Nath Radhamony, R. and Mohan Prasad, A., 2005. T-DNA insertional mutagenesis in Arabidopsis: a tool for functional genomics. *Electronic Journal of Biotechnology*, 8(1).

Stewart, P.S. and William Costerton, J., 2001. Antibiotic resistance of bacteria in biofilms. *The Lancet*, 358, pp.135-138.

Stirrett, K.L., Ferreras, J.A., Jayaprakash, V., Sinha, B.N., Ren, T. and Quadri, L.E.N., 2008. Small molecules with structural similarities to siderophores as novel antimicrobials against Mycobacterium tuberculosis and Yersinia pestis. *Bioorg. Med. Chem. Lett*., 18, pp.2662-2668

Stoodley, P., Sauer, K., Davies, D. and Costerton, J., 2002. Biofilms as complex differentiated communities. *Ann. Rev. Microbiol*., 56, pp.187-209.

Strieker, M., Tanović, A. and Marahiel, M.A., 2010. Nonribosomal peptide synthetases: Structures and dynamics. *Current Opinion in Structural Biology*, 20, pp.234-240.

Sultana, M., Vogler, S., Zargar, K., Schmidt, A., Saltikov, C., Seifert, J. and Schlömann, M., 2012. New clusters of arsenite oxidase and unusual bacterial groups in enrichments from arsenic-contaminated soil. *Archives of Microbiology*, 194(7), pp.623-635.

Sun, X., Cao, Y., Yang, Z., Xu, C., Li, X., Wang, S. and Zhang, Q., 2004. Xa26, a gene conferring resistance to *Xanthomonas oryzae pv. oryzae* in rice encodes an LRR receptor kinase-like protein. *The Plant Journal*, 37(4), pp.517-527.

Szpunar, J., 2005. Advances in analytical methodology for bioinorganic speciation analysis: metallomics, metalloproteomics and heteroatom-tagged proteomics and metabolomics., *36 Analyst*, 130(4), pp.442-465.

Telford, J.R. and Raymond, K.N., 1997. Amonabactin: a family of novel siderophores from a pathogenic bacterium. *J. Biol. Inorg. Chem*., 2(6), pp.750-761.

Teng, T., Xi, B., Chen, K., Pan, L., Xie, J. and Xu, P., 2018. Comparative transcriptomic and proteomic analyses reveal upregulated expression of virulence and iron transport factors of aeromonas hydrophila under Iron Limitation. *BMC Microbiology*, 18(1).

Tietze, A., Shi, Y., Kronenwerth, M. and Bode, H., 2020. Nonribosomal Peptides Produced by Minimal and Engineered Synthetases with Terminal Reductase Domains. *ChemBioChem*, 21(19), pp.2750-2754.

Toulza, E., Tagliabue, A., Blain, S. and Piganeau, G., 2012. Analysis of the global ocean sampling (GOS) project for trends in iron uptake by surface ocean microbes. *PLoS One*, 7(2), pp.30931.

Troxell, B. and Hassan, H., 2013. Transcriptional regulation by Ferric Uptake Regulator (Fur) in pathogenic bacteria. *Frontiers in Cellular and Infection Microbiology*, 3.

Tyanova, S., Temu, T. and Cox, J., 2016. The MaxQuant computational platform for mass spectrometry-based shotgun proteomics. *Nature Protocols*, 11, pp.2301-2319.

Ueoka, R., Shinzato, N., Kagaya, N., Suenaga, H. and Shin-ya, K., 2020. Pseudoalteropeptide A, a novel lipopeptide from the marine bacterium Pseudoalteromonas piscicida SWA4_PA4 isolated from marine seaweed. *The Journal of Antibiotics*, 74(2), pp.105-110.

Van Doan, H., Hoseinifar, S., Ringø, E., Ángeles Esteban, M., Dadar, M., Dawood, M. and Faggio, C., 2019. Host-Associated Probiotics: A Key Factor in Sustainable Aquaculture. *Reviews in Fisheries Science & Aquaculture*, 28(1), pp.16-42.

Vandenende, C., Vlasschaert, M. and Seah, S., 2004. Functional Characterization of an Aminotransferase Required for Pyoverdine Siderophore Biosynthesis in Pseudomonas aeruginosa PAO1. *Journal of Bacteriology*, 186(17), pp.5596-5602.

Vernyik, V., Karcagi, I., Tímár, E., Nagy, I., Györkei, Á., Papp, B., Györfy, Z. and Pósfai, G., 2020. Exploring the fitness benefits of genome reduction in Escherichia coli by a selection-driven approach. *Scientific Reports*, 10(1).

Verstraeten, S., Aimo, L. and Oteiza, P., 2008. Aluminium and lead: molecular mechanisms of brain toxicity. *Archives of Toxicology*, 82(11), pp.789-802.

Vettoretti, L., Plésiat, P., Muller, C. and El Garch, F., 2009. Efflux unbalance in Pseudomonas aeruginosa isolates from cystic fibrosis patients. *Antimicrob. Agents Chemother*., 53, pp.1987-1997.

Vogel, A., 1987. Class reactions (reactions for functional groups). In: *Elementary Practical Organic Chemistry*. New Delhi: CBS Publishers, pp.190-194.

Vraspir, J.M., Holt, P.D. and Butler, A., 2011. Identification of new members within suites of amphiphilic marine siderophores. *Biometals*, 24(1), pp.85-92.

Wang, W., Chi, Z., Chi, Z., Li, J. and Wang, X., 2009. Siderophore production by the marine-derived Aureobasidium pullulans and its antimicrobial activity. *Bioresource Technology*, 100(9), pp.2639-264

Wang, X., Wang, H., Liu, T. & Xin, Z., 2014. A PKS I gene-based screening approach for the discovery of a new polyketide from Penicillium citrinum Salicorn 46. *Applied Microbiology and Biotechnology*, 98(11), pp.4875-4885.

Weber, T., Baumgartner, R., Renner, C., Marahiel, M. and Holak, T., 2000. Solution structure of PCP, a prototype for the peptidyl carrier domains of modular peptide synthetases. *Structure*, 8(4), pp.407-418.

Weber, T., Blin, K., Duddela, S., Krug, D., Kim, H., Bruccoleri, R., Lee, S., Fischbach, M., Müller, R., Wohlleben, W., Breitling, R., Takano, E. and Medema, M., 2015. antiSMASH 3.0—a comprehensive resource for the genome mining of biosynthetic gene clusters. *Nucleic Acids Research*, 43(W1), pp.W237-W243.

Weber, T., Rausch, C., Lopez, P., Hoof, I., Gaykova, V., Huson, D. and Wohlleben, W., 2009. CLUSEAN: A computer-based framework for the automated analysis of bacterial secondary metabolite biosynthetic gene clusters. *Journal of Biotechnology*, 140(1-2), pp.13-17.

Wencewicz, T.A. and Miller, M.J., 2013. Biscatecholate-monohydroxamate mixed ligand siderophore- carbacephalosporin conjugates are selective sideromycin antibiotics that target Acinetobacter baumannii. *J. Med. Chem.*, 56, pp.4044-4052.

Wencewicz, T.A., Long, T.E., Mollmann, U. and Miller, M.J., 2013. Trihydroxamate siderophore-fluoroquinolone conjugates are selective sideromycin antibiotics that target Staphylococcus aureus. *Bioconjugate Chem*., 24, pp.473-486.

Whitehead, N., Barnard, A., Slater, H., Simpson, N. and Salmond, G., 2001. Quorum-sensing in Gram-negative bacteria. *FEMS Microbiology Reviews*, 25(4), pp.365-404.

Wilderman, P.J., Vasil, A.I., Johnson, Z. and Wilson, M.J., 2001. Characterization of an endoprotease (PrpL) encoded by a PvdS-regulated gene in Pseudomonas aeruginosa. *Infect. Immun*., 69, pp.5385-5394.

Wilson, B., Bogdan, A., Miyazawa, M., Hashimoto, K. and Tsuji, Y., 2016. Siderophores in Iron Metabolism: From Mechanism to Therapy Potential. *Trends in Molecular Medicine*, 22(12), pp.1077-1090.

Winkelmann, G., 1991. *CRC handbook of microbial iron chelates*. Boca Raton u.a.: CRC Press.

Winkelmann, G., 2002. Microbial siderophore-mediated transport. *Biochemical Society Transactions*, 30(4), pp.691-696.

Xiao, R. and Kisaalita, W.S., 1997. Iron acquisition from transferrin and lactoferrin by Pseudomonas aeruginosa pyoverdine. *Microbiology*, 143, pp.2509.

Xu, K.D., McFeters, G.A. and Stewart, P.S., 2000. Biofilm resistance to antimicrobial agents. *Microbiology*, 146, pp.547.

Yamanaka, K., Reynolds, K.A., Kersten, R.D., Ryan, K.S., Gonzalez, D.J., Nizet, V., Dorrestein, P.C. and Moore, B.S., 2014. Direct cloning and refactoring of a silent

lipopeptide biosynthetic gene cluster yields the antibiotic taromycin A. *Proceedings of the National Academy of Sciences of the United States of America*, 111(5), pp.1957-1962.

Yavuz, E., Tokalıoğlu, Ş. and Şahan, S., 2013. FAAS Determination of Ag(I) in Water, Anode Slime, Rock and Cream Samples by Solid Phase Extraction Method based on Sepabeads SP207/5-(p-Dimethylaminobenzylidene) Rhodanine Combination. *Journal of the Brazilian Chemical Society*.

Yokel, R., Ackrill, P., Burgess, E., Domingo, J., Flaten, T. and Savory, J., 1996. Prevention and treatment of aluminum toxicity including chelation therapy: status and research needs. *Journal of Toxicology and Environmental Health*, 48(6), pp.667-684.

Yuan, X., Couto, J., Glidle, A., Song, Y., Sloan, W. and Yin, H., 2017. Single-Cell Microfluidics to Study the Effects of Genome Deletion on Bacterial Growth Behavior. *ACS Synthetic Biology*, 6(12), pp.2219-2227.

Zawadzka, A.M., Abergel, R.J., Nichiporuk, R., Andersen, U.N. and Raymond, K.N., 2009. Siderophore-mediated iron acquisition systems in Bacillus cereus: identification of receptors for anthrax virulence-associated petrobactin. *Biochemistry*, 48, pp.3645-3657.

Zhang, F., Ramos Alvarenga, R., Throckmorton, K., Chanana, S., Braun, D., Fossen, J., Zhao, M., McCrone, S., Harper, M., Rajski, S., Rose, W., Andes, D., Thomas, M. and Bugni, T., 2022. Genome Mining and Metabolomics Unveil Pseudonochelin: A Siderophore Containing 5-Aminosalicylate from a Marine-Derived Pseudonocardia sp. Bacterium. *Organic Letters*, 24(22), pp.3998-4002.

Zhang, G., Amin, S.A., Küpper, F.C., Holt, P.D., Carrano, C.J. and Butler, A., 2009. Ferric stability constants of representative marine siderophores: marinobactins, aquachelins, and petrobactin. *Inorg. Chem.*, 48(23), pp.11466-11473.

Appendices

Appendix A

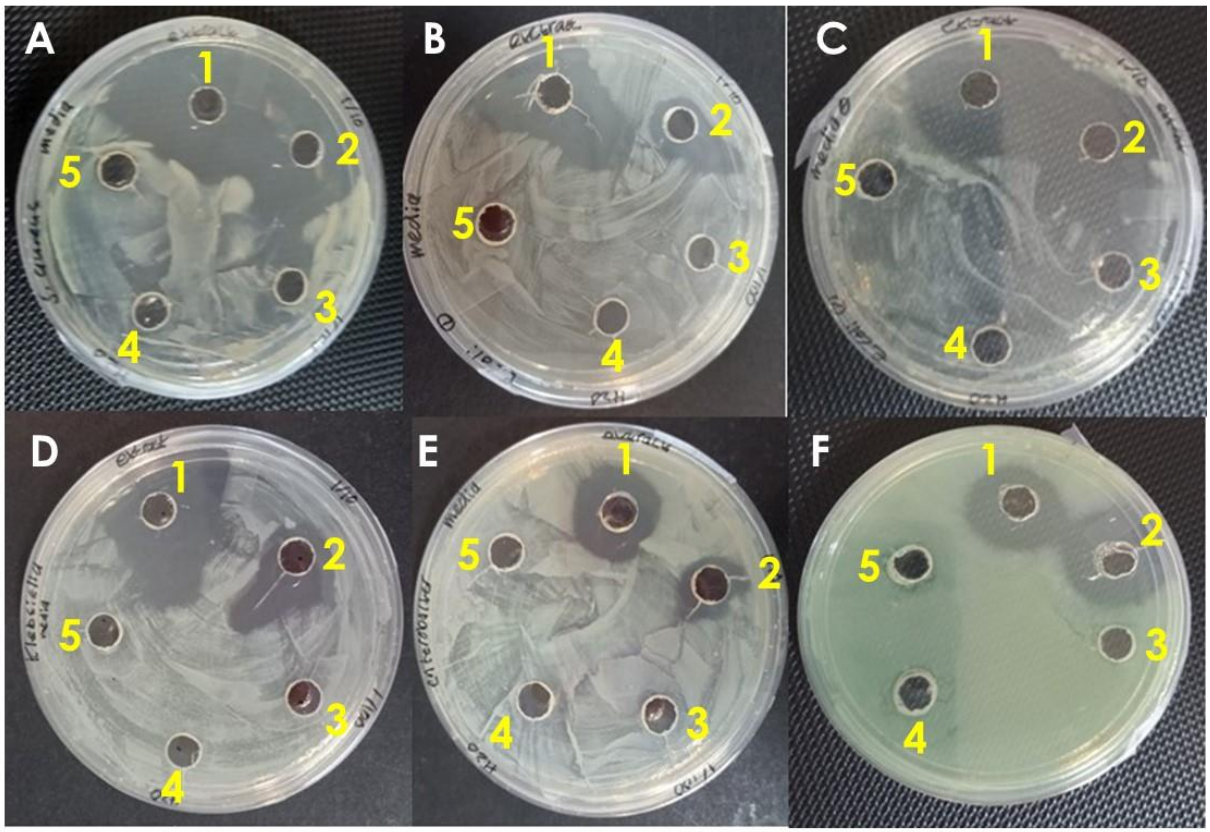

A 1: Antibacterial activity of concentrated cell-free culture supernatant of T. viridans. Zone of clearance indicates inhibition of test strains S. aureus (A), E. coli ATCC 35218 (B), E. coli ATCC 25922 (C), K. pneumoniae (D), E. cloacae (E), and P. aeruginosa (F). Each test strain was tested against an undiluted sample from T. viridans (wells 1), a one-in-ten dilution of the sample (wells 2), and a one-in-one hundred dilution of the sample (wells 3). For the purpose of negative controls, wells 4 and 5 were loaded with dH2O and sterile MMM Fe- respectively. These results could not be repeated.

Appendix B

A 2: MS2 peak masses for peaks with intensities of 0.015 and above found within spectra of compounds with masses of 1050.39 Da, 1032.38 Da and 1034.40 Da. Masses with the same values across compounds are shown in red. Mass

differences of 17 Da within compounds are highlighted in orange. Mass differences of 60 Da within compounds are highlighted in green. Mass differences of 45 Da within compounds are highlighted in purple.

1050.39	1032.38	1034.40
737,18	419	419
755,19	437,01	437,01
796,25	755,19	755,19
814,26	773,23	884,38←944,41
840,24	882,4←942,39	885,37←902,39
858,22← 918,42	883,39←900,41	902,39←962,39
859,25←919,39←979,4	900,41←960,38	903,42←963,39
859,25←876,26	901,41←961,38	918,36←963,39
877,26	916,39←961,38	924,38
918,39←978,4	922,4	925,36←942,39
918,42←935,36←952,41	934,4←979,35	936,38←981,36
934,4←979,4	935,39←952,41	943,42←960,4
940,41	935,39←978,35	954,42←997,38
952,41←997,4	935,39←980,38	955,38←1015,39
953,41←1013,4	940,41	963,39←980,36←997,38
953,41←970,42	941,41←958,42	972,4←1017,38
953,41←998,36	952,41←997,4	974,37
958,42	953,41←970,42	981,36←998,38←1015,39
959,38	953,41←996,4	999,37←1016,39
960,41	953,41←998,4	
970,38←1015,37	961,38←978,35←995,37	
971,42←988,43	970,42←1015,37	
971,42←1016,37	971,42←1016,37	
972,42←1032,38	972,4	
972,42←989,39	979,35←996,4←1013,38	
972,42←1017,41	980,38←997,1	
976,39	997,4←1014,37	
977,4	998,4←1015,37	
977,44		
979,4←996,4←1013,4		
988,43←1033,38		
989,39←1034,38		
997,4←1014,37		
998,36←1015,37←1032,38		
1016,37←1033,38		
1017,41←1034,38		